

SEISMIC PERFORMANCE ANALYSIS OF SPUN PRECAST CONCRETE  
PILE IN RECLAIMED SOIL



A thesis submitted

by

Kh. Afia Farzana Haque

Student No. 0419042213

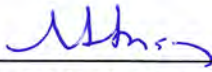
A thesis submitted to the Department of Civil Engineering,  
Bangladesh University of Engineering and Technology, Dhaka, in partial fulfillment  
of the degree of Masters of Science in Civil Engineering (Geotechnical)

**DEPARTMENT OF CIVIL ENGINEERING**  
**BANGLADESH UNIVERSITY OF ENGINEERING AND TECHNOLOGY**

January, 2022

The thesis titled “SEISMIC PERFORMANCE ANALYSIS OF SPUN PRECAST CONCRETE PILE IN RECLAIMED SOIL”, submitted by Kh. Afia Farzana Haque, Roll No.:0419042213, Session: April 2019, has been accepted as satisfactory in partial fulfillment of the requirement for the degree of Master of Science (Civil and Geotechnical Engineering) on 8th January, 2022.

### BOARD OF EXAMINERS



---

Dr. Mehedi Ahmed Ansary  
Professor  
Dept. of Civil Engineering  
BUET, Dhaka-1000.

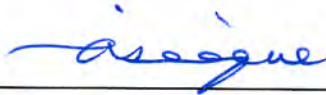
Chairman  
(Supervisor)



---

Dr. Md. Delwar Hossain  
Professor and Head  
Dept. of Civil Engineering  
BUET, Dhaka-1000.

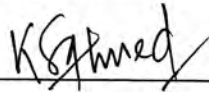
Member  
(Ex-Officio)



---

Dr. Abu Siddique  
Professor  
Dept. of Civil Engineering  
BUET, Dhaka-1000.

Member



---

Dr. Khondaker Sakil Ahmed  
Associate Professor  
Dept. of Civil Engineering  
MIST, Dhaka-1206

Member  
(External)

## DECLARATION

I hereby declare that this thesis is my original work and it has been written by me in its entirety. I have duly acknowledged all the sources of information which have been used in the thesis. This thesis has also not been submitted for any degree in any university previously.

Afia Farzana

Kh. Afia Farzana Haque

## **ACKNOWLEDGEMENT**

At the very outset the author express her sincere gratitude to almighty ALLAH for granting the ability to complete this thesis work successfully.

The author expresses her gratitude and profound indebtedness to her supervisor, Dr. Mehedi Ahmed Ansary, Professor, Department of Civil Engineering, Bangladesh University of Engineering and Technology, Dhaka for his continuous guidance, valuable suggestions and encouragement throughout the research work. His sincere help and valuable advice at every stage made this research work possible.

The author is grateful to Dr. Md. Delwar Hossain, Professor and Head, Department of Civil Engineering, Bangladesh University of Engineering and Technology, for the valuable time he provided as a board member. The author would also like to take the opportunity of expressing sincere appreciation to Dr. Abu Siddique, Professor, Department of Civil Engineering, Bangladesh University of Engineering and Technology and Dr. Khondaker Sakil Ahmed, Associate Professor, Military Institute of Science and Technology, Dhaka, for his kind consent to be the member of my defense board. The author would like to express deep gratitude to Mohiuddin Ahmed, Associate Professor, Military Institute of Science and Technology for the support provided by Geotech laboratory of MIST. Their co-operation and essential suggestions helped me to understand the importance of research.

I greatly express gratitude to my family for their love, uncountable support and encouragement to complete this research.

## ABSTRACT

Precast Spun Prestressed Concrete (SPC) piles are a well-established foundation type in many parts of the world, but it is newly introduced in Bangladesh, particularly in soft soil. As a result, assessing the bearing capacity of SPC pile has an added interest for local engineers and researchers. Also, to analyze the seismic performance of pile foundation embedded in liquefiable soil during an earthquake event is imperative. Among different types of precast piles, the spun pile is popular for using in building and bridge structures for attaining proper axial and lateral load considering pile-soil interaction. In a seismic region, a laterally loaded pile needs to be safe against structural and geotechnical failure to sustain large deflection.

This study systematically investigates the applicability of SPC pile and also determine the liquefaction potential of the reclaimed soil. At the very beginning, a number of subsoil investigations are conducted and required soil samples are collected for basic laboratory tests. Based on the test result and seismic consideration, the liquefaction assessment is performed following the simplified SPT method and compared with some analytical approaches. The results have showed that the soil of that particular area is liquefiable up to a depth of 4.5 m, and SPC piles may be suitable for this weak soil condition. The ultimate load test of the SPC pile has been performed in the Jolshiri area to determine the in-situ pile capacity. It should be mentioned that the vertical load-bearing capacity of the pile has been reduced in a range of 3.8% to 4.5% after considering liquefaction through analytical approach.

In this investigation, the SPC pile is simulated under axial and earthquake loading conditions to observe the static and dynamic pile response through an advanced numerical finite element code PLAXIS 3D. The static numerical model is validated using pile load test data. The PLAXIS 3D soil modeling parameters are determined from field and laboratory tests using established formulas and correlations. For earthquake analysis, Hardening Soil Model is used and liquefaction phenomenon is captured through UBC3D-PLM model.

It is found that the pile deflection increases by 40 times for earthquake with large acceleration compared to only static loading. Total stress and shear stress have increased about 7.2% and 8.5% respectively in case of earthquake loading than axial loading. Parametric study has also been conducted in the analysis and noted that pile length and diameter has significant effect to limit pile displacement at considerable level but mesh size has no considerable effect on pile displacement. It has been observed from the liquefaction analysis in PLAXIS 3D that the pore water pressure ratio becomes 1 which means the loose sand layer completely liquefied. In liquefied soil, pile shows larger displacement about 30-60 % than non-liquefied soil condition during earthquake. The liquefaction causes large bending moment at the interface of liquefiable and non-liquefiable soil. A comparison of pile moment generation has been made considering liquefaction, without liquefaction and improved soil under earthquake loading. It has been found that soil improvement up-to almost 15 m can help to reduce large moment generation about 90% to 100% during liquefaction. The soil improvement measures significantly ameliorate the pile response and flexural capacity. SPC pile is a good alternative compared to conventional driven and cast-in-situ pile in reclaimed areas in terms of axial loading but their application under earthquake loading needs to be analyzed to improve the flexural capacity and lateral stiffness.

## TABLE OF CONTENTS

<b>DECLARATION</b>	iii
<b>ACKNOWLEDGEMENT</b>	iv
<b>ABSTRACT</b>	v
<b>TABLE OF CONTENTS</b>	vi
<b>LIST OF FIGURES</b>	ix
<b>LIST OF TABLES</b>	xii
<b>NOTATION AND ABBREVIATIONS</b>	xiii
<b>CHAPTER 1 INTRODUCTION</b>	1
1.1 General	1
1.2 Background of the Study	2
1.3 Objectives of the Study	4
1.4 Scope of the Study	4
1.5 Organization of the Thesis	6
<b>CHAPTER 2 LITERATURE REVIEW</b>	7
2.1 Introduction	7
2.2 Bearing Capacity and Dynamic Response of Precast Pile in Liquefiable Soil	9
2.3 Seismic Performance of Spun Pile Foundation	18
2.3.1 Experimental Investigation (Monotonic and Cyclic Load Test on PHC Pile)	18
2.3.2 Crack Pattern and Failure Mode	21
2.3.2 Numerical Modeling	29
2.3.3 PHC Pile in Liquefiable Soil	30
2.4 Shear Wave and Shear Modulus Estimation	32
2.5 Liquefaction Susceptibility Analysis	33
2.6 Bearing Capacity Determination of Pile	34
2.6.1 Bearing Capacity Determination by Analytical Procedure	34
2.6.2 Bearing Capacity Determination from Static Pile Load Test	35
2.7 FEM Analysis: PLAXIS 3D	36
2.7.1 Hardening Soil (HS Model)	37
2.7.2 UBC-3D PLM Model	38

2.7.3	PLAXIS Embedded Beam (Rows)	40
2.8	Summary	41
<b>CHAPTER 3 FIELD DATA COLLECTION AND BEARING CAPACITY ANALYSIS</b>		
	<b>ANALYSIS</b>	43
3.1	Introduction	43
3.2	Geometry of SPC Pile	44
3.3	Laboratory Test Results	46
3.3.1	Grain Size Analysis	50
3.3.2	Atterberg Limit Test	52
3.3.3	Unconfined Compression Test	53
3.3.4	Consolidated Drained Direct Shear Test	54
3.3.5	Consolidated Drained Triaxial Compression Test	56
3.3.6	One-Dimensional Compression Test	57
3.4	Field Test	60
3.4.1	Pile Load Test	60
3.5	Liquefaction Analysis in Jolshiri Site	63
3.6	Bearing Capacity Analysis of SPC pile	64
3.7	Summary	70
<b>CHAPTER 4 NUMERICAL MODELING</b>		71
4.1	Introduction	71
4.2	FEM Model in PLAXIS 3D	71
4.3	Derivation of Soil Stiffness Parameters	71
4.3.1	Field and Laboratory Tests Performed for Determination of Soil Parameters	72
4.4	Modeling Parameters	72
4.4.1	Soil Modeling Parameters	72
4.4.2	Embedded Pile Modeling Parameters	74
4.5	Numerical Modeling	75
4.5.1	Validation with Field Pile Load Test Data	79
4.5.2	Pile Deflection under Axial Loading	79
4.5.3	Stress Distribution	82
4.6	Parametric Study	84
4.6.1	Influence of Mesh Size	84
4.6.2	Effect of Pile Length	87
4.6.3	Effect of Pile Diameter	88

4.7	Earthquake Analysis	89
4.7.1	Dynamic Soil Behavior	90
4.7.2	Boundary Condition	91
4.7.3	Earthquake Input Signal	93
4.8	Pile Deformation under Earthquake Loading	94
4.9	Liquefaction Analysis	104
4.9.1	Liquefiable Sand Layer Parameters	104
4.10	Soil Improvement Impact on Liquefiable Soil	109
4.11	Summary	117
<b>CHAPTER 5 CONCLUSIONS AND RECOMMENDATIONS</b>		118
5.1	Conclusions	118
5.2	Recommendations for Future Work	120
<b>REFERENCES</b>		122



## LIST OF FIGURES

Figure 1.1	Flowchart of the study	5
Figure 2.1	a) Lateral spreading Kaushaltar-Lokanthali in Nepal, 2015. (Gautam et al.,2017). b) Tilting of pile supported building on level ground during 1995 Kobe earthquake in Japan Bhattacharya et al.(Bhattacharya et al.,2008). c) The Showa Bridge collapsed during the 1964 Niigata earthquake in Japan. Bhattacharya et al.(Bhattacharya et al.,2008)	8
Figure 2.2	i) Soil surface condition at end of shakings, a) Site 1; and b) Site 2. ii) Schematic diagram of piles deformation: a) Site 1; b) Site 2 (C. Xu et al.,2020)	11
Figure 2.3	Schematic of soil and pile displacements for cases where piles could not resist downslope passive force from crust (C) and cases where piles resisted passive force of crust with either upslope resisting forces from loose sand (B) or downslope driving forces from loose sand (A). (Brandenberg et al.,2005)	12
Figure 2.4	(a) Schematic diagram of soil profiles in Case I, II and III. (Rahmani and Pak.2012)	14
Figure 2.5	a) Cross section of proposed pile. b) Experimental setup for bending test, (Akiyama et al.,2012)	19
Figure 2.6	Prefabrication process of prestressed piles, (Xizhi et al.,2020)	20
Figure 2.7	Test setup and arrangements of instruments (Xizhi et al.,2020)	21
Figure 2.8	Slip surface and displaced shape of the damaged pile based on the investigation by (Akio Nakazawa 1996; Akio Nakazawa and Nakazawa.1999)	22
Figure 2.9	(a) Compression failure of hollow pile. (b) Buckled dowel	23
Figure 2.10	(i) Damages of the models after the tests. (ii) Pile soil separation. (Huang et al.,2018)	25
Figure 2.11	Failure modes of PHC piles. Xizhi et al. (2020)	26
Figure 2.12	Modes of failures for plies under lateral loads: (a) free head piles (b) fixed head (Fatahi et al.,2014; Poulos and Davis.1980)	27
Figure 2.13	Brittle plastic hinge mechanism of hanging PHC pile (Setiawan et al.,2020)	27
Figure 2.14	HS yield surface with cap presented in principal stress space	37
Figure 2.15	Definition of $E_{50}^{ref}$ and $E_{ur}^{ref}$ for drained triaxial test results	37
Figure 2.16	Original UBCSAND hardening rule	39
Figure 3.1	Jolshiri abashon project (Google Map)	43
Figure 3.2	Geomtery of SPC pile: (a) Circular hollow cross section; (b) SPC pile after Fabricated ready for transportation; (c) Long section os SPC piles showing the spiral reinforcement schedule.	45

Figure 3.3	a) Standard Penetration Test (SPT) b) Borehole Location	47
Figure 3.4	Borehole cross-sections	48
Figure 3.5	SPT N values for three boreholes	50
Figure 3.6	Laboratory test (a) Disturbed soil sample (b) Undisturbed soil sample (c) specific gravity test (d) Direct shear test (e) Atterberg limit test (f) Triaxial test.	51
Figure 3.7	Particle size distribution curve	52
Figure 3.8	Casagrande Plasticity Chart	53
Figure 3.9	(a) Relationship between axial strain and stress and (b) brittle failure mode	54
Figure 3.10	Direct shear test, relationship between (a) maximum shear stress and normal stress (b) deformation and root time (c) shear stress and horizontal displacement (d) vertical and horizontal displacement	55
Figure 3.11	Relationship between (a) Shear stress and principal stress (b) Deviator stress and axial strain (c) Volumetric strain and axial strain and (d) shear failure modes of soil samples	57
Figure 3.12	Relationship between void ratio and applied pressure	58
Figure 3.13	a) Depth vs Shear wave Velocity b) Depth vs Shear Modulus, $G_{max}$	59
Figure 3.14	Push-in test in study area	61
Figure 3.15	a) Performing static load test b) Schematic diagram of static load test c) spun pile for driving in soil d) Hydraulic jack and dial gauge setup during the test	62
Figure 3.16	Comparison of liquefaction assessment	64
Figure 3.17	(a) Bearing capacity without considering liquefaction by analytical method (b) Bearing capacity considering liquefaction by analytical method	65
Figure 3.18	(a) Comparison of skin friction considering with and without liquefaction (b) comparison of bearing capacity considering with and without liquefaction	66
Figure 3.19	Load vs Settlement plot of conducted load tests	67
Figure 3.20	Load-Settlement curve derived from pile load test by Davisson offset method	68
Figure 3.21	Load-Settlement curve derived from pile load test by tangent method	68
Figure 3.22	Comparison of pile bearing capacity determined from Push-in test and analytical method	69
Figure 4.1	Parameters for hardening soil model	73
Figure 4.2	FEM model developed in PLAXIS 3D	76
Figure 4.3	(a) Axially loaded embedded pile. (b) connectivity plot	78
Figure 4.4	Comparison of PLAXIS 3D obtained results with field measured result	79
Figure 4.5	Pile depth vs axial load	80
Figure 4.6	(a) Displacement field around pile. (b) Top view of displacement contour	81
Figure 4.7	Total principle stress at surrounding soil at pile bottom	82
Figure 4.8	Total strain in z direction	83
Figure 4.9	Stress-strain relationship	83
Figure 4.10	Mesh element connectivity plot	85

Figure 4.11	Total displacement of pile with respect to full loading stage for different meshing condition	86
Figure 4.12	Distribution of displacement with pile depth for different meshing condition	86
Figure 4.13	Comparison of moment for different mesh size	87
Figure 4.14	Distribution of displacement with pile depth for different pile length	88
Figure 4.15	Distribution of displacement with pile depth for different pile diameter	89
Figure 4.16	Assigned Rayleigh damping for soil	91
Figure 4.17	3-D view of boundary condition	92
Figure 4.18	Original earthquake frequency (a) 1995 Kobe (b) 1989 Loma Prieta	93
Figure 4.19	Kobe earthquake input signal	94
Figure 4.20	Soil deformation due to earthquake loading (Kobe)	95
Figure 4.21	Vertical displacement of soil under earthquake loading	95
Figure 4.22	Lateral displacement of soil under earthquake loading	96
Figure 4.23	Top view of lateral displacement of soil under earthquake loading	96
Figure 4.24	Displacement comparison of pile under both axial and earthquake loading	97
Figure 4.25	Acceleration response spectrum of analysed model for Kobe earthquake at different depth	98
Figure 4.26	Earthquake acceleration at different depth of soil	99
Figure 4.27	Amplification spectrum	100
Figure 4.28	Maximum strain at top of soil profile for earthquake loading	101
Figure 4.29	Maximum strain at bottom of soil profile for earthquake loading	101
Figure 4.30	Maximum shear stress under earthquake loading	102
Figure 4.31	Maximum shear stress under maximum axial loading	103
Figure 4.32	Principle total stress under earthquake loading	103
Figure 4.33	Deformation at the top soil layer due to liquefaction	107
Figure 4.34	Maximum pore pressure ratio at top soil layer for Kobe earthquake	107
Figure 4.35	Maximum pore pressure ratio at top soil layer for Loma Prieta earthquake	108
Figure 4.36	Maximum excess pore water pressure generated during Kobe and Loma Prieta earthquake	108
Figure 4.37	Displacement comparison of pile under earthquake loading	109
Figure 4.38	Comparison of moment developed under earthquake loading condition	110
Figure 4.39	Comparison of moment developed both considering and without considering liquefaction	111
Figure 4.40	Comparison of moment reduction after soil improvement for Kobe earthquake	114
Figure 4.41	Comparison of moment reduction after soil improvement for Loma Prieta earthquake	115
Figure 4.42	Comparison of moment considering liquefaction, withoutout liquefaction and soil improvement for (a) Kobe (b) Loma Prieta earthquake	116

## LIST OF TABLES

Table 2.1	Proposed empirical relationships between uncorrected SPT-N and shear wave velocity	32
Table 3.1	Properties of SPC pile used in this study	46
Table 3.2	SPT and Subsoil Classification	58
Table 4.1	Material properties for the soil layers	74
Table 4.2	Required parameters of the embedded pile	75
Table 4.3	Stage construction phases for compressive loading	77
Table 4.4	Stage construction phases for incremental loading and unloading stages	77
Table 4.5	Element size factor with elemnt distribution	84
Table 4.6	Stage construction phases for earthquake analyis	90
Table 4.7	Input parameters of liquefied sand layer of UBC3D-PLM model	105
Table 4.8	Material properties for soil improvement up-to 5 m	112
Table 4.9	Material properties for soil improvement up-to 15 m	113

## NOTATION AND ABBREVIATIONS

<b>Symbol</b>	<b>Description</b>
CD	Consolidated Drained triaxial test
$c'$	Cohesion
$e_{init}$	Initial void ratio
$e_{max}$	Maximum void ratio
E	Young's modulus
$E_{50}$	Secant elastic modulus at 50% peak strength
$E_{oed}$	Oedometer modulus
$E_{ur}$	Unloading/reloading modulus
k	Coefficient of permeability
$k_o^{nc}$	Coefficient of earth pressure at rest for normally consolidated soil
m	Power for stress level dependency stiffness
OCR	Over Consolidated Ratio
$p^{ref}$	Reference Pressure
q	Deviatoric stress
$q_a$	Asymptotic value of deviatoric stress
$q_f$	Deviatoric stress at failure
$R_f$	Failure ratio
$R_{int}$	Strength reduction factor
$S_u$	Undrained shear strength
$\phi_{pi}$	Peak friction angle
$\phi_{cv}$	Constant volume friction angle
$n_p$	Plastic shear modulus index
$f_{dens}$	Densification factor
$f_{Epost}$	Post liquefaction factor
$\alpha$	Adhesion factor
$\alpha$	Cap parameter
$\beta$	Cap parameter

<b>Symbol</b>	<b>Description</b>
$\varepsilon$	Axial strain
$\varepsilon_1$	Major Principal strain
$\varepsilon_a$	Axial strain
$\varepsilon^{p1}$	Plastic shear strain
$\varepsilon^{pv}$	Plastic volumetric strain
$\varepsilon^{pc}$	Volumetric cap strain
$\nu$	
$\phi$	Angle of friction
$\phi'_{mob}$	Effective mobilized angle of friction
$\gamma$	Unit weight of soil
$\nu$	Poisson's ration
$\nu_{ur}$	Unloading/reloading poisson's ratio
$\sigma_1, \sigma'_1$	Major total, effective principal stress
$\sigma_3, \sigma'_3$	Minor total, effective principal stress
$\sigma_h, \sigma'_h$	Total, effective horizontal stress
$\sigma_v, \sigma'_v$	Total, effective vertical stress
$\tau$	Shear stress
$\psi$	Dilatancy angle
$\psi'_{mob}$	Effective mobilized dilatancy angle
LL	Liquid limit
PI	Plasticity index
SPC	Spun Prestressed Concrete
BNBC	Bangladesh National Building Code
BS	British Standard
IS	Indian Standard
PHC	Prestressed High Strength Concrete
HS	Hardening Soil
HSS	Hardening Soil Small
UBC3D	University of British Columbia 3D Formulation
SPT	Standard Penetration Test
ASTM	American Society for Testing and Materials
MC	Mohr-Coulomb
MCE	Maximum Considered Earthquake
FEM	Finite Element Model
FS	Factor of safety

# CHAPTER 1

## INTRODUCTION

### 1.1 General

Increased demand for high-rise buildings for the ever-growing urban population made engineers build structures in poor ground condition. In this case, heavy loads coming from structures near the ground drive the engineers to adopt a deep foundation. Pile foundations can be classified into two categories: displacement piles and replacement piles. The displacement pile is installed by pushing into the ground which causes soil displacement around the pile. In replacement piles, the soil is replaced with subsequent placement of pile material. A Prestressed spun concrete pile is a displacement pile driven into an end bearing layer. It is newly introduced in Bangladesh for its better-quality control technique and quiet piling operation. A precast prestressed spun pile can provide high bearing capacity from large shaft resistance and toe bearing.

The main reason for the pile foundation is to limit the settlement and control damage of the structure due to the soft layer underground. If the loose sand under the structure is saturated, it tends to behave like a liquid during earthquake shaking and tries to flow laterally. This makes the foundation vulnerable to extensive damage as the soil loses shear strength due to pore water pressure generation. The extensive damage caused by liquefaction of both superstructure and foundation is observed during past earthquakes namely Niigata earthquake in Japan 1964, 1995 Kobe Earthquake. Bangladesh and north Indian states are seismically active regions in the world. In the last 200 years, it has experienced numerous large magnitude of earthquakes. Though Dhaka did not encounter large to moderate magnitude earthquakes in the past but researchers pointed out four vulnerable points as a source of an earthquake that makes Dhaka a risky city among 20 unsafe cities in the world. Recently a mild tremor of 3.4 magnitudes was felt in Sylhet, Bangladesh. An earthquake of 4.5 magnitudes was felt in 2001 with a focal depth of 10 km near Dhaka. With the increased population, Dhaka city is going through rapid urbanization. As a result, many lowland areas are now being used and filled up with loose sandy dredged soil which is susceptible to liquefaction during seismic action.

Most piles are designed considering the axial load coming from the structure but during seismic events, it can suffer from substantial lateral pressure and large settlement in liquefiable soil. Previous studies showed that a pile can sustain axial load during the earthquake but it fails in

lateral load, so it is mandatory to design a pile in the seismic region considering both axial and lateral load to overcome unwanted sudden damage of foundation and superstructure.

Numerical analysis is a reliable way to determine the seismic performance of a pile for a particular subsoil condition. By considering both geological properties and structural loading conditions, numerical investigation can evaluate the pile-soil response during seismic wave propagation. Researchers use finite element modeling to determine the factors affecting pile behavior in seismically vulnerable areas where piles can encounter possible failure due to weak soil during the liquefaction phenomenon.

For simulating pile-soil behavior, PLAXIS 3D finite element software is used in this thesis. Emphasis is given on soil modeling with earthquake loading and its effect on the pile. Different constitutive models are incorporated in PLAXIS such as Mohr-Coulomb (MC) model, the elastic-plastic non-linear stress-dependent stiffness Hardening Soil (HS) model, UBC3D-PLM, etc. In this study, the Hardening soil model is used for soil modeling for analysis of static and earthquake loading conditions. UBC3D-PLM model is used to capture the liquefaction probability during earthquake in loose sandy soil. The pile is modeled as an embedded beam row element. The function of embedded beam row is widely acknowledged by researchers in simulating dynamic pile response.

In this investigation, a static SPC pile load test has been conducted, and also SPT test has been also carried out in the study site. After the field tests, a numerical model is validated with the pile load test data and pile is simulated under static loading. A detailed numerical investigation has been conducted to observe the SPC pile response in earthquake loading in liquefiable soil situated in Jolshiri reclaimed land.

## **1.2 Background of the Study**

Researchers have found much evidence of pile damages during earthquakes due to inertia forces of superstructures and piles lateral displacement. Spun Prestressed Concrete (SPC) pile has become a convenient choice for engineers in cohesionless liquefiable soil for building structures because of its low construction cost, high bearing capacity, and good reliability. The pile foundation is designed to sustain vertical and lateral load but sufficient lateral resistance



needs to be considered for resisting structural damage of piles during an earthquake. The SPC piles are widely used abroad and many researchers have conducted experimental and numerical investigations to see the SPC pile capacity under axial and lateral load. The present study intends to investigate the seismic performance of SPC pile foundation in a reclaimed area of Dhaka susceptible to earthquake-induced liquefaction using three-dimensional numerical modeling.

Spun Prestressed Concrete (SPC) pile is a reliable alternative to conventional driven or bored pile due to its high ultimate load capacity and skin friction (Akiyama et al., 2012). Under dynamic loading prestressed pile showed larger peak displacement for saturated soil rather than unsaturated soil but prestressed pile can resist the damage well (Huang et al., 2017; Huang and Yu, 2017). A pile can be yielded before the complete liquefaction took place in the reclaimed layer (Uzuoka et al., 2007). The static load test can accurately measure the ultimate bearing capacity of prestressed high strength concrete pile compared to SPT blow count, CPT method (Wei et al., 2020). Numerical investigations are also done by researchers to observe pile performance in different soil characteristics (Kyi and Yangon; Lozovyi and Zahoruiko, 2014; Mohey Mohamed et al., 2020; Shafiqu and Sa'ur, 2017). Belinchón et al. (2016) have carried out a numerical investigation to model the negative skin friction of hollow prestressed pile driven into soft soil. The increased reinforcement ratio, pile depth, and prestressing level can move the plastic hinge location of the pile at a deeper depth and improve soil-pile interaction (Huang et al., 2020). Yang et al. (2018) have observed that the increase in reinforcement ratio of prestressed tendons and concrete infilling can improve ductility and bearing capacity of the piles.

Though SPC is widely used worldwide for its high strength capacity but in the context of Bangladesh SPC pile is newly introduced for reclaimed areas. Again, there is gap in literature to study SPC pile in loose soil susceptible to liquefaction during seismic excitation. Very few researchers addressed the problem of pile behavior in weak liquefiable soil. So, it is imperative to understand the pile behavior both in terms of vertical loading and lateral loading condition in subsoil conditions like reclaimed areas where the soil is highly susceptible to liquefaction phenomenon. The accurate way to measure the bearing capacity of pile foundation is to conduct in situ static pile load test. In the study area, this test is conducted to know the ultimate pile vertical load-bearing capacity. Pile foundation analysis is a three-dimensional problem. This study uses 3D finite element software to validate the vertical bearing capacity with field load test data and simulate the seismic behavior of the SPC pile under earthquake loading.

### **1.3 Objectives of the Study**

The following are the main objectives of the research:

- (i) To investigate the soil characteristics of the study site by conducting field and laboratory tests.
- (ii) To develop a 3D finite element numerical model of SPC pile of at the site soil condition and compare it with the static pile load test data.
- (iii) To observe SPC pile performance numerically under seismic excitation and conduct the parametric study.

### **1.4 Scope of the Study**

Firstly, to know the soil characteristics of the soil Standard Penetration Test (SPT) has been done and soil samples has been collected to the laboratory for determining soil index and shear strength properties. A static pile load has also been performed to estimate pile capacity in Jolshiri Abashon area.

Secondly, a numerical finite element modeling has been done in PLAXIS 3D using Hardening soil model and embedded beam row to simulate static pile load test behavior. The developed model has been validated with the results of the static pile load test. A parametric study has also been done to observe the influence of mesh size, pile length and diameter on pile response.

Thirdly, the numerical model has been subjected to earthquake ground motion to observe the pile dynamic response using proper boundary condition. Liquefaction behavior of pile and soil has been simulated using UBC3D-PLM model during earthquake excitation.

Figure 1.1 shows the flowchart of the work procedure used to conduct the study.

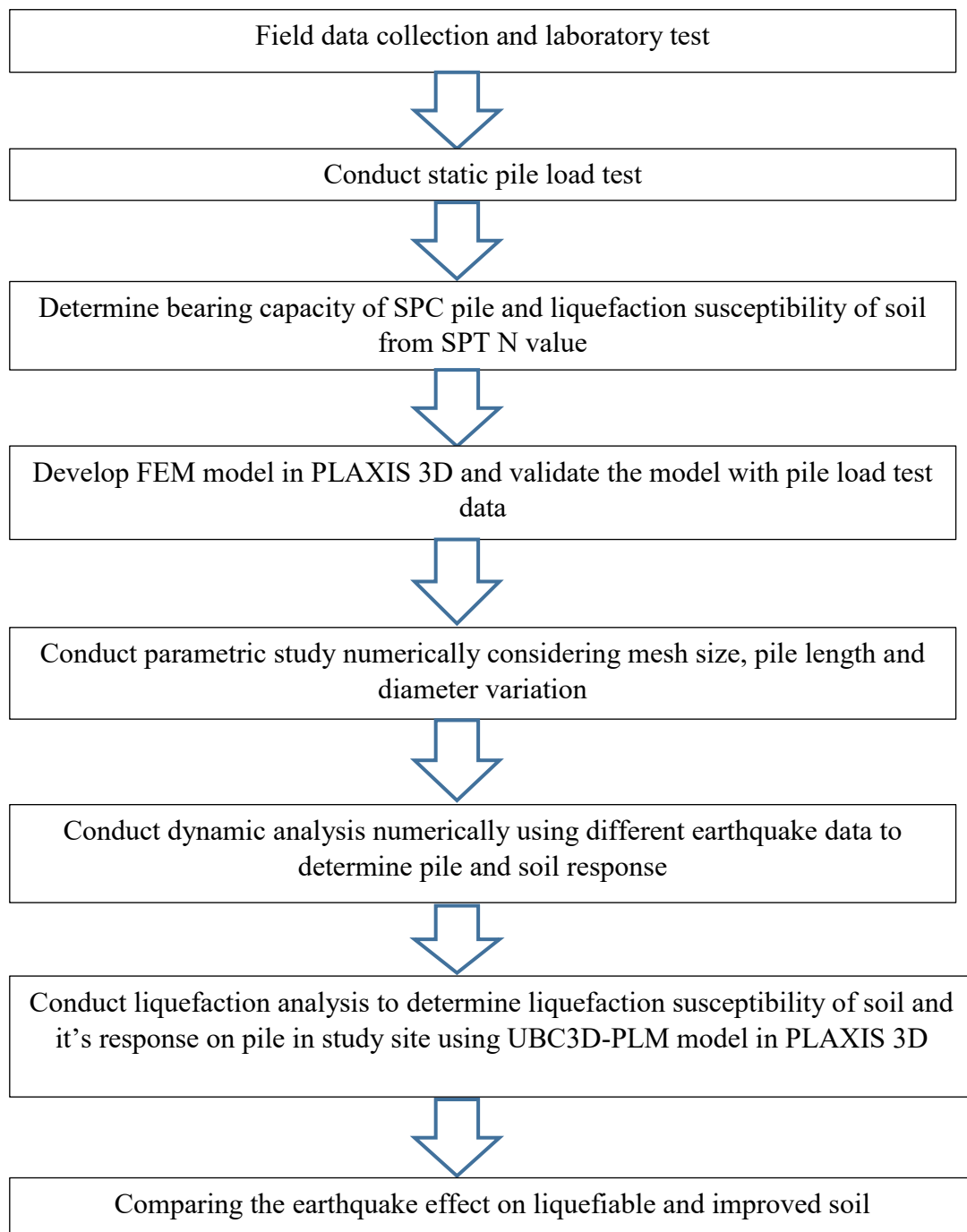


**Figure 1.1:** Flowchart of the study

## **1.5 Organization of the Thesis**

The thesis is divided into several chapters to achieve the stated objectives. The chapters are structured as follows:

Chapter one discusses an introduction of the relevant research background, statement of problems as well as the objectives of this research.

Chapter two presents the previous researches on dynamic response of precast pile and recent progress of SPC piles in seismic zones and liquefiable soil including experimental, numerical and theoretical investigation.

Chapter three represents the Standard Penetration Test (SPT) test and laboratory test that is conducted to know the sub-soil condition of Jolshiri reclaimed area. Also, the static pile load test carried out in the study area to determine the bearing capacity of the soil is discussed. The liquefaction susceptibility of soil is determined in this chapter using SPT N value. The validation of the FEM model in PLAXIS 3D with pile load test data has also been shown for the study site here. Several parametric studies are conducted here that can affect the finite element model.

Chapter four describes the modeling procedures of dynamic analysis of pile and soil using finite element analysis to observe the pile-soil response in an earthquake wave motion. The liquefaction phenomenon is considered using UBC3D-PLM model parameters for loose sand soil layers in reclaimed areas. In the end, pile and soil response in liquefiable soil is discussed considering improved soil.

Chapter five presents the findings of the research program. Also, recommendations are stated in this chapter for future research scope.

## CHAPTER 2

### LITERATURE REVIEW

#### 2.1 Introduction

Pile foundation gives stability to any structure by transferring load from weak layer of soil to stiff layer. After installation, a pile foundation performance can be influenced by many uncertainties for seismic activities. One of the devastating results of seismic activity that leads to a phenomenon called liquefaction if the soil layer is weak or loose. When a saturated loose sandy or silty soil is subjected to significant ground shaking during an earthquake, that can increase the pore water pressure in the soil as it cannot pass through during this short time and it behaves like liquid decreasing the effective stress in soil then this occurrence is called liquefaction. In a sloping ground due to liquefaction, a downslope displacement may occur if the soil shear strength is minimum, this phenomenon is called lateral spreading. A non-liquefiable layer is at the top of the liquefied layer then the liquefaction may increase the chance of lateral flow of the non-liquefied layer which causes damage to the pile. Earthquake-induced liquefaction can cause significant damage in any structure build on cohesionless loose sandy soil by causing failure in the foundation. Kathmandu valley in Nepal has witnessed a strong earthquake of 7.8 magnitudes in 2015, April 25. Due to this earthquake different locations in Nepal has experienced severe damage because of liquefaction in form of sand boiling and lateral spreading, see Figure 2.1 (a). Such failure has also been observed during the Niigata earthquake 1964 and the Kobe earthquake 1995, see Figure 2.1 (b,c).

The pile can encounter failure due to bending caused by deformation of surrounding soil or buckling when the pile lacks lateral support. Nowadays precast piles are extensively used in building and bridge constructions especially in weak soil as they can sustain large bending moments (Harries and Patrou, 2001). There are various types of precast piles namely the H-shaped steel pile, prestressed hollow concrete pile or spun pile, prestressed high-strength concrete pile and reinforcement concrete pile, etc. Among them, prestressed concrete piles are getting attention among the engineers because of their high load carrying capacity, low cost, good quality, and wide range of applicability (Cao et al., 2020; Shi, 2004).



**Figure 2.1:** a) Lateral spreading Kaushaltar-Lokanthali in Nepal, 2015 (After Gautam et al., 2017) b) Tilting of pile supported building on level ground during 1995 Kobe earthquake in Japan ( After Bhattacharya et al., 2008) and c) The Showa Bridge collapsed during the 1964 Niigata earthquake in Japan (After Bhattacharya et al., 2008)

The increase in buried depth, prestressing level, and reinforcement ratio can increase the pile-soil interaction of concrete piles (Huang et al., 2020). The prestressing in piles can reduce pile damage effect and degradation. The bearing capacity of the prestressed concrete pile under earthquake loading has been studied by performing seismic analysis both experimentally and numerically (Wang et al., 2014; Tao et al., 2017; Yang et al., 2018; Au et al., 2011). A precast prestressed concrete piles can fail in liquefiable soil during earthquakes due to a lack of flexural strength and ductile capacity (Uzuoka et al., 2007). A detailed literature review consisting of experimental, numerical, and theoretical related studies conducted previously are discussed in this chapter. Also, a review on the constitutive model of soil used in this study namely the Hardening soil model and UBC3D-PLM model is presented here in this section.

## **2.2 Bearing Capacity and Dynamic Response of Precast Pile in Liquefiable Soil**

The precast pile is popular in the seismic regions due to its cost-effectiveness and high strength capacity. Precast pile failure during a strong earthquakes has been witnessed in previous years. Horizontal bearing properties of pile foundation during lateral earthquake loading have been determined by many researchers previously. This section reviewed precast pile foundation dynamic response and bearing capacity during an earthquake in liquefiable soil.

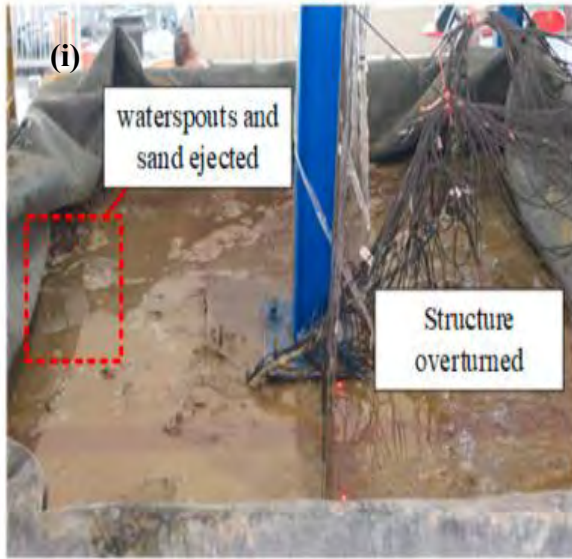
Lateral displacement near the pile head and bending moment near the pile shaft can increase due to gap formation. The lateral displacement of the square pile is found to be smaller than the circular pile whereas the Hollow precast pile showed larger displacement than the solid RC pile (Heidari et al., 2014b; Heidari et al., 2014a). The RC pile displacement compared to steel pile is found to be larger due to the formation of cracks which leads to increased deflections in the pile. Inadequate length of the pile in liquefiable layer and extreme ground motion can occur severe damage to pile foundation during seismic activities.

Elgamal et al. (2006) have performed shake table test and nonlinear elastoplastic model in Opensees of laterally loaded pile embedded in liquefied soil. Zhang (2009) has mentioned a method of nonlinear analysis of laterally loaded rigid pile in cohesionless soil where ultimate soil resistance and modulus of subgrade reaction linearly increased with depth. Zhang and Hutchinson (2012) has determined the inelastic behavior of piles embedded in layered soil with or without the effect of liquefaction by conducting nonlinear pushover analysis. The results from the analysis showed a larger yield drift for piles in liquefied soil. Maximum

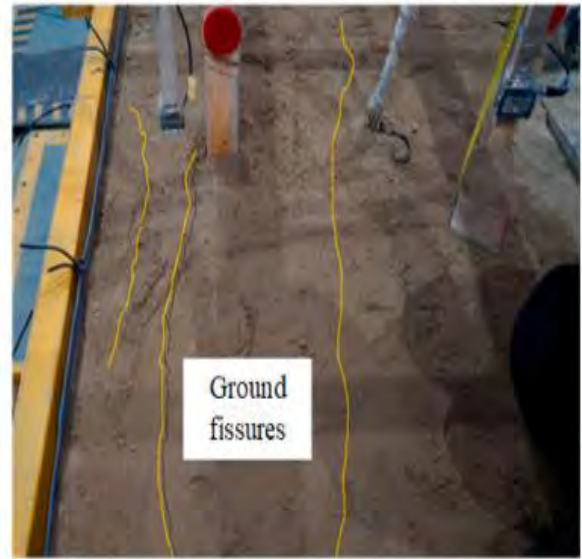
moment location for pile in liquefied soil ranges from 3-5.5 times the diameter of pile and 0.5-3 D for non-liquefied soil for both high and low strength piles with diameter ranges from 0.8-1.2 m. Xu et al. (2020) have conducted shake table test to observe the seismic performance and failure pattern of the pile group in both liquefiable and non-liquefiable sand deposits. For the experiment, two site conditions have been considered one is with liquefiable saturated sand layer and another one is with loose sand layer, for both cases the top clay layer and bottom dense sand layer were fixed in position. The results from the experimental analysis has showed that the liquefied site experienced waterspouts and sand boiling after shaking while the non-liquefied site showed ground fissures as shown in Figure 2.2 (i). The non-liquefiable site has showed higher acceleration amplification with larger displacement than the liquefiable site, see Figure 2.2 (ii). The soil in liquefied sites has showed larger stiffness degradation and piles showed larger bending moment than piles in non-liquefied site.

In a sloping ground, lateral spreading is the after effect of liquefaction phenomenon if there is non-liquefiable layer above or below the liquefied soil layer and in most pile and structural damage occur due to this occurrence. Different experimental tests have been conducted by scholars (Cubrinovski et al., 2006; Motamed et al., 2010; He et al., 2006; Towhata et al., 2006; Ashford et al., 2006; Abdoun and Dobry, 2002) to determine pile response in laterally spreading ground. The lateral behavior of pile foundation in non-liquefiable sloping soil crust over liquefied loose sand layer was studied by Brandenberg et al.(2005). The direction of lateral loading has been explained in terms of pile and liquefiable soil displacement. As shown in Figure 2.3, three different loading cases have been considered during centrifuge test. In case A, pile displacement is lesser as the pile reacted stiff under crust loading so a downslope load attracted the pile, in case B, the pile also behaved stiff enough to resist the load on clay crust and an upslope resisting force is attracted by pile. In case C, the pile is too flexible to resist the load and has showed larger displacement near pile head. Laterally spreading crust displaced more than liquefiable sand layer in earthquake event (Brandenberg et al., 2005).



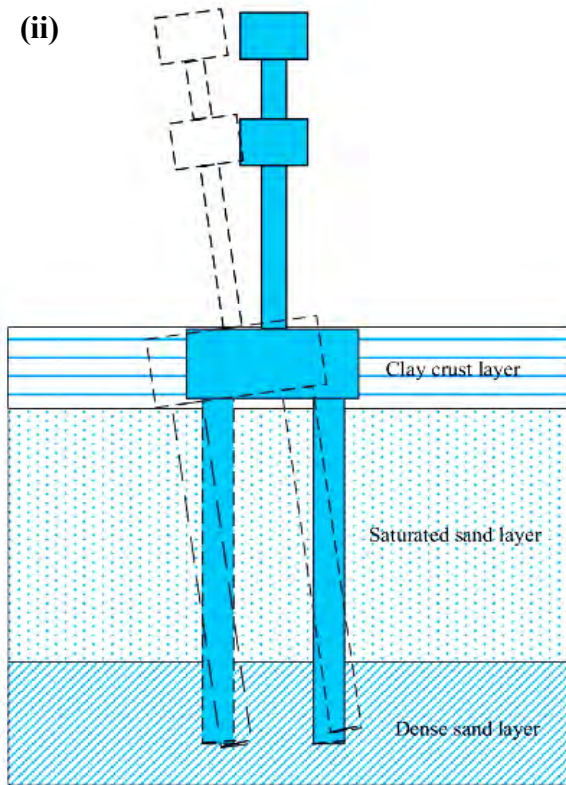


a)

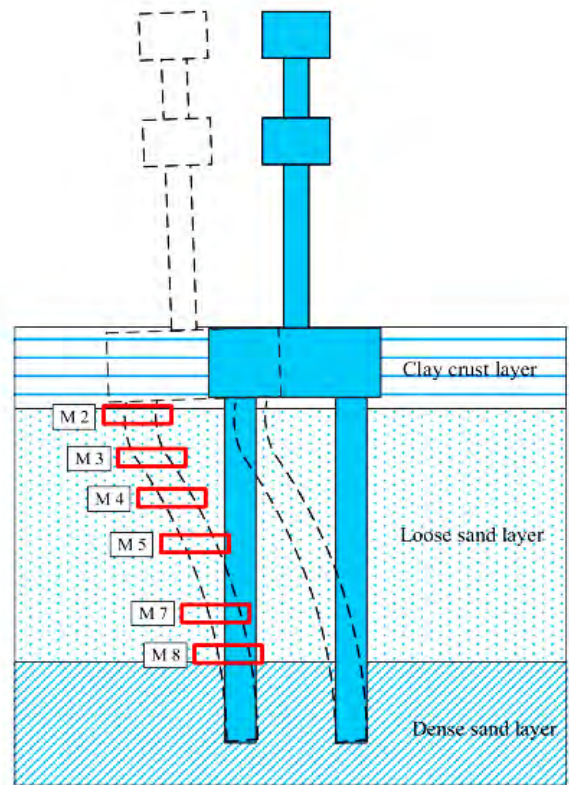


b)

(ii)



a)



b)

**Figure 2.2:** i) Soil surface condition at end of shakings, a) Site 1; and b) Site 2. ii) Schematic diagram of piles deformation: a) Site 1; b) Site 2 (After Xu et al., 2020)

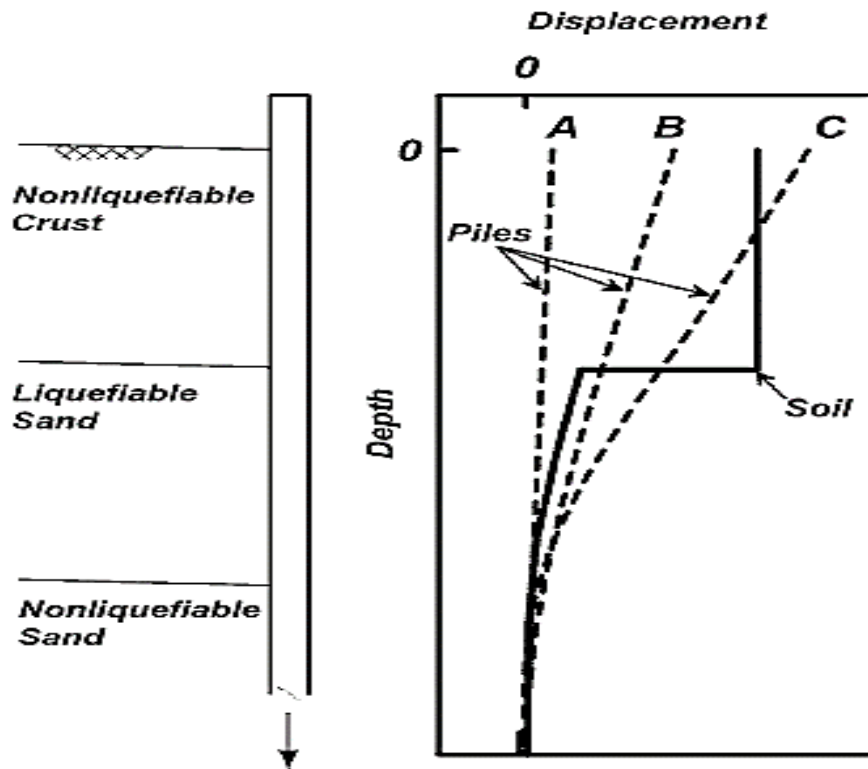


**Figure 2.3:** Schematic of soil and pile displacements for cases where piles could not resist downslope passive force from crust (C) and cases where piles resisted passive force of crust with either upslope resisting forces from loose sand (B) or downslope driving forces from loose sand (A). (After Brandenberg et al., 2005)

Different researchers (Maheshwari et al., 2004; Maheshwari et al., 2005; Maheshwari et al., 2008; Haldar and Babu, 2010) have studied the effect of soil liquefaction on dynamic response of pile foundation by carrying numerical investigation. Soil nonlinearity and pore pressure generation in saturated soil affect the dynamic response of pile as well (Chen and Baladi, 1985; Baladi and Rohani, 1979; Byrne, 1991; Martin et al., 1975). By considering soil nonlinearity and pore pressure generation during liquefaction in soil model a 2x2 pile-soil model has been investigated by (Maheshwari and Sarkar, 2011) in MATLAB by three dimensional finite element code to see the effect of loading intensity and stiffness of soil under seismic excitation. The result showed that effect of nonlinearity is prominent for soft soil for both case of with or without pore pressure in soil. Soil loses its dynamic stiffness if liquefaction occurs due to pore pressure generation and group effect of pile is reduced by soil nonlinearity (Sarkar and Maheshwari, 2012).

For designing pile against seismic loading in liquefiable soil, both the translation and rotation needs to be considered (Maheshwari and Sarkar, 2012). The dynamic lateral stiffness is influenced by the properties of top layer of soil, size of pile and installation process. The driven precast pile can generate four to five time's higher stiffness than driven cast in situ piles (Boominathan and Ayothiraman, 2006) . The group pile in clay under dynamic lateral loading shows higher peak displacement than single pile due to reduction of stiffness. The closer spacing of group piles has dominant pile soil interaction and group pile shows strong pile-soil interaction under dynamic loading than static loading with increased magnitude of moment and active pile length (Chandrasekaran et al., 2013). Different researchers (Abdoun and Dobry, 2002; Abdoun et al., 2003; Suzuki et al., 2006; Dungca et al., 2006; Bhattacharya et al., 2004; Tamura and Tokimatsu, 2006; Han et al., 2007; Hokmabadi et al., 2015) have done experimental investigation to determine dynamic response of pile in liquefiable soil. Due to the popularity of finite element software's and to avoid the problems encountered in physical test for liquefaction analysis of pile, numerical investigation has been conducted by many researchers to get more accurate results (Cheng and Jeremić, 2009; Finn and Fujita, 2002; Klar et al., 2004; Oka et al., 2004; Uzuoka et al., 2007; Comodromos et al., 2009).

With the intention of finding out the critical parameters that influence the dynamic behavior of pile in liquefiable soil under seismic excitation, Rahmani and Pak (2012) has conducted three dimensional dynamic analysis in Opensees considering permeability coefficient for excess pore water pressure during liquefaction. The effect of pile fixity, length, relative density, frequency input motion and thickness of liquefiable layer on pile response have been identified. Three types of soil profiles have been taken into account to study the parameters as shown in Figure 2.4. It has been observed that maximum bending moment is developed at 2 m below pile top for free head pile and at pile head for fixed head pile. Pile length has no significant influence on the location of bending moment. The fixed head pile has showed larger bending moment at pile head in liquefiable soil but reduced lateral displacement. It has also been found that 10% increase in relative density in liquefiable soil layer decreased the lateral displacement and bending moment about 10-15%.

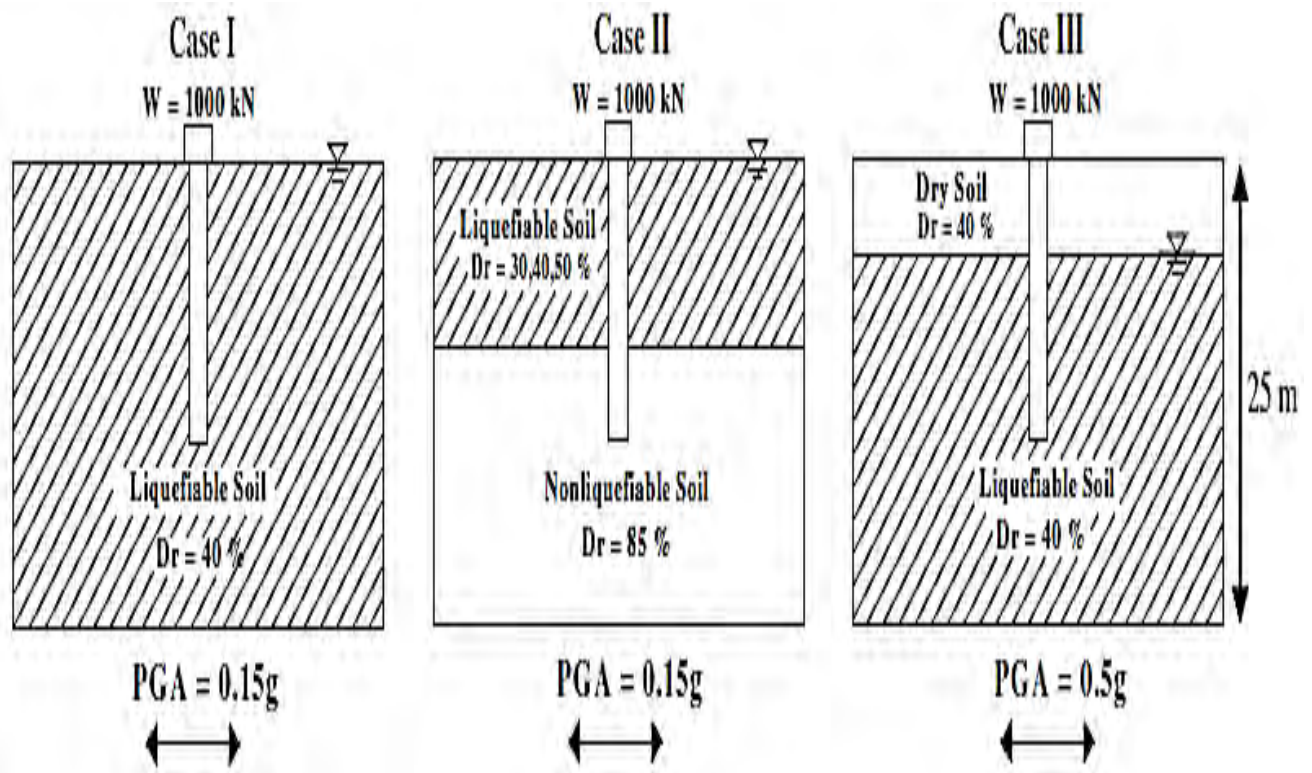


**Figure 2.4:** (a) Schematic diagram of soil profiles in Case I, II and III. (After Rahmani and Pak, 2012)

Hokmabadi et al. (2015) have studied the seismic soil-pile interaction on dynamic response of buildings with different heights in soft soil by conducting shake-table test. The experimental result has showed that the pile-soil interaction of end bearing pile caused an increase in the lateral displacement and interstory drift of buildings compared to fixed base structure.

Belinchón et al. (2016) have addressed the problem of designing piles in soft cohesive soil. They have carried out numerical investigation to model the negative skin friction of hollow prestressed pile driven into soft soil and to observe the influence of pile coating, length and load on the location of neutral plane of pile. From the analysis it was observed that coated pile caused less drag load and less settlement compared to uncoated pile. The increase in vertical load can reduce the negative skin friction and depth of neutral plane. Effect of interface strength is very negligible on neutral plane position (El-Mossallamy et al., 2013). Researchers (Bhattacharya et al., 2004; Knappett and Madabhushi, 2006; Knappett and Madabhushi, 2009; Bhattacharya et al., 2003) have reported the pile instability and failure pattern in liquefiable soil under dynamic loading. Mokhtar et al. (2014) have explained pile instability and lateral displacement due to soil liquefaction through numerical modeling considering seismic excitation in submerged condition. The author reported that pile top experienced maximum

lateral displacement in submerged condition than dry mode and large diameter of pile can reduce lateral displacement. Increase in pile diameter can increase the lateral pile resistance and flexural rigidity and increase in pile soil contact area can enhance the soil passive resistance with pile fixation length. Fatahi et al. (2014) have done a comprehensive study of soil characteristics, stress field and soil-pile interface influence on the performance of horizontally loaded pile. The author has summarized that pile constructed in soft clay can produce soil heave, soil separation and tension crack near ground surface. The boundary element method in PLAXIS 3D has been found to be sensitive to young's modulus of soil. The coefficient of lateral earth pressure has minimum influence on depth-lateral displacement but interface strength reduction factor has significant effect on performance of pile (Fatahi et al., 2014). Phanikanth et al. (2013) and Asaadi and Sharifipour (2015) have performed numerical modelling to see the pile behavior in liquefied soil. Asaadi and Sharifipour (2015) has carried out numerical analysis to observe the effect of relative density, earthquake frequency and acceleration on pile in liquefaction susceptible soil. The result has found that the liquefaction potential of soil decreases with increase in depth and relative density of soil. For high peak ground acceleration liquefaction has initiated at an early stage and with high intensity earthquake the pile displacement and settlement also increased. But liquefaction susceptibility has decreased in near pile and free field areas with increased frequency of earthquake and dissipation capacity increased with frequency. Artificially filled soil has more susceptibility to liquefaction and here the use of driven pile can increase the density of liquefiable filled soil up to 4.4% - 4.8% (Saha et al., 2012). Janalizadeh and Zahmatkesh (2015) has observed the pile response by numerical analysis considering various parameters such as soil layering, kinematic and internal forces, pile head boundary condition and ground slope in liquefiable soil.

Rostami et al. (2017) have carried out a numerical investigation to observe the pile response in liquefiable soil under both axial and earthquake loading. Three cases have been considered in the study i) Liquefiable soil ii) liquefiable layer between non-liquefiable layers and iii) upper layer is liquefiable soil, for analyzing pile capacity, failure pattern, and plastic hinge formation. The author has found that the pile response was significantly influenced by material properties, length, free and fixed head condition and surrounding soil. For case I the location of bending moment is in the middle of the pile in liquefiable layer for free, and fixed headed pile. In cases II and III the bending moment of the pile has been developed at the boundary of the model Rostami et al. (2017). It is found that pile length had no effect on the location of bending moment but the plastic hinge location is influenced by pile diameter, reinforcing steel, ductility



and soil condition. In a homogenous liquefied soil layer the plastic hinge may form in the middle of pile. Chatterjee and Choudhury (2018) has proposed analytical process to find out the effect of vertical load on bending moment and deflection on a laterally loaded pile embedded in liquefiable soil. The result showed that the maximum bending moment has occurred at the interface of liquefiable and non-liquefiable soil layer (Chatterjee and Choudhury, 2018; Choudhury et al., 2014; Liyanapathirana and Poulos, 2005). Pile has experienced maximum bending moment and deflection in liquefiable soil due to significant reduction in soil shear strength and subgrade modulus. With the increase in internal loading, the bending moment and deflection of pile has increased by 52%. The shear strength become zero due to liquefaction which cause to increase the effective length of pile and subsequent failure happens (Chatterjee and Choudhury, 2018). So vertical load consideration is important to determine pile response. The bending moment and deflection at the pile head is influenced by the thickness of liquefiable soil layer (Chatterjee, 2019).

For understanding field behavior of precast pile, the vertical and horizontal bearing capacity determination can provide the practical information to engineers. Different researchers (Marcos et al., 2013; Chen and Marcos, 2018; Yu and Yang, 2012; Zhou et al., 2017) have focused on determining bearing capacity of precast pile and their interpretation method. Behavior of precast pile under compressive loading has been studied by Zhou et al. (2019). Three design codes have been compared for designing bearing capacity. All the codes have been found conservative but the double tangent method is more conservative and Chin's method has given highest value of pile capacity. Flexural rigidity of pile influences the lateral response of pile dominantly than soil flow and also the bending moment along the pile length is independent of soil flow (Banerjee and Shirole, 2014). Zhanfang et al. (2020) have realized the necessity to determine the vertical bearing capacity of pile in horizontal earthquake load in liquefiable sandy soil using Shake table test. Four conditions have been considered for the test such as, natural foundation, 3D, 3.5D and 4D pile spacing and different vibration settlement time history has been analyzed for those conditions. After that a settlement dynamic amplification factor (SDAF) has been proposed. From the study, they have observed that proper selection of pile spacing can improve anti-liquefaction soil properties, form the test 3D condition gave higher anti-liquefaction property. The dynamic problem for pile has been converted into static problem by multiplying SDAF to static load. Al-abboodi and Sabbagh (2019) has reported that decrease in pile diameter can increase lateral displacement in pile under lateral loading and pile configuration, position in a pile group can influence the performance of laterally loaded passive

piles. The spacing to diameter ratio and length to diameter ratio have influence on the bearing capacity of pile raft foundation. Increase in Pile diameter can reduce the settlement significantly than increase in Pile length (Singh et al., 2021). Similar conclusion has been drawn by Johnson et al. (2019) for pile-raft foundation in multilayered soil. Pile spacing is important parameter to influence pile load-settlement curve (Ukritchon et al., 2016). Choosing appropriate material model in FEM analysis is very important to predict the actual field condition. Gowthaman et al. (2017) have suggested that at higher working load above 15000 kN, the combination of Hardening soil and Mohr Coulomb model can provide better prediction of pile settlement. Whereas the Mohr Coulomb model can predict settlement realistically up-to a working load below 13000 kN. Young modulus of soil plays a significant role in predicting bending moment along the pile length (Al-Abboodi et al., 2015). Ter-Martirosyan. (2020) has reported that liquefied soil can pull down a pile to specific depth due to self-compaction and can increase the pile settlement up-to 87% compared to non-liquefied soil. For pile supported wharf structures Kardoğan and Bhattacharya (2017) has suggested to use fewer large modulus piles to avoid buckling related problems in liquefied soil during earthquake. Zein et al. (2021) have studied the suitability of modeling pile as plate element to analyze dynamic soil-structure response in PLAXIS. From the study, it has been found that pile modelled as plate element overestimated shear stress, moment values, displacement during earthquake. They have recommended to use plate model only in case of dense sand and in all other cases embedded row model is found to be appropriate for representing real performance of pile. The increase in pile length and diameter can reduce maximum amplitude of displacement (Al-Qayssi et al., 2001). Embedded pile can predict the pile group behavior better than volume pile and embedded pile is sensitive to finite element mesh sizes (Marjanović et al., 2016). Lozovyi and Zahoruiko (2014) has compared static pile load test of four piles in different soil condition with PLAXIS 3D finite element simulation. Both the load-settlement curves have showed good correlation. When the adhesion between pile-soil interface increases and rough friction sleeves are present then the shear stress also increases (Hamouma et al., 2020). A pile group efficiency depends on the number of pile in it and pile spacing. Larger the number of piles in a pile group, lower the group efficiency. Higher Soil stiffness modulus also increases efficiency (Dewi and Liang, 2011). The maximum acceleration, displacement and bending moment are reduced with increase in length to diameter ratio of pile under cyclic loading. Shafiqu and Sa'ur (2017) has studied the seismic behavior of pile using finite element program PLAXIS 3D. Using dynamic soil properties and earthquake data, the pile-soil system has been modeled in the analysis.

The study has concluded that the 3D model can analyze the real behavior of seismic activity than 2D analysis in PLAXIS. Mohamed et al. (2020) have used UBC3D-PLM model in PLAXIS to model seismic liquefaction behavior of soil and HS small model to capture the soil dynamic behavior. Jawad et al. (2018) have investigated the effect of dynamic loading, number of piles on vertical settlement, pore water pressure ratio and liquefaction zone. The analysis has showed that increase in dynamic loading increases the pore water pressure which will cause liquefaction with a higher vertical settlement. Increased number of piles decrease the vertical settlement and pore water pressure. The HS small model is reported to be suitable for seismic ground response analysis without considering liquefaction (Amorosi et al., 2016). The increase in embedded length of pile can decrease the value of bending moment but overall pile capacity increases (Deendayal, 2017). Pile embedded in sand underlain by clay shows higher bearing capacity (Tradigo et al., 2015). Piles spaced closely in a pile group shows larger displacement than a single pile when subjected to lateral loading. In a pile group first row carries highest load than middle and back rows.

### **2.3 Seismic Performance of Spun Pile Foundation**

Among different types of precast pile, now-a-days prestressed piles are extensively used in building and bridges. These piles are manufactured in factory by using centrifugal casting method. Prestressed concrete pile (spun pile) is a reliable alternative to conventional driven or bored pile due to its high ultimate load capacity and skin friction (Akiyama et al., 2012). The seismic damage of PHC piles under vertical and lateral loading have encouraged the researchers to study the performance of piles in earthquake events. An experimental investigation is a reliable approach to analyze the behavior of pile under both axial and lateral loading. Also, for numerical validation the experimental results are extremely useful despite high initial cost. The result obtained from different experimental and numerical investigations of PHC piles are presented below considering performance criteria and failure pattern.

#### **2.3.1 Experimental Investigation (Monotonic and Cyclic Load Test on PHC Pile)**

Different researchers (Xizhi et al., 2020; Budek and Priestley, 2005; Xu and Ma, 2017; Zhang et al., 2019; Joen and Park, 1990; Wang et al., 2014; Wang et al., 2015; Yang and Wang, 2016; Kokusho et al., 1987; Zhang et al., 2011; Gao, 2012) have conducted experimental investigation on the seismic behavior of PHC pile. To enhance the bearing capacity of pile



researchers proposed different ideas. From the result of anti-symmetric bending shear test on PHC pile Kishida et al. (1998) have proposed an idea to fill up the hollow part of pile with concrete and to increase the amount of spiral reinforcement which can enhance the ultimate shear strength and deformation capacity of pile. Lignola et al. (2009) and Yazici (2012) have found that the FRP wrapping around a hollow prestressed pile can increase the ductility and ultimate load carrying capacity of hollow part. Zhang et al. (2011) have investigated the flexure and shearing properties of concrete pipe piles. The results of shearing test has showed that after incorporating non-prestressed bar the stress and crack distribution have changed and the pile has showed less deformation.

Akiyama et al. (2012) have proposed a prestressed concrete pile with carbon- fiber sheets and concrete infilling to increase the flexural capacity of pile.

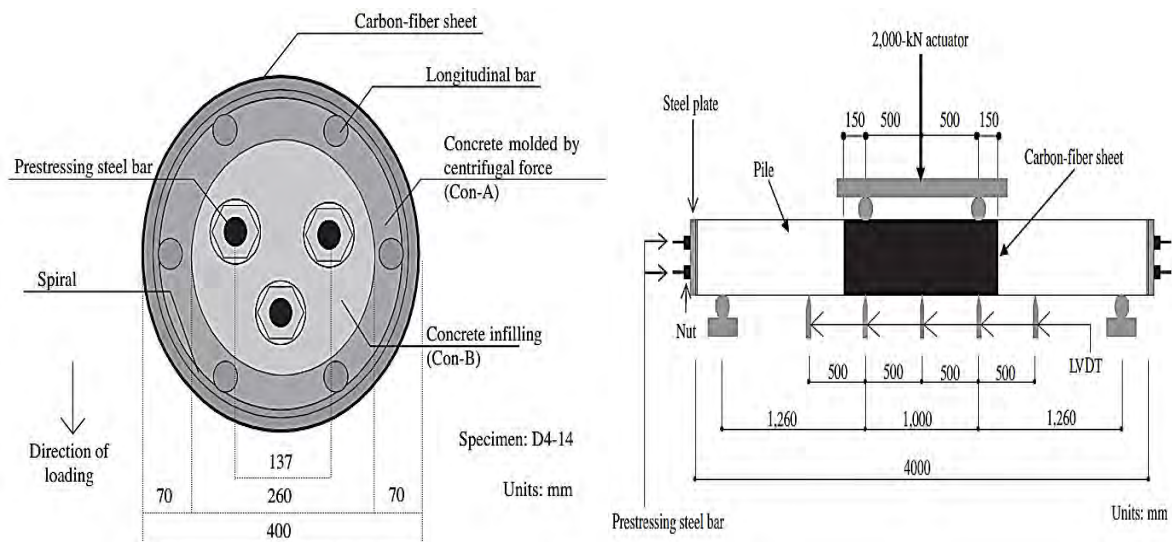


**Figure 2.5:** a) Cross section of proposed pile. b) Experimental setup for bending test, (After Akiyama et al., 2012)

From bending test as shown in Figure 2.5, Akiyama et al. (2012) have found that the proposed pile has higher flexural capacity than conventional precast pile. Furthermore, an analytical approach has been presented to obtain relationship between bending moment and curvature of proposed pile, even if the pile experiences soil liquefaction during an earthquake event. Yanyan (2013) has noted that normal strength deformed bar can enhance the flexural strength capacity of PHC piles under low-cyclic loading.

Shin et al. (2013) have conducted an experimental investigation on square hollow rectangular concrete pile to observe the shear strength under cyclic loading with single layer longitudinal

reinforcement and without transverse reinforcement. They have concluded that under cyclic loading the piles damaged due to flexural crack and in monotonic loading the concrete section remained uncracked. Li et al. (2013) have mentioned that the arrangement pattern, number of piles and configuration of upper structure can affect the strain and bending moment of PHC pile. With increase in seismic intensity the soil-pile interaction and nonlinearity effect also go up.

Xizhi et al. (2020) have conducted experimental investigation on nine prestressed high strength concrete pile with partial normal strength deformed bar to see the seismic behavior under both axial compression load and cyclic load. The prefabrication process of piles and experimental setup is shown in Figure 2.6.



**Figure 2.6:** Prefabrication process of prestressed piles: (a) Reinforcement cage (b) Connection details (c) Into the mold (d) Concrete pouring (e) Tensioned prestressed tendons (f) Centrifugal casting (g) Curing (h) Completion, (After Xizhi et al., 2020)

In cyclic loading test, the dynamic response of the pile can be observed. The experimental setup is shown in Figure 2.7. During an earthquake event a pile may suffer from damage. In prestressed pile, concrete cover spalling can be seen as a regular phenomenon in horizontal loading but the ductile behavior of the pile is found satisfactory despite the effect of concrete cover crushing and lateral strength reduction. This crushing of concrete cover causes sudden degradation of load carrying capacity with higher residual displacement of the system.

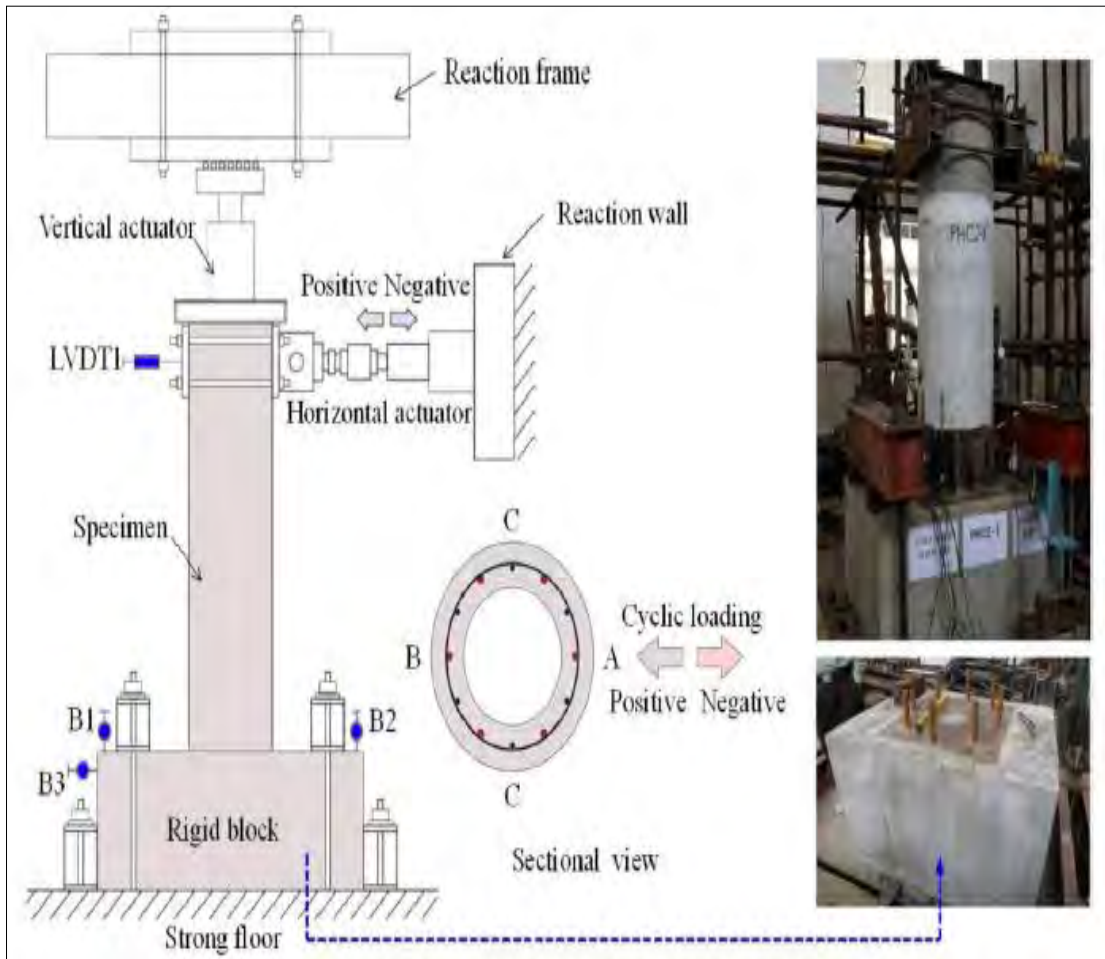


**Figure 2.7:** Test setup and arrangements of instruments (After Xizhi et al., 2020)

### 2.3.2 Crack Pattern and Failure Mode

Previous researchers have showed that damage in prestressed pile occurred in different earthquake hazard mostly due to bending failure (Sugimura et al., 2004; Yamazoe et al., 2012). Nakazawa (1996, 1999) has mentioned the possibility of slip surface occurrence due to lateral flow in liquefied reclaimed soil, see Figure 2.8. Au et al. (2011) have analyzed the bending response of PHC piles based on the nonlinearity and stress dependence of consecutive materials.

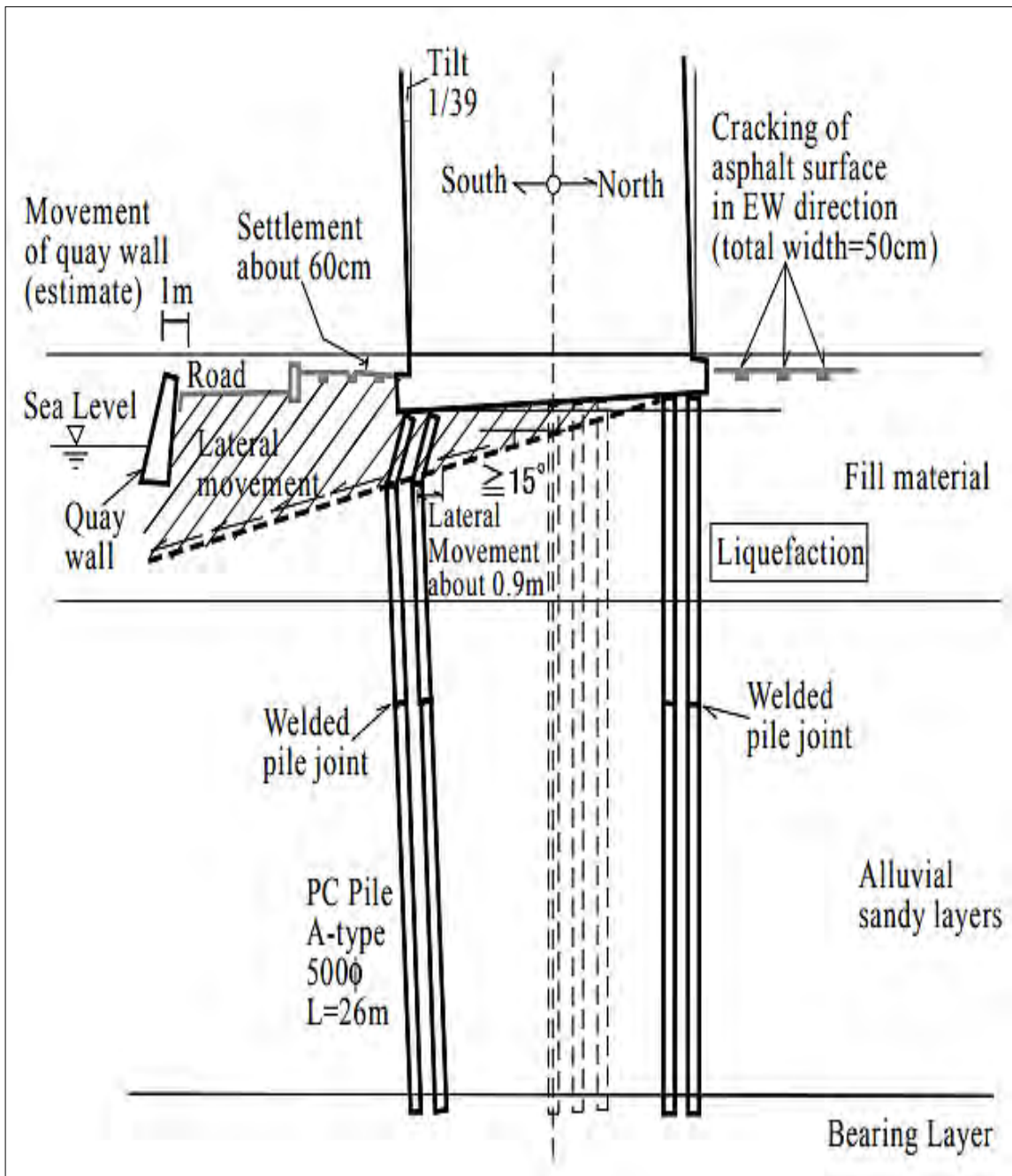


**Figure 2.8:** Slip surface and displaced shape of the damaged pile based on the investigation (After Nakazawa, 1996, 1999)



Different researchers (Xizhi et al., 2020; Li et al., 2015; Xu and Ma, 2017; Yang and Wang, 2016; Zhang et al., 2019) have performed cyclic load test on different PHC pile and have observed failure pattern under cyclic loading. Back in 1987 Banerjee et al. (1987) have found that performance of pile is influenced by axial load, embedment condition and spiral steel. Joen and Park (1990) has recommended to use spiral steel in pile head embedded in pile cap to improve bond in strands and to assist lateral load transfer in surrounding concrete area of pile cap. Precast hollow pile have lighter weight and give more structural efficiency due to its prefabrication process. Harries and Petrou (2001) has suggested that the prestressed pile embedded plainly in cast-in-situ square pile cap can increase the flexural capacity of pile cap connection region if the pile is placed with sufficient minimum embedded length equal to the width of pile. Budek and Priestley (2005) has performed a parametric study of prestressed hollow circular pile shaft. The parameters like transverse reinforcement, confinement ratio and presence of nonprestressed steel bar in plastic hinge area have been varied to see the flexural response of pile. The study has concluded that the incorporation of nonprestressed bar in plastic region decreases the curvature capacity of pile and causes compression failure due to bond slip. Also the confinement to the plastic hinge zone has no effect on displacement ductility capacity of pile. Figure 2.9 (a) and (b) shows spalling of concrete cover under axial loading and buckling of dowel bar during pile failure. The shear strength of oblique section of prestressed pile can be influenced by concrete strength, loop bar percentage and effective prestress (Yongchao et al., 2011).



**Figure 2.9:** (a) Compression failure of hollow pile. (b) Buckled dowel

The pretensioned spun concrete pile shows poor load carrying capacity in flexure. Bang et al. (2013) have proposed concrete infilled prestress pile with transverse and longitudinal reinforcement to increase the flexural load carrying capacity. The seismic behavior of PHC pile to pile cap connection has been studied by Wang et al. (2014). The experimental results showed that the connections were damaged due to anchor bar yielding and formation of plastic hinge. Yang et al. (2016) have mentioned two main failure modes in the research on experimental and numerical investigation on PHC pile-pile cap connection. The first reason is tensile rupture of prestressed tendons and pile headings which causes loss of bearing capacity. The second reason is the formation of plastic hinge and yielding of anchor bar. The concrete crushes in the compression region can be improved by increasing lateral reinforcement (Nagae and Hayashi, 2003). But low amount of spiral reinforcement ratio results in poor confinement in spun pile concrete section and cannot resist the compression damage of concrete in pile (Irawan and Djameluddin, 2018). PHC piles failure pattern is sudden and violent with significant loss in lateral resistance (Wang et al., 2014). The residual stress on pile after test can affect the pile shaft and end resistance significantly (Chung et al., 2007). Xu and Ma (2017) has tested steel fiber reinforced PHC pile under low-reversed cyclic loading where all the piles failed in bending and mostly brittle failure happened due to the piles. In PHC pile the quantity of cracks are more than steel fiber reinforced PHC piles.

Huang et al. (2018) have conducted low-cycle pseudo static test to observe the seismic performance of PHC piles at different prestressing level. PHC 1, PHC 2, PHC 3 and PHC 4 piles have been prestressed with  $0$ ,  $0.25 \lambda$ ,  $0.5 \lambda$ ,  $0.57 \lambda$ , where  $\lambda =$  prestressing force. The test result has showed that the damages in the PHC piles ranges within  $4D-8D$  of embedded depth. Increased amount of prestressing can redistribute the internal forces of pile and crushing location as shown in Figure 2.10 (i). In case (d) the PHC-4 had three location of damage whereas the other piles have showed one location for damage. Huang has mentioned four stages for describing the mechanical behavior of pile i) elastic stage which considers the pile head displacement occurs below  $8-10$  mm. ii) elastic-plastic stage, where concrete cracks in tension side iii) plastic-hardening state, where concrete crushes in compression zone and pile stiffness starts to degrade iv) failure stage, in this state the bearing capacity of pile is affected and decreased suddenly. At failure stage the lateral load has decreased with increase in pile displacement and the pile-soil separation occurred as shown in Figure 2.10 (ii).

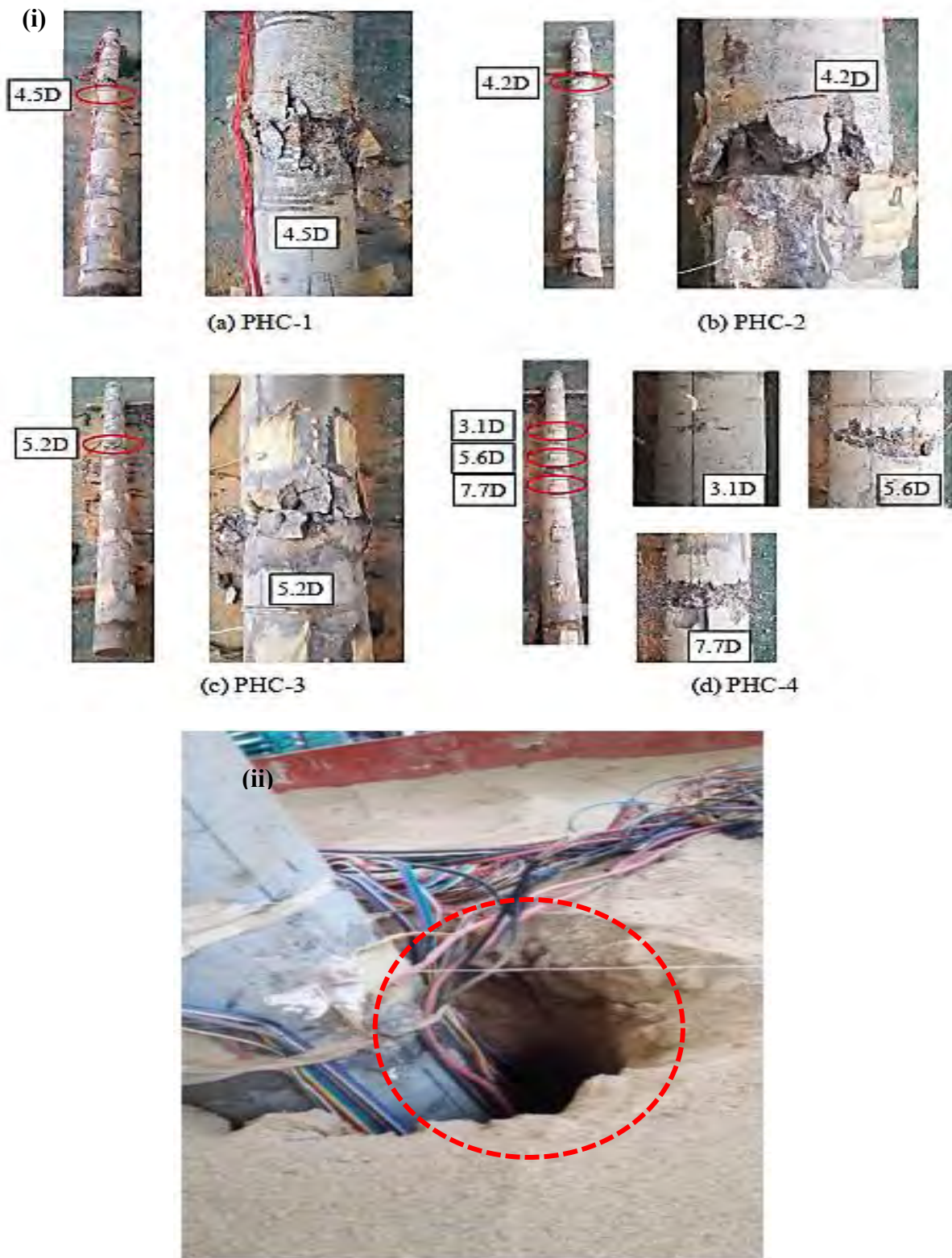


**Figure 2.10:** (i) Damages of the models after the tests. (ii) Pile soil separation. (After Huang et al., 2018)

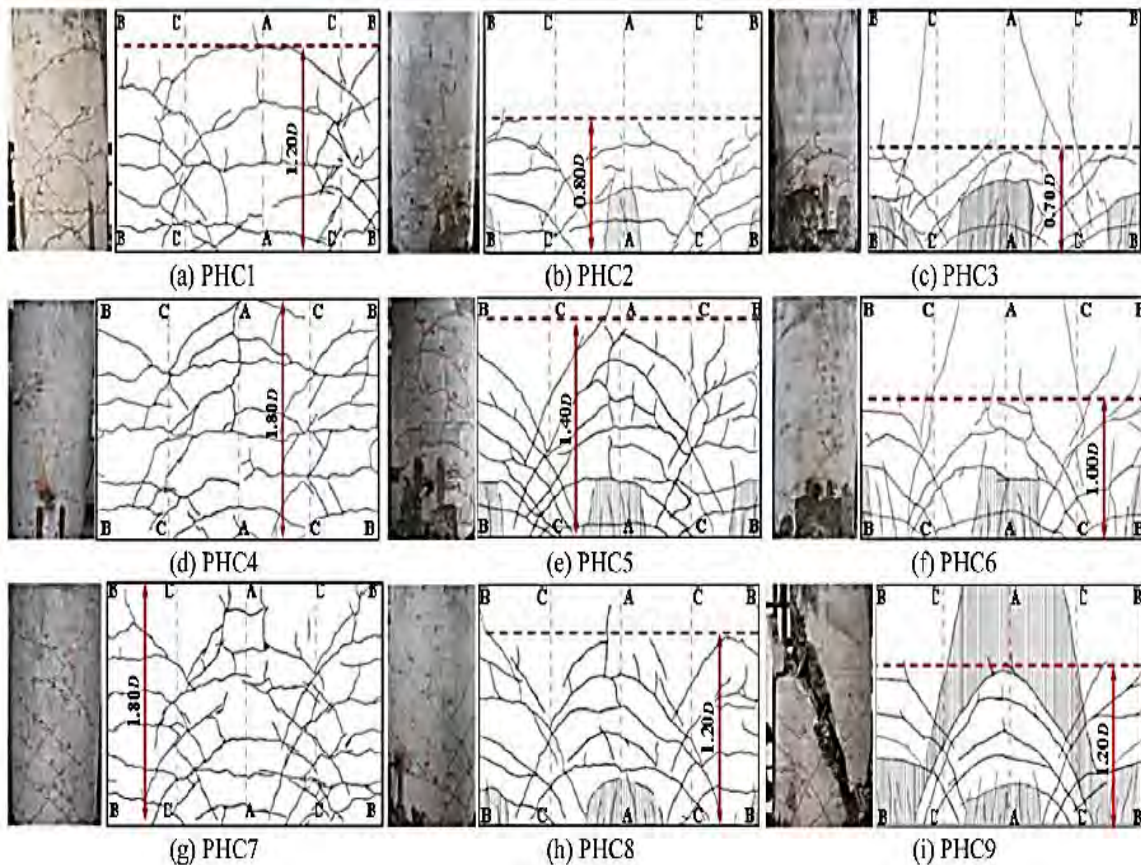


**Figure 2.11:** Failure modes of PHC piles. (After Xizhi et al., 2020)

Flexural crack first will develop in the root region of PHC pile as shown in Figure 2.11 as per Xizhi et al. (2020). With the increment of load the crack propagates along the height of the piles. After yielding, the cracks spread towards the sides of the piles. The two of failure modes have been observed in the study, one is flexural failure and other one is shear failure. As the normal strength bar increases the amount of flexural crack and height of cracks also increases. It have also been observed that if the amount of normal strength increases then the ductility of PHC pile decreases (Xizhi et al., 2020; Nagae and Hayashi, 2003). Pile failure under lateral loading may occur due to degradation of lateral bearing capacity or formation of plastic hinge shown in Figure 2.12 mode-1 and mode-2 respectively (Fatahi et al., 2014). Another reason may be the support condition at the pile head. Pile head can be fixed at position called fixed head pile and if there is no constraint then it is called free head pile. In mode-3 for fixed head pile two plastic hinge formation just below pile cap can cause pile failure. In free head pile structural failure formed a hinge below ground level.



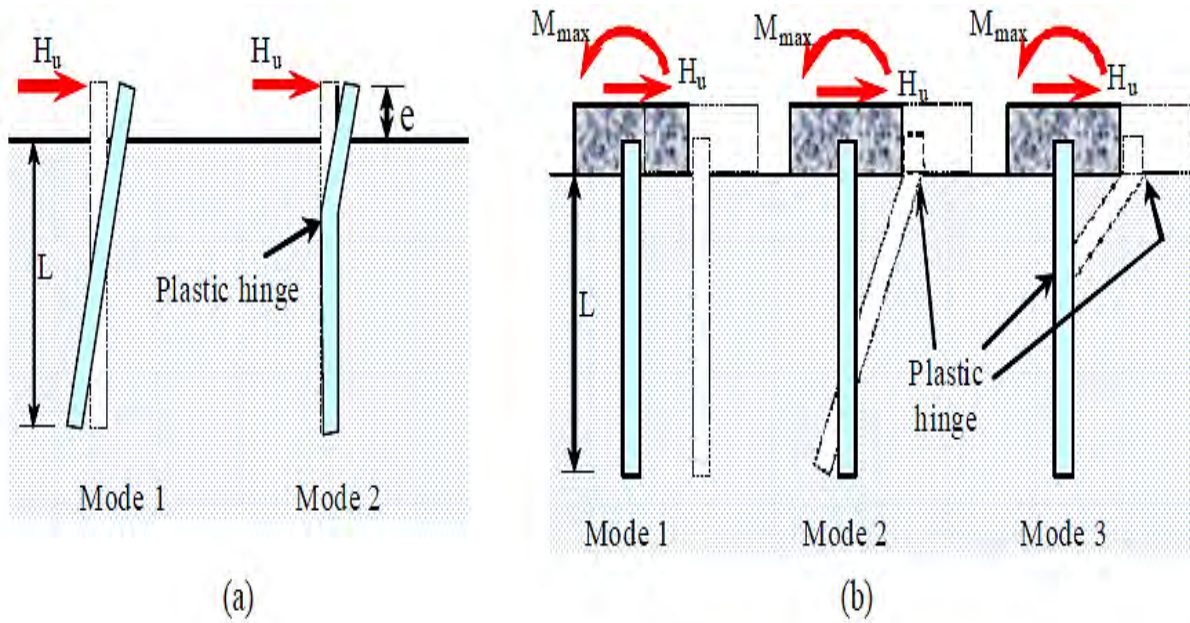


**Figure 2.12:** Modes of failures for piles under lateral loads: (a) free head piles (b) fixed head  
(After Poulos and Davis, 1980; Fatahi et al., 2014)

Setiawan et al. (2020) have found that in pile supported slab viaduct system, the PHC pile has showed two brittle plastic hinge location, see Figure 2.13.

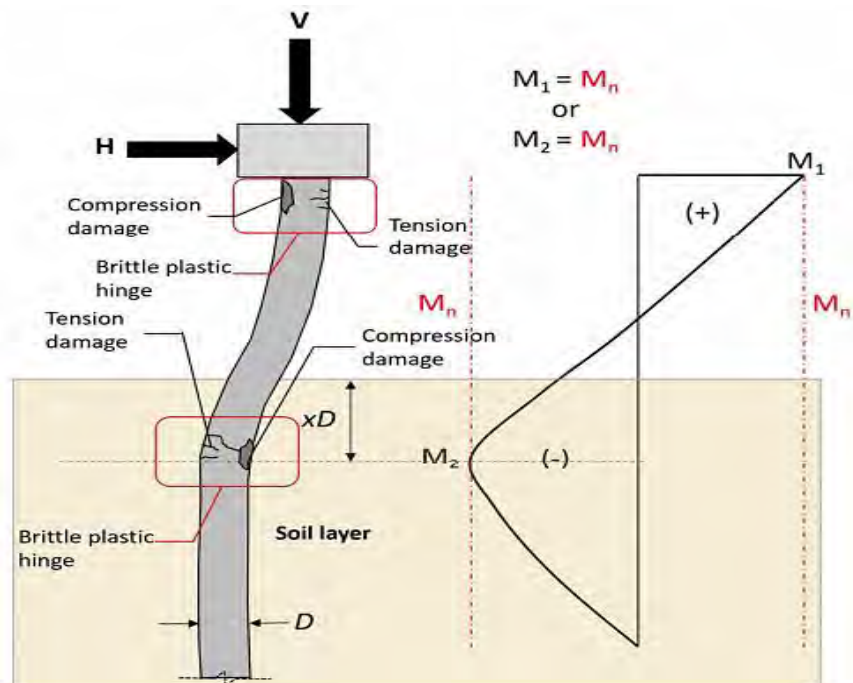


**Figure 2.13:** Brittle plastic hinge mechanism of hanging PHC pile (After Setiawan et al., 2020)

Huang et al. (2020) have found that the increased reinforcement ratio, pile depth and prestressing level can move the plastic hinge location of pile at deeper depth and improve soil-pile interaction. Also the crack resistance of reinforced pile has improved with increased reinforcement and prestressing level. A study conducted by Wu et al. (2020) has revealed that prestressed concrete piles reinforced with Basalt Fiber Reinforced Polymer (BFRP) hybrid bar has higher flexural capacity than steel bars. The failures in BFPR reinforced pile has been caused by gradual concrete crushing and in steel bar reinforced pile large crack width occurred.

The seismic behavior of precast prestressed pile in cast in situ reinforced concrete bent cap has been assessed by Sweigart (2010). The three piles of 18 inch diameter with 18 inch embedment have been tested to observe the moment capacity and displacement ductility of the connections. The two interior piles have showed better ductility than exterior pile and increase in embedment depth also resulted in sufficient ductility and moment bearing capacity. The concrete infilled pipe pile has showed more ductility and moment bearing capacity than unfilled one (Bingkang and Hai, 2007). From study of Li et al. (2015), it has been found that for a filled core pipe pile, adding non-prestressed reinforcing bar enhance the ductile and bearing capacity of pile. Similar phenomenon has been pointed out by Yang et al. (2018) that increase in reinforcement ratio of prestressed tendons and concrete infilling can improve ductility and bearing capacity. The PHC pile reinforced with steel fiber can improve the ductility and enhance the bearing capacity of the pile (Xu and Ma, 2017). The ductile performance of prestressed pile depends on soil pile system. The intrinsic connection type and axial load variation influences the ductile behavior of pile. By conducting cyclic loading test on PHC pipe piles Tao et al. (2017) have identified the influence of reinforcement ratio, embedded depth, axial compression ratio and shear strength on PHC pile in undrained soil. The obtained results have showed that the reinforcement ratio did not influence the displacement ductility but had influence on hysteretic energy dissipation. With the increase in buried depth and decreased axial compression ratio both the displacement ductility and energy dissipation capacity increased. The shear strength of soil have no influence on the displacement ductility and energy dissipation. The hysteretic curve found by (Xizhi et al., 2020) is almost linear with flexural crack that developed at the root zone of the pile under cyclic loading. Under axial and lateral loading the circular prestressed hollow pile has showed minimum energy dissipation capacity with thinner hysteretic curve (Budek and Priestley, 2005). PHC piles with longitudinal normal strength deformed bar has more stable hysteresis curve and dissipates more energy than without longitudinal normal strength deformed bars. The equivalent viscous damping increases with

the increase in prestressing level. With considering the pile-soil interaction, it is evident that the PHC pile has energy dissipation and plastic deformation capacity (Huang et al., 2018). Cao et al. (2020) have conducted experimental investigation to determine the seismic performance of PHC pile. Cao has found from the study that the Basalt Fiber Reinforced Polymer (BFRP) warped pile has showed larger bearing capacity. The PHC piles with steel bar and strands has showed better seismic performance by dissipating more energy resulting fatter hysteresis loop than other piles. It has been concluded that the reinforcement ratio and stirrup has no effect on improving bearing capacity of pile rather it can improve the ultimate bending moment capacity of pile.

### **2.3.2 Numerical Modeling**

A set of numerical investigation has been done by many researchers based on finite element method using software such as ANSYS (Xu and Ma, 2017), Opensees (Yang and Wang, 2016, Setiawan et al., 2020), ABAQUS (Zhang et al., 2019; Wang et al., 2014) etc. Wang et al. (2014) have observed the effect of different parameters on PHC pile in ABAQUS where the considerations are i) diameter of stirrup. ii) Spacing of stirrup. iii) Concrete strength. iv) effective prestressed stress. It has been identified from the analysis that increase in concrete strength and prestressed tendon improved the flexural strength and stiffness. In Opensees software behavior of PHC pile has been observed by implementing plastic hinge length using force based beam-column element by Setiawan et al. (2020). Xia et al. (2013) have simulated single PHC pile in ANSYS under different conditions such as pile effective area, wall thickness, bending moment, pile elastic modulus to investigate the effect on flexural strength. Zhou and Fang (2015) has simulated PHC pipe pile under static load test in FLAC 3D and the results have showed good agreement with load-displacement curve. Lin et al. (2016) have evaluated vertical bearing capacity of PHC-steel composite pile using FLAC 3D. The interface of composite pile and soil has been found to be feasible to model in FLAC 3D. The bearing capacity provided by PHC pile is higher than steel pipe. Increase in embedded pile cap depth can increase the horizontal bearing capacity of PHC pipe pile group (Bai et al., 2020). Spun pile foundation analysis and design in cohesion less soil for a sixteen storied building has been numerically studied by Kyi and Yangon (2019).

The pile has satisfied the allowable limits of deflection and settlement. Xu and Ma. (2017) has performed numerical modeling in ANSYS software by varying number of PHC pile in pile group under horizontal force. From the study it can be seen summarized that for free end pile

top, bending moment is zero at top but when the pile top is embedded end then bending moment at pile top is maximum. The non-prestressed bar have no influence on bending moment of pile. Mixing the reinforced pipe pile alongside the non-prestressed reinforcement can help to reduce the bending moment of pile body. Peak ground acceleration at free head pile top is more which results in a larger deflection and displacement in liquefiable soil (Rao et al., 2013). Teguh et al. (2005) has done numerical study on square prestressed concrete pile-to-pile connection under lateral loading and have found that if the shear strength of non-critical section can be reduced then joint performance of pile will be improved. Flexible foundation system can reduce columns ductility demand and reduce ultimate structural damage in earthquake event. Again head embedded pile can provide effective confinement to the joints and longer headed embedment can produce strong connection with fewer crack damage at the interface (Teguh et al., 2006). Prestressed pile in pile cap can resist moment considerably and it can be calculated by combining flexural capacity of pile and resistant of embedment (Xiao, 2003).

The numerical investigation on precast or prestressed pile to cast in situ pile cap connection has been performed by Fuziol (2009) and Ziehl et al. (2012). Guo et al. (2017) has performed both experimental and numerical investigation of prestressed concrete high-strength pile cap connection damage by considering common connection, strengthened connection and T-shaped steel connection. The numerical model of pile cap connection has been simulated in FEM software ABAQUS under lateral load and constant axial loading. The results have showed that all the failure in specimens were due to flexure. The common connection detailed specimen lost bearing capacity due to anchor bar yielding, cracking and spalling of pile cap. The other two specimens are damaged due to crack in pile cap and pile. The common connection pile cap has showed lower dissipation capacity than the other two specimens. The analysis has concluded that the pile cap with strengthened and T-shaped steel connection performed better in terms of strength and stiffness than common connection in earthquake event.

### **2.3.3 PHC Pile in Liquefiable Soil**

Possibility of soil liquefaction during earthquake has got less consideration in research. Especially the pile-soil interaction in soft soil needs to be taken care of while designing pile. Uzuoka et al. (2007) have performed numerical analysis to determine the dynamic response of group pile in reclaimed soil. The three dimensional analysis has been done considering soil-water coupled analysis. The result has showed that pile yielded before the complete liquefaction

has took place. Before complete liquefaction of the reclaimed layer, the inertial effect of superstructure has influenced the pile curvature at both head and bottom end. After completion of liquefaction the kinematic effect dominates the pile curvature at bottom of reclaimed layer. Dung et al. (2011) have compared the applicability of SPT based method to determine toe bearing capacity of PHC pile with the CPT, pile driven test and field load test results and observed that SPT based method was less reliable. Shafieezadeh et al. (2012) have observed the seismic performance of battered prestressed concrete pile-supported wharf structure in liquefied soil numerically. Both gravity and lateral load condition have been simulated and the pile is found to be severely damaged. The observed damage location are the pile sections near the interface between loose and dense sand layers, pile sections close to the surface of the embankment and pile-deck connections. Huang et al. (2017) have introduced dynamic response of PHC pipe piles in liquefiable soil by performing shake-table test. Two types of typical earthquake Chi-Chi and El-Centro with an artificial wave have been selected as input excitation for the test. The results have showed larger peak displacement of pile for saturated soil rather than unsaturated soil. With larger peak acceleration, pore water pressure increases to maximum. An overlaying clay layer can help to decrease the pore pressure slowly and lessen the chance of liquefaction. The soil condition greatly influence the damage response of pile but prestressed pile can resist the damage well. Wen (2016) has performed shake table test of PHC pipe piles in saturated soil and looked for the failure modes of piles considering pile-soil interaction. Kim et al. (2017) have found that extended end pile can increase bearing capacity up-to 24% compared to PHC pile. Dissipation of pore water pressure at the pile-soil interface can influence the shear strength of soil and bearing capacity of PHC pile (Wang et al., 2020). Zhou et al. (2019) have determined the uplift bearing capacity of PHC pile in clayey soil and also in the soil treated with cement paste by conducting field test. It has been observed that the uplift bearing capacity of PHC pile in cemented soil has increased.

The ultimate skin friction for PHC pile-cemented soil interface is much higher compared to cement soil-soil interface. Wei et al. (2020) have determined the ultimate bearing capacity of PHC pile using three methods JGJ94-2008 method, Meyerhof method and Schmertmann method from SPT blow count in saturated sandy layer. It has been found that the results from static load test, SPT and CPT values are in good agreement. But static load test is required for accurate measure of bearing capacity in soil stratum.

## 2.4 Shear Wave and Shear Modulus Estimation

Standard Penetration Test (SPT) is the most common in-situ geotechnical test which is effective to use for determining soil properties. So, different researchers tried to correlate  $V_s$  in terms of various soil indexes including depth, soil type and SPT-N value. A large number of studies has been found showing the relationship between  $V_s$  and soil geotechnical parameters such as standard penetration resistance. Some studies considering soil types (gravel, sand, silt or clay) and some other studies considering depth, fine content of soil and corrected or uncorrected standard penetration resistance. In almost all relationships have used the functional form as shown in equation 2.1 for shear wave velocity and equation 2.2 for shear modulus.

$$V_s = A * N^B \quad (2.1)$$

Here  $V_s$  is shear wave velocity (m/s);  $N$  is SPT value;  $A$  and  $B$  are constant parameters accompanied by correlation coefficient  $R$ .

$$G_{\max} = \rho V_s^2 \quad (2.2)$$

Here  $G_{\max}$  is shear modulus;  $\rho$  is soil mass density;  $V_s$  is shear wave velocity (m/s).

Different researchers, (Ansary et al., 2010; Hasancebi and Ulusay, 2007; Imai, 1977; JRA, 1980; Lee, 1992; Ohba and Toriuma, 1970; Ohta and Goto, 1978; Seed and Idriss, 1981) have proposed a relation between SPT  $N$  value and shear wave velocity are presented in Table 2.1. The equations are categorized for all types of soils and also, for cohesive and cohesionless soil.

**Table 2.1:** Proposed empirical relationships between uncorrected SPT-N and shear wave velocity

Proposed by	All Soils	Cohesionless	Cohesive
Ohba and Toriuma (1970)	$V_s = 85.34 N^{0.31}$	-	-
Imai (1977)	$V_s = 91 N^{0.337}$	$V_s = 80.6 N^{0.331}$	$V_s = 80.2 N^{0.292}$
Ohta and Goto (1978)	$V_s = 85.35 N^{0.348}$	-	-
Seed and Idriss (1981)	$V_s = 61 N^{0.5}$	-	-
Lee (1992)	$V_s = 76.2 N^{0.24}$	-	$V_s = 138.4 (N+1)^{0.242}$
Hasancebi and Ulusay (2007)	$V_s = 90 N^{0.309}$	$V_s = 90.82 N^{0.319}$	$V_s = 97.89 N^{0.269}$
Japanese Highway Bridge Design Code (1980)	-	$V_s = 80 N^{0.33}$	$V_s = 100 N^{0.33}$
Ansary et al.(2010)	-	$V_s = 84.16 N^{0.34}$	$V_s = 109.92 N^{0.28}$

## 2.5 Liquefaction Susceptibility Analysis

In 1971 Seed and Idriss (1971) has developed a procedure of determining liquefaction potential using SPT N values where a factor of safety ratio was defined.  $FS = \text{Cyclic resistance of soil} / \text{Cyclic stress}$ . If FS value falls below one for a soil layer then there is chance of liquefaction. Researchers (Youd and Idriss, 2001; Tokimatsu and Yoshimi, 1983; Idriss and Boulanger, 2006) have studied liquefaction analysis process following seed and Idriss method and formulated different other methods to determine factor of safety. An updated procedure of Seed and Idriss proposed by (Idriss and Boulanger, 2006) is used in this study. The adopted method is briefly described below.

$$FS = CRR / CSR \quad (2.3)$$

Here CRR = Cyclic Resistance Ratio, CSR = Cyclic Stress Ratio.

The cyclic resistance ratio is calculated by equation 2.4 after Idriss and Boulanger

$$CSR = 0.65 \frac{a_{max}}{g} \frac{\sigma_0}{\sigma'_0} r_d \quad (2.4)$$

Here,  $a_{max}$  is peak surface acceleration,  $\sigma_0$  is total overburden pressure,  $\sigma'_0$  is effective overburden pressure, g is acceleration due to gravity,  $r_d$  is stress reduction factor depending on z which is the depth from ground surface in meter.

For 7.5 magnitude earthquake the CSR can be written by equation 2.5

$$CSR_{7.5} = \frac{CSR}{MSF} \quad (2.5)$$

MSF = Magnitude scaling factor, The MSF can vary according to earthquake magnitude. MSF can be modified by equation 2.6 with respect to magnitude (M)

$$MSF = 6.9e \left( -\frac{M}{4} \right) - 0.058 \leq 1.8 \quad \text{for } M > 5.2 \quad (2.6)$$

$$MSF = 1.8 \quad \text{for } M < 5.2$$

For calculating cyclic resistance ration SPT N value is obtained and N values needs to be corrected for overburden pressure, rod length, hammer efficiency, borehole diameter and sampler lining. After the corrected  $N_{60}$  value the clean sand correction was done by equation 2.7.

$$(N_1)_{60CS} = (N_1)_{60} + \Delta (N_1)_{60} \quad (2.7)$$

$$\Delta (N_1)_{60} = \exp\left(1.63 + \frac{9.7}{(FC+0.1)} - \left(\frac{15.7}{(FC+0.1)}\right)^2\right) \quad (2.8)$$

FC = Fine content of corresponding layer

The value of CRR was determined from the curve of SPT blow count to CRR ratio corresponding to fine content after (Bolton Seed et al. 1985). The following equation 2.9 modified after Idriss and Boulanger approximates this curve and can also be used to calculate the CRR<sub>M=7.5</sub> for a given (N1)<sub>60cs</sub>

$$CRR = \exp\left[\frac{(N_1)_{60cs}}{14.1} + \left(\frac{(N_1)_{60cs}}{126}\right)^2 - \left(\frac{(N_1)_{60cs}}{23.6}\right)^3 + \left(\frac{(N_1)_{60cs}}{25.4}\right)^4 - 2.8\right] \quad (2.9)$$

## 2.6 Bearing Capacity Determination of Pile

In this section pile bearing capacity determination procedure from both analytical method and field test has been discussed.

### 2.6.1 Bearing Capacity Determination by Analytical Procedure

For determining the driven pile bearing capacity Meyerhof (1976) equation is used widely. This method is based on N-values obtained from Standard Penetration Test (SPT). This method has been described in Indian Standard IS 2911 and BNBC 2020. The correlation suggested by Meyerhof using standard penetration resistance, N in saturated cohesionless soil to estimate the ultimate load capacity of driven pile is given below. The ultimate load capacity of pile ( $Q_u$ ), in kN, is given in equation 2.10.

$$Q_u = 40N \frac{L_b}{D} A_p + \frac{\bar{N}}{0.5} A_s \quad (2.10)$$

Where,

N = Average N value at the pile tip;

$L_b$  = Length of penetration of pile in the bearing strata, in m;

D = Diameter or minimum width of pile shaft, in m;

$A_p$  = Cross-sectional area of pile tip, in  $m^2$ ;

$\bar{N}$  = Average N along the pile shaft; and



$A_p$  = Surface area of pile shaft, in  $m^2$ .

The end-bearing resistance should not exceed  $400 NA_p$

For non-plastic silt or very fine sand the equation has been modified as given in equation 2.11.

$$Q_u = 30N \frac{L_b}{D} A_p + \frac{\bar{N} A_s}{0.60} \quad (2.11)$$

## 2.6.2 Bearing Capacity Determination from Static Pile Load Test

For determining bearing capacity, in-situ test is a reliable procedure. In Bangladesh this is a well adopted technique to find pile bearing capacity in construction site. Ansary et al. (2001) discussed on the status of pile load test in Bangladesh. In this study pile load test has been done in site and capacity has been determined using BNBC (2020). According to BNBC (2020), the recommended various criteria used for evaluating the ultimate and allowable load carrying capacity of piles and drilled shaft/bored cast in situ piles are summarized below.

- a. Terzaghi (1942) reported that the ultimate load capacity of a pile may be considered as that load which causes a settlement equal to 10% of the pile diameter.
- b. The allowable load capacity of pile should be 50% of the final load, which causes the pile to settle a depth of 10% of pile width or diameter (BS 8004).
- c. Ultimate load capacity of pile is smaller of the following two criteria (IS:2911 Part-4):
  - (i) Load corresponding to a settlement equal to 10% of the pile diameter in the case of normal uniform diameter pile or 7.5% of base diameter in case of under-reamed or large diameter cast in-situ pile.
  - (ii) Load corresponding to a settlement of 12 mm.
- d. Allowable load capacity of pile is smaller of the following (IS: 2911 Part-4):
  - (i) Two thirds of the final load at which the total settlement attains a value of 12 mm.
  - (ii) Half of the final load at which total settlement equal to 10% of the pile diameter in the case of normal uniform diameter pile or 7.5% of base diameter in case of under-reamed pile.

- e. A very useful method of computing the ultimate failure load has been reported by Davisson (1973). This method is based on offset method that defines the failure load. The elastic shortening of the pile, considered as point bearing, free standing column, is computed and plotted on the load-settlement curve, with the elastic shortening line passing through the origin. The slope of the elastic shortening line is  $20^\circ$ . An offset line is drawn parallel to the elastic line. The offset is usually 0.15 inch plus a quake factor, which is a function of pile tip diameter. For normal size piles, this factor is usually taken as 0.1D inch, where D is the diameter of pile in foot. The intersection of offset line with gross load-settlement curve determines the arbitrary ultimate failure load. This method is recommended for driven precast piles.
- f. Butler and Hoy (1977) states that the intersection of tangent at initial straight portion of the load-settlement curve and the tangent at a slope point of 1.27 mm/ton determines the arbitrary ultimate failure load.
- g. The Brinch Hansen (1963) proposed a definition for ultimate load capacity as that load for which the settlement is twice the settlement under 90 percent of the full test load.
- h. Where failure occurs, the ultimate load may be taken to calculate the allowable load using a factor of safety of 2.0 to 2.5

Again there is popular Tangent method used in this study to determine ultimate pile capacity. In Tangent method, the ultimate bearing capacity of piles can be determined by drawing first tangent lines to the starting and ending portions of the load-settlement curves; the intersection point of these two tangents is assumed to represent the ultimate bearing capacity of pile.

## **2.7 FEM Analysis: PLAXIS 3D**

In PLAXIS 3D foundation analysis can either be modelled by an embedded pile or by a volume pile, which is a volume with the material properties of a certain pile type. In this part the material models and embedded beam modelling, which are used in this thesis, are elaborated.

### 2.7.1 Hardening Soil (HS Model)

For modelling the soil behavior in this study, the Hardening Soil small strain is applied. For liquefaction potential analysis UBC-3D PLM model is considered. A description of these models are provided below.

This HS-model is an improvement of the MC-model and can be used for more accurate predictions of displacements and failure for static types of geotechnical problems both in soft as in stiffer soils. The hardening soil model supersedes the hyperbolic model by using theory of plasticity rather than the theory of elasticity, by including soil dilatancy and yield cap. The Mohr-Coulomb failure surface in combination with a “yield” cap is used in this model as shown in Figure 2.14. The advantage of the Hardening soil model over the Mohr-Coulomb model is not only that the Hardening soil model considers a hyperbolic stress-strain curve instead of a bi-linear curve, but also it controls the stress-dependency level.

In the Mohr-Coulomb model, the user selects a fixed value of Young’s modulus but for real soil behavior the stiffness depends on the stress level. It is necessary to estimate the stress levels within the soil and use these to obtain required values. As a result of plastic straining, the yield surface will expand, which is called hardening. In this model, two types of hardening can be distinguished: compression and shear hardening. With both compression and shear hardening, the elastic region is enlarged.

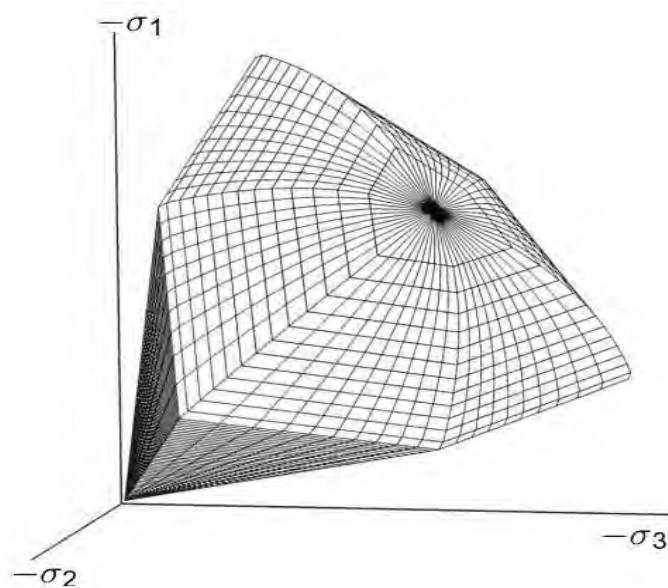


**Figure 2.14:** HS yield surface with cap presented in principal stress space (After PLAXIS manual, 2016)

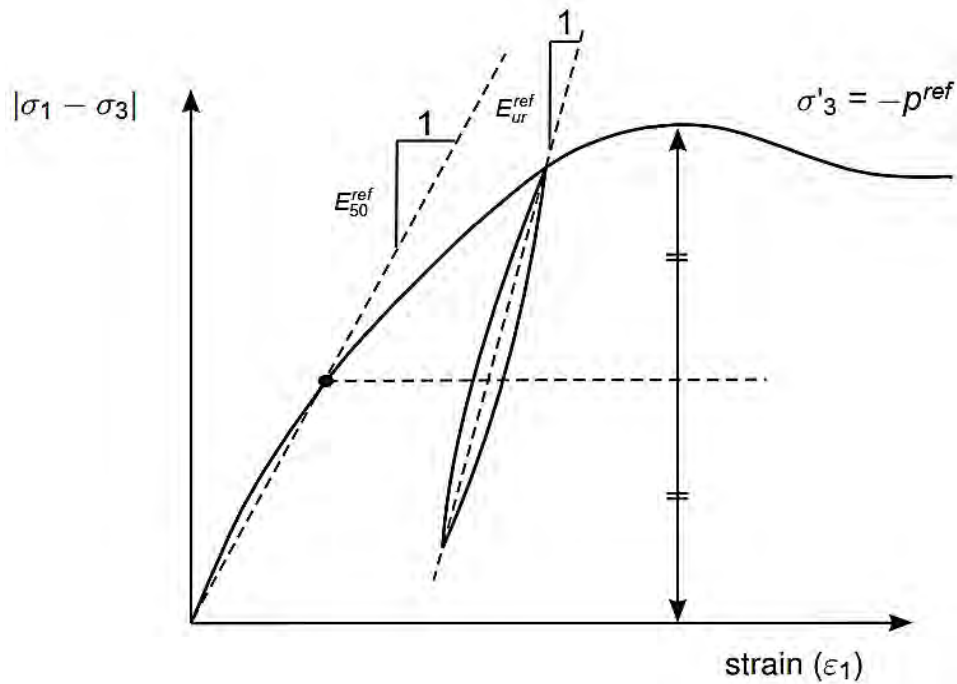


**Figure 2.15:** Definition of  $E_{50}^{ref}$  and  $E_{ur}^{ref}$  for drained triaxial test results (After PLAXIS manual, 2016)

A stiffness modulus  $E_{50}^{ref}$  is defined for a reference of minor principle effective stress of  $-\sigma_3' = P^{ref}$ , see Figure 2.15. It is secant stiffness at 50% of maximum deviatoric stress at cell pressure equal to  $P^{ref}$ .  $E_{ur}^{ref}$  is the unloading/reloading stiffness that can be determined also from shear modulus. Inside the yield contour the material governs elastic behavior, where the stiffness is defined by  $E_{ur}^{ref}$ . The key features of Hardening soil model in PLAXIS are

- i. Stress dependent stiffness
- ii. Shear hardening: plastic strain due to primary deviatoric-loading
- iii. Independent behaviour for unloading/reloading
- iv. Mohr-Coulomb failure surface with cap
- v. Taking loading history into account
- vi. Compression hardening: plastic strain due to primary compression

### 2.7.2 UBC-3D PLM Model

The UBC3D-PLM model is an effective stress elasto-plastic model which is capable of simulating the liquefaction behavior of sand and silty sand under seismic loading. The UBC3D-PLM model formulation is based on original UBCSAND (University of British Columbia

Sand) model introduced by Puebla et al. (1997) and Beaty and Byrne (1998). The UBCSAND model contains a 2D Mohr-Coulomb yield surface and a corresponding non-associated potential function. The main difference between the UBCSAND model and the UBC3D-PLM model is generalized 3D formulation. The UBC3D-PLM model uses the Mohr-Coulomb yield condition in 3D principle stress space for primary loading. A potential function based on Drucker-Prager's criterion is used for the primary yield surface. The UBC3D-PLM model incorporates a non-linear, isotropic law for the elastic behavior that is defined in terms of elastic bulk modulus  $K$  and elastic shear modulus  $G$ . Here these two parameters are defined by the equation 2.12 and 2.13.

$$K = k_B^{*e} P^{ref} \left( \frac{p'}{P^{ref}} \right)^{me} \quad (2.12)$$

$$G = k_G^{*e} P^{ref} \left( \frac{p'}{P^{ref}} \right)^{ne} \quad (2.13)$$

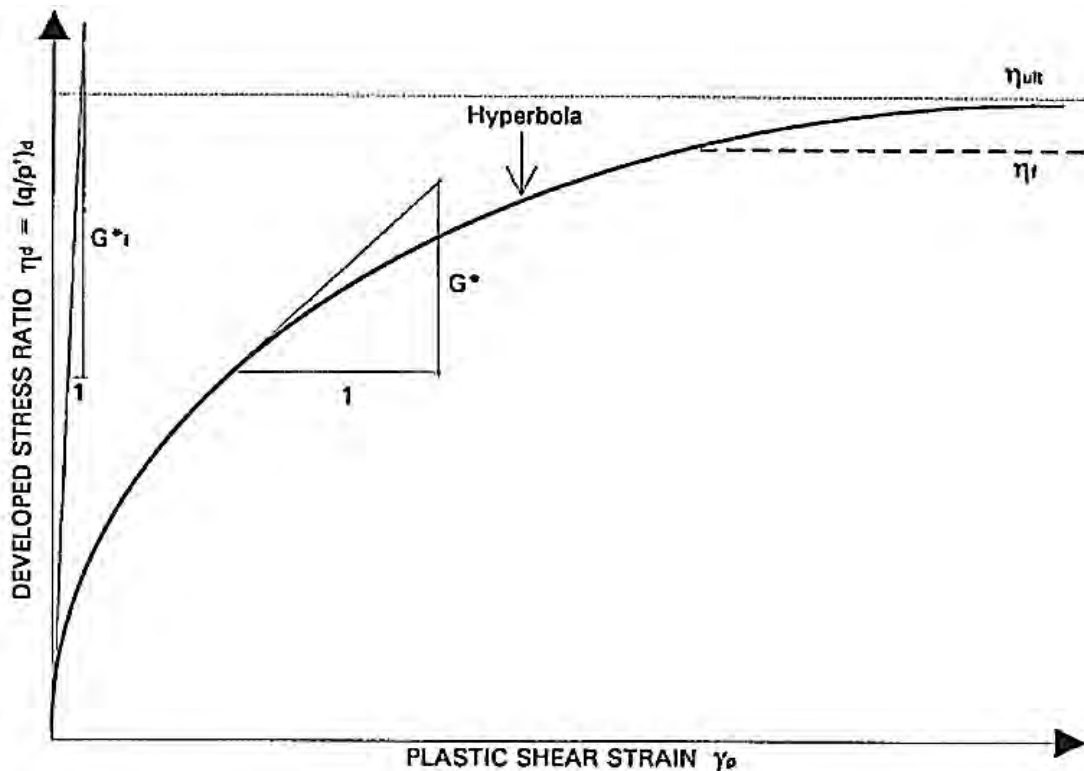


**Figure 2.16:** Original UBCSAND hardening rule (After PLAXIS manual, 2016)

$k_B^{*e}$  and  $k_G^{*e}$  are input parameters of the UBC3D-PLM model and represent the bulk and shear modulus factors respectively.  $P^{ref}$  is reference pressure. The factors **me** and **ne** are parameters that define the rate of stress dependency of stiffness. Once the stress state reaches the yield surface, plastic behavior is taken into account as long as the stress point is not going

immediately back into the elastic zone. The first yield surface is defined from a set of Mohr-Coulomb functions. The position and size of the yield surface is defined based on the hardening law. Plastic hardening based on the principle of strain hardening is used in the model similar to the Hardening Soil model. The hyperbolic hardening rule is presented in Figure 2.16. The hardening rule for UBC3D-PLM model is presented by equation 2.14.

$$d\sin\varphi_{mob} = 1.5 k_G^{*p} \left( \frac{P'}{P^{ref}} \right)^{np} \frac{P^{ref}}{P'} \left( 1 - \frac{\sin\varphi_{mob}}{\sin\varphi_p} R_f \right) 2 d\lambda \quad (2.14)$$

Here,  $k_G^{*p}$  is plastic shear modulus;  $np$  is plastic shear modulus exponent;  $\varphi_{mob}$  is mobilized friction angle;  $R_f$  is failure ratio ranging from 0.5-1.0;  $d\lambda$  is plastic strain increment multiplier.

This model employs two yield surfaces for smooth transition into liquefied state of the soil and enable the distinction between primary and secondary loading. A rule of stress reversals of loading to unloading and vice versa is used to define to count the cycles. This tends to increase the excess pore pressure during undrained cyclic loading with decreasing rate until liquefied state is approached.

### 2.7.3 PLAXIS Embedded Beam (Rows)

The embedded beam (row) is a function within PLAXIS, which implements a beam that can cross soil volume elements at any arbitrary location and orientation. This beam is connected to the surrounding soil by means of special interfaces, which describe the skin and foot resistance. Although this beam does not occupy a volume, a particular volume around the pile (elastic zone) is assumed in which plastic soil behavior is neglected. The size of this zone is based on the input of the (equivalent) pile diameters. The embedded beam almost behaves as a volume pile, because of this zone. But on the contrary to volume piles, the embedded beam does not influence the finite element mesh as generated from the geometry model. The mesh refinements are therefore lower and save calculation time. However, the installation effects of the pile are not included into the embedded beam. In PLAXIS 3D the embedded beam or pile is available. The beam elements can be linear elastic or elastoplastic.

The special interfaces of the embedded beams model the soil-structure interaction. The interaction between the soil and shaft is modelled by means of line-to-volume interface elements, the interaction between soil and base by point-to-volume interface elements. These interface elements determine the strength and stiffness of this interaction. An elasto-plastic

model is used to describe the behavior of the special interfaces. The interface is divided into skin resistance (in unit of force per circumference per length) and tip resistance (in unit of force). These two resistances provide the bearing capacity of the pile in axial direction, which is an input parameter in PLAXIS. The material parameters of embedded beam distinguish between the parameters of beam and the parameters of skin resistance and foot resistance.

## 2.8 Summary

This chapter focuses on the previous studies by different researchers on the importance of using analyzing pile foundation in liquefiable soil during earthquake and performance of prestressed concrete piles in liquefiable soil in seismic excitation. Significance of performing both the experimental and numerical investigations are described by scholars are summarized here.

1. (Elgamal et al., 2006; Xu et al., 2020; Cubrinovski et al., 2006; Motamed et al., 2010; He et al., 2006; Towhata et al., 2006; Ashford et al., 2006; Abdoun and Dobry, 2002; Bhattacharya et al., 2004; Tamura and Tokimatsu, 2006; Han et al., 2007; Hokmabadi et al., 2015; Maheshwari et al., 2004) have conducted experimental test to determine the precast pile response in liquefiable soil. It has been found that end bearing pile can cause more lateral displacement than precast pile under dynamic loading. In liquefiable layer pile can show larger stiffness degradation and higher bending moment generation than non-liquefiable soil.
2. (Phanikanth et al., 2013; Asaadi and Sharifipour, 2015; Rostami et al., 2017) have done numerical investigations to predict pile behavior in liquefied soil. The results have shown that soil liquefaction potential decreases with increased depth and reclaimed soils are more susceptible to liquefaction. Use of driven pile can increase density of liquefiable soil up-to 4.4% - 4.8%. Increase in pile length has no effect on reducing bending moment but plastic hinge location can be influenced by pile diameter, ductility and soil condition.
3. (Xizhi et al., 2020; Budek and Priestley, 2005; Xu and Ma, 2017; Zhang et al., 2019; Joen and Park, 1990; Wang et al., 2014, 2015; Yang and Wang 2016; Kokusho et al., 1987; Zhang et al., 2011; Gao, 2012) have done experimental investigation to observe the performance of PHC pile. PHC pile can encounter concrete cover spalling but the ductile behavior of the pile is found to be satisfactory. Increased amount of prestressing

and concrete filling in hollow part can increase flexural capacity of the pile. The reinforcement ratio and stirrup can improve the ultimate bending moment capacity of pile.

4. (Uzuoka et al., 2007; Huang et al., 2017; Wang et al., 2020; Zhou et al., 2019) have studied the PHC pile response in liquefiable soil. PHC pile yield before the complete liquefaction takes place in reclaimed soil. Static pile load test is an accurate method to determine bearing capacity of PHC pile in saturated sandy soil (Wei et al., 2020).
5. Numerical modeling is a reliable way to determine the dynamic response of pile in liquefiable soil during earthquake excitation. PLAXIS 3D is a finite element software where liquefaction analysis can be done using UBC3D-PLM soil modeling. Pile can be modelled using embedded beam row or volume pile. For earthquake analysis HS model shows more accuracy than MC model.
6. Prestressed concrete pile is widely used in reclaimed soil due to its cost effectiveness and load carrying capacity. A large number of numerical and experimental investigations have been conducted on SPC pile. It is a recently introduced in Bangladesh for using in reclaimed areas for its numerous advantages and economic purposes. But still there is lacking in finite element investigations of SPC piles under earthquake loading. This study focuses on the analysis of static and dynamic analysis of SPC pile in reclaimed area of Jolshiri site using PLAXIS 3D.



## CHAPTER 3

### FIELD DATA COLLECTION AND BEARING CAPACITY ANALYSIS

#### 3.1 Introduction

In this present study, the Jolshiri Abashon project area has been selected which is a reclaimed land located at the center of the eastern side of the DMDP area, Dhaka, Bangladesh. Jolshiri Abashon is 1.3 km from the south side of Purbachal's new town and it is surrounded by the Balu River on the west and the Shitalakkhya River on the east. Figure 3.1 shows the site location.

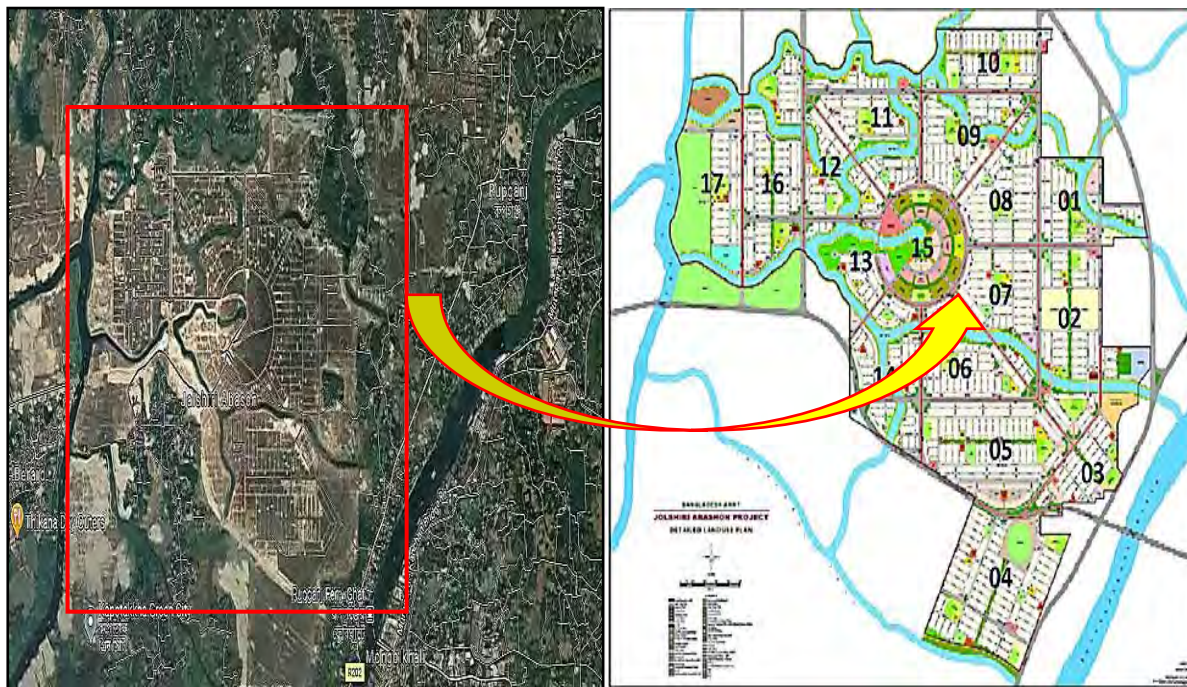


**Figure 3.1:** Jolshiri Abashon area

Primarily, at this site the subsoil investigation has been carried out and required soil properties are determined in the laboratory. A pile load test has also been conducted on a SPC pile in Jolshiri area for determining in-situ vertical bearing capacity. The results are verified with different existing empirical methods to estimate the bearing capacity.

### 3.2 Geometry of SPC Pile

Hollow prestressed precast reinforced concrete piles are termed as spun prestressed concrete (SPC) pile. SPC pile's geometry is commonly used in electric poles and they can be fabricated at the same factory. The concept of using spun pile as the foundation of soft soil particularly in the coastal zone has gained popularity for the last two decades mainly due to its easier installation, low cost, higher bearing capacity and easier insurance of material quality before pile casting. The hollow circular geometry of the SPC pile used in this study is shown in Figure 3.2 (a), the fabricated SPC pile and the long section of the pile with reinforcement are shown in Figure 3.2 (b), and Figure 3.2 (c), respectively. The SPC piles are fabricated through a special arrangement of caging, prestressing followed by the procedure of concrete pouring, rotating, steam curing etc. The aggregate size is usually 12mm and downgrade and ordinary portland cements (OPC) are used in the construction of SPC piles. PCC cements are also used in some construction. Relatively, high strength concrete (a concrete strength 50 MPa and above) and high strength strands (a nominal strength of 1860 MPa) are used for SPC pile casting. A prestress of 50 MPa is used in these piles to enhance the bending capacity that can ensure the piles to sustain lifting and handling stress. The basic features of the used SPC piles in this study are presented in Table 3.1.

Generally, the bearing capacity of the SPC pile is governed by the structural capacity of the pile. The length of the pile is designed based on the ability to penetrate through the soil. Subsequently, the lateral capacity of the pile is also designed as per the requirement of the site condition. The cross-sectional area of the SPC piles are low therefore shear reinforcement plays a key role against shear forces generated from seismic excitation. The allowable vertical capacity of SPC piles may be given by the API guideline as shown in equation 3.1 (Piling.2019).

$$P_a = A_g(0.33 f'_c - 0.27f_{pc}) \quad (3.1)$$

Where

$P_a$ , the allowable service level axial load bearing capacity of SPC pile

$A_g$ , gross cross-sectional area of pile

$f'_c$ , compressive strength of concrete at 28 days

$f_{pc}$  = effective prestress in the pile

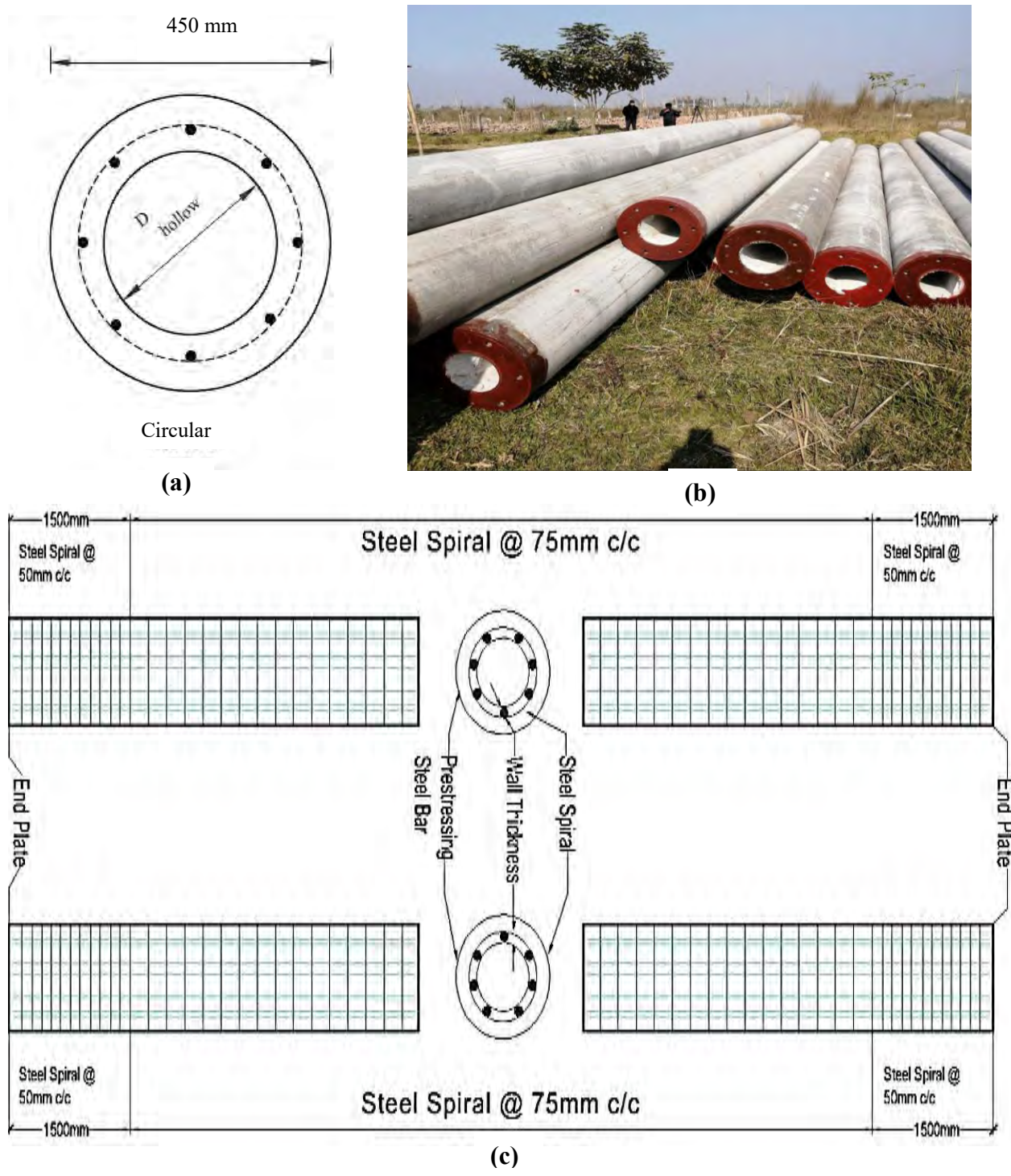


**Figure 3.2:** Geometry of SPC pile: (a) Circular hollow cross section; (b) SPC pile ready for transportation; (c) Long section of SPC piles showing the spiral reinforcement details.

**Table 3.1:** Properties of SPC pile used in this study

SI	Description	Properties (Unit)
1.	Diameter	450 mm
2.	Length	12 m / 9 m / 6 m
3.	Cement used	OPC/PCC
4.	Concrete Mix Ratio FM of Sand Max Agg Size	1:1.25:2.5 2.5 FM (4-8) mm and (12 to 16) mm
5.	Wall Thickness	110 mm
6.	Material Spec: Concrete Strength Strands: 9mm dia 4mm MS wire ultimate load	7 Nos (pre-stressed) 50 MPa 1860 MPa 440 MPa
7.	4mm MS wire @50mm c/c 4mm MS wire @75C/C	At top and bottom 1.5 m At the middle
8.	Design Compressive Load (12m)	2500 kN
9.	Bending Strength	180 kN-m

### 3.3 Laboratory Test Results

To obtain the soil stratification of the selected site, subsoil investigation has been carried out. Three boreholes have been conducted within a residential building site. Each boring is associated with a Standard Penetration Test (SPT) and collection of disturbed and undisturbed samples from different depths of the boreholes. Figure 3.3 (a, b) shows the schematic diagram of borehole location for Standard Penetration Test (SPT). Figure 3.4 also shows the different soil stratum which are obtained from the subsoil investigation. In Figure 3.5, three boreholes are presented with respect to SPT blow count at different depths. As can be seen from the Figure, the top layer of the soil (up to 4.5 m depth) is consisting of very loose sand with an SPT value below 11. All three boreholes confirmed that there is a 33 m thick soft clayey sandy silt.



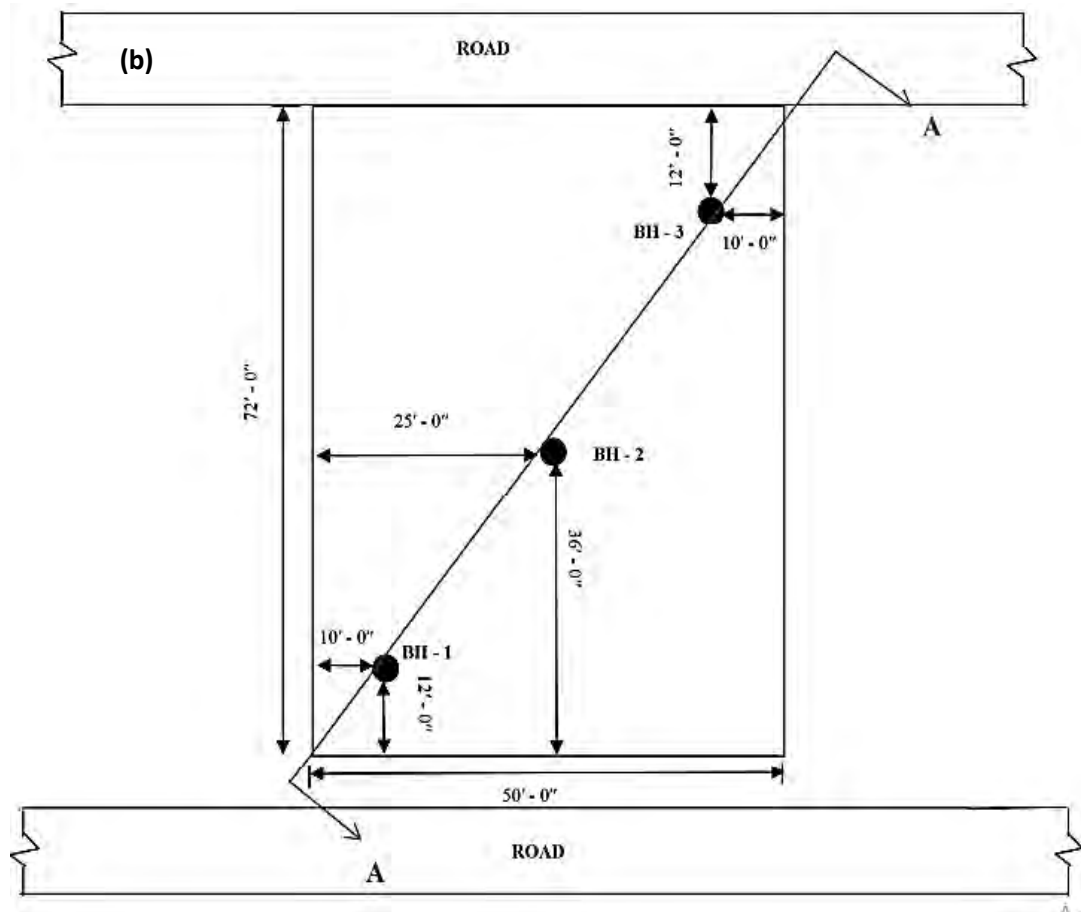
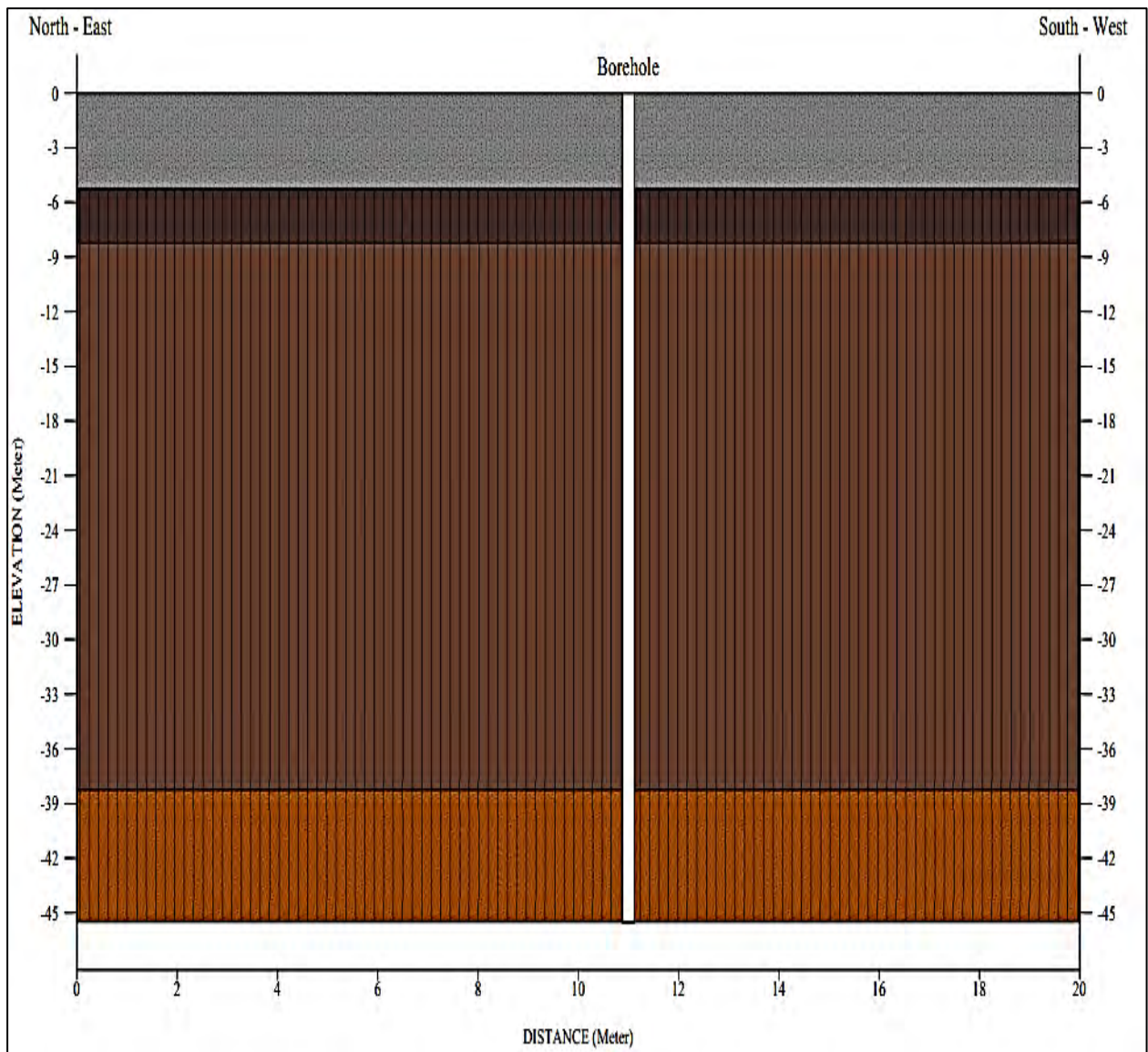


**Figure 3.3:** a) Standard Penetration Test (SPT) b) Borehole Location



### LEGEND



**Figure 3.4:** Borehole cross-sections

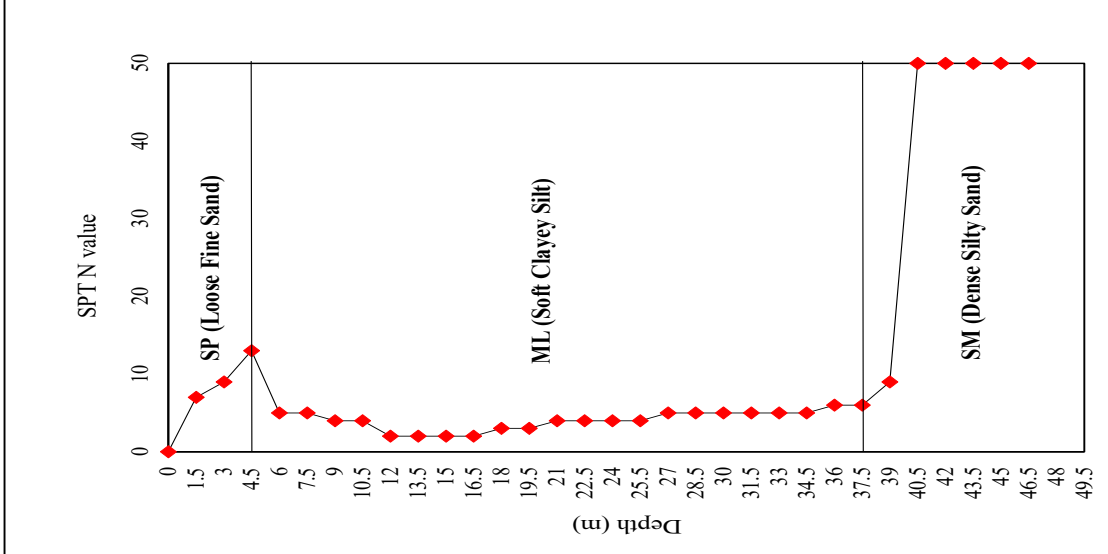
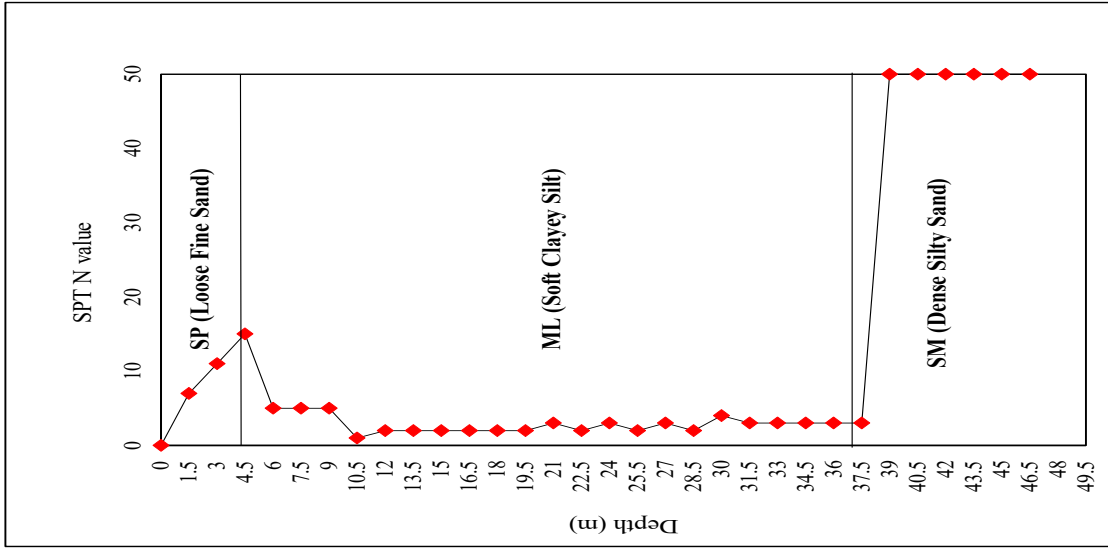
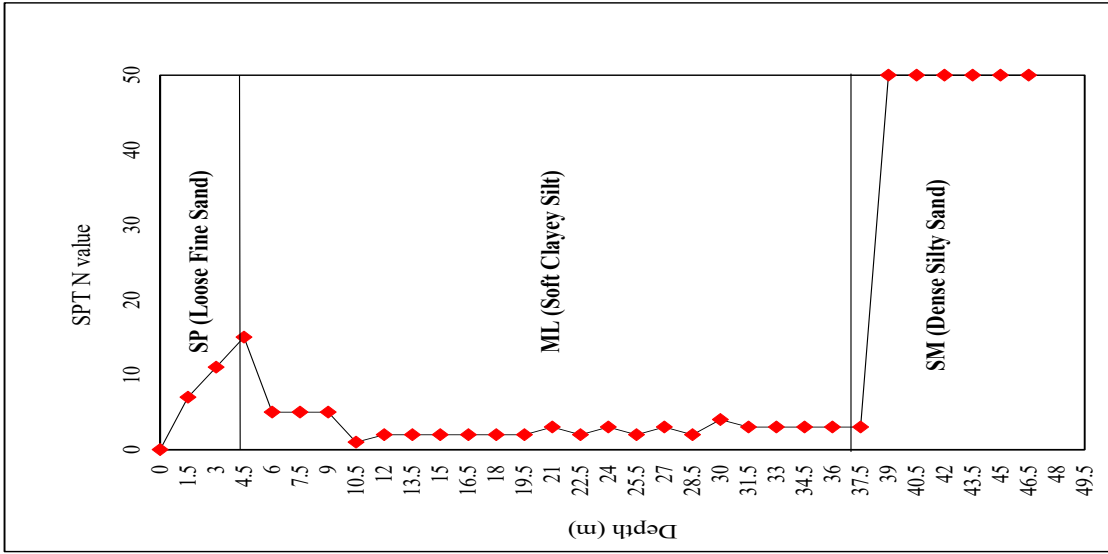


**Figure 3.5:** SPT N values for three boreholes

The first layer shows loose sandy soil, the second layer is soft clayey silt, third layer is dense silty sand layer. A hard stratum is found once the depth of penetration exceeds 37.5 m. The soil classifications are done with the data found from laboratory test results such as grain size analysis, CD triaxial test, Atterberg limit, moisture content, direct shear test, organic content test, unit weight, consolidation test, unconfined compressive strength test etc. Disturbed and undisturbed test samples have been collected from the study site at different depths. The laboratory tests are performed to identify the soil index and strength properties. The Laboratory tests are conducted by following the provisions of the standard code of practices such as BNBC, AASHTO and ASTM as shown in Figure 3.6. The soil layers are classified on the basis of laboratory test results according to the Unified Soil Classification System (USCS) for three boreholes. In absence of test results for any depth of a borehole, standard correlation with SPT-N values is followed based on soil characterization presented in this study.

### **3.3.1 Grain Size Analysis**

Sieve Grain Size Analysis is done to determine the particles' size ranging from 0.075 mm to 100 mm. Particles smaller than 0.075 mm is distributed using the Hydrometer Method. The particle-size distribution curve is used to calculate the coefficient of uniformity and the coefficient of curvature. Based on the lab test results, grain size distribution curve is presented on Figure 3.7. The  $D_{50}$  mean for loose and medium sand are 0.1850 mm and 0.3038 mm, while the fine fraction < 0.075 mm are 11% and 9%, respectively. For clayey silt the  $D_{50}$  mean is 0.0125 mm and fine contents is 95%. In dense sand,  $D_{50}$  mean is 0.255 mm and fine contents are between 44% and 25%. The SPT, soil classification, basic strength and index properties are presented in Table-3.2. The tables show that the soil strata containing ML is highly plastic with a LL of 32-38% and PI of 6-12%. Nearly 90-95% of the particle is passing #200. When the depth exceeds 37.5 m, dense silty sand is found with a SPT value of 50 and above. From 7.5 m to 37.5 m a layer of dark gray soft clayey silt layer exists which is not suitable for supporting end bearing resistance of pile foundation. Beyond 37.5 m brown dense silty sand continues which is capable of withstanding deep foundation's end bearing. Based on the geotechnical parameters, it is decided that the toe of the SPC piles will rest at this layer.



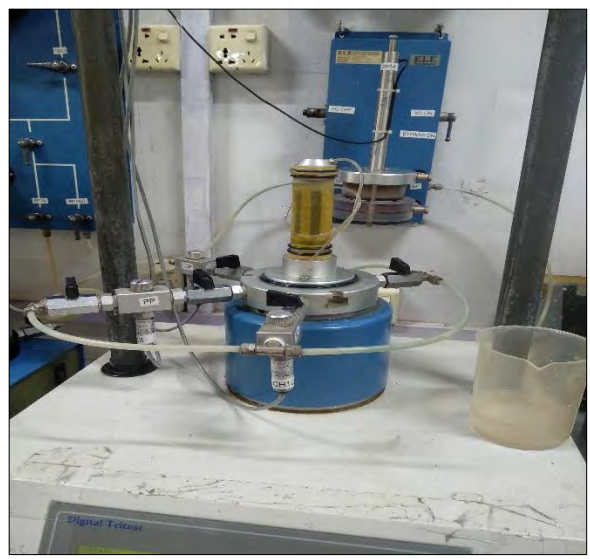
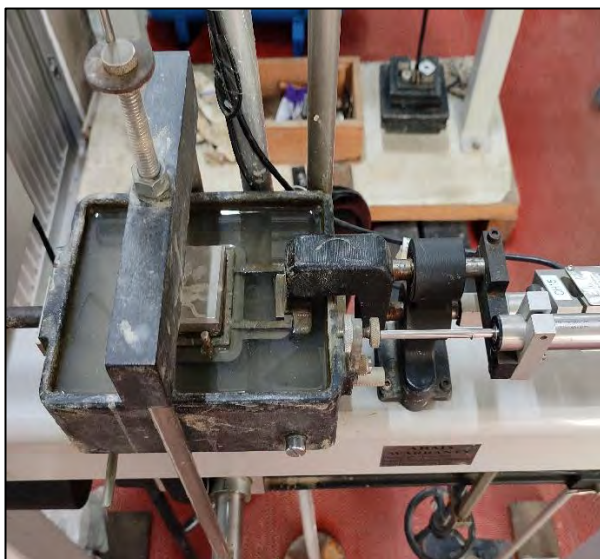


**Figure 3.6:** Laboratory test (a) Disturbed soil sample (b) Undisturbed soil sample (c) Specific gravity test (d) Direct shear test (e) Atterberg limit test (f) Triaxial test.

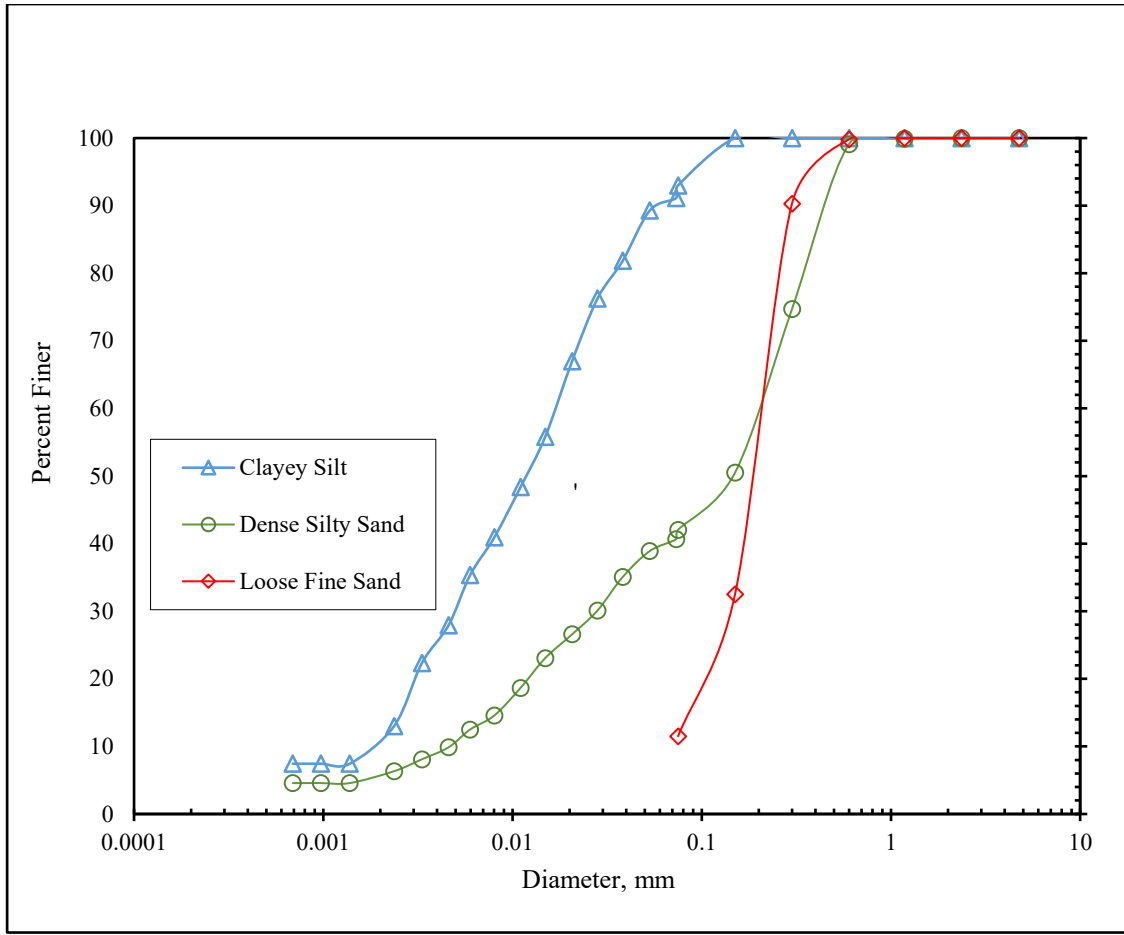


**Figure 3.7:** Particle size distribution curve

### 3.3.2 Atterberg Limit Test

Atterberg limit tests has been conducted with the soil samples collected from different depts to estimate the liquid limit, plastic limit and plasticity index of soil. Thus the soil is classified at depth 16 m using Casagrande Plasticity Chart as shown in Figure 3.8. At depth 21 m, 16 m and 30 m the Atterberg limit test has been done and it is found that the LL is between 36-37%, PI ranges from 6-9 %. The soil at this layer is classified as Clayey silt soil.

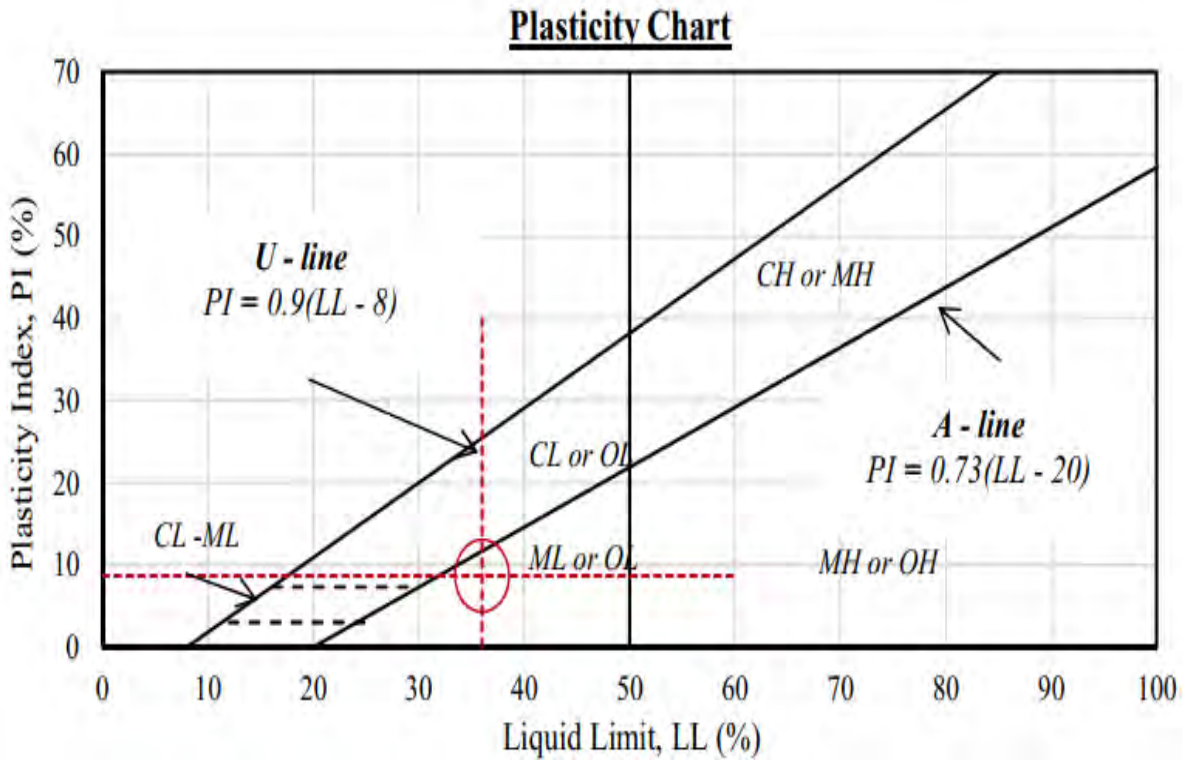
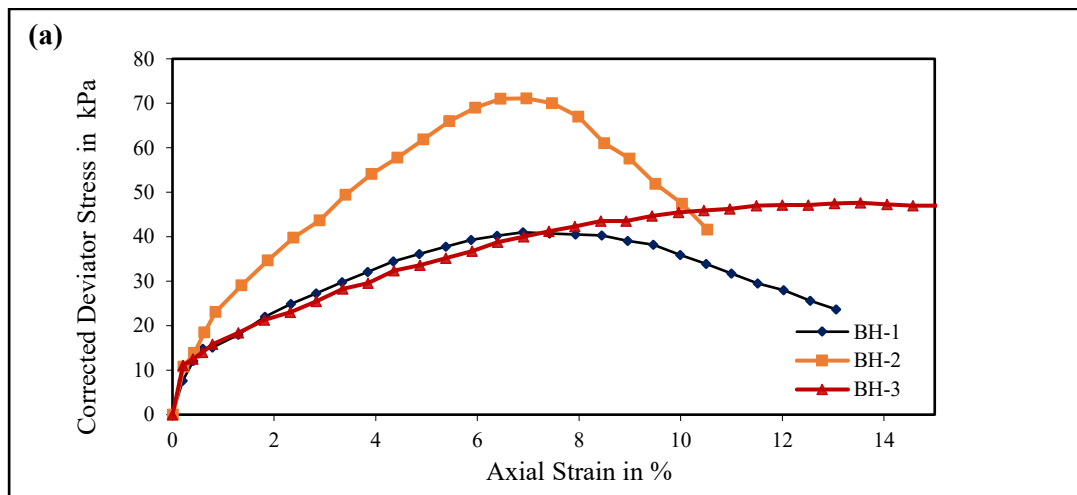


**Figure 3.8:** Casagrande Plasticity Chart

### 3.3.3 Unconfined Compression Test

The unconfined compression test is also called unconfined compressive strength test. It is done under uniaxial compression condition to determine undrained shear strength of saturated soil  $C_u$ . In this study unconfined compression test has been done at a depth of 8.7 m. The  $C_u$  value ranges from 20-35 kPa for different borelogs, see Figure 3.9 (a). The shear failure of soil samples are shown in Figure 3.9 (b).





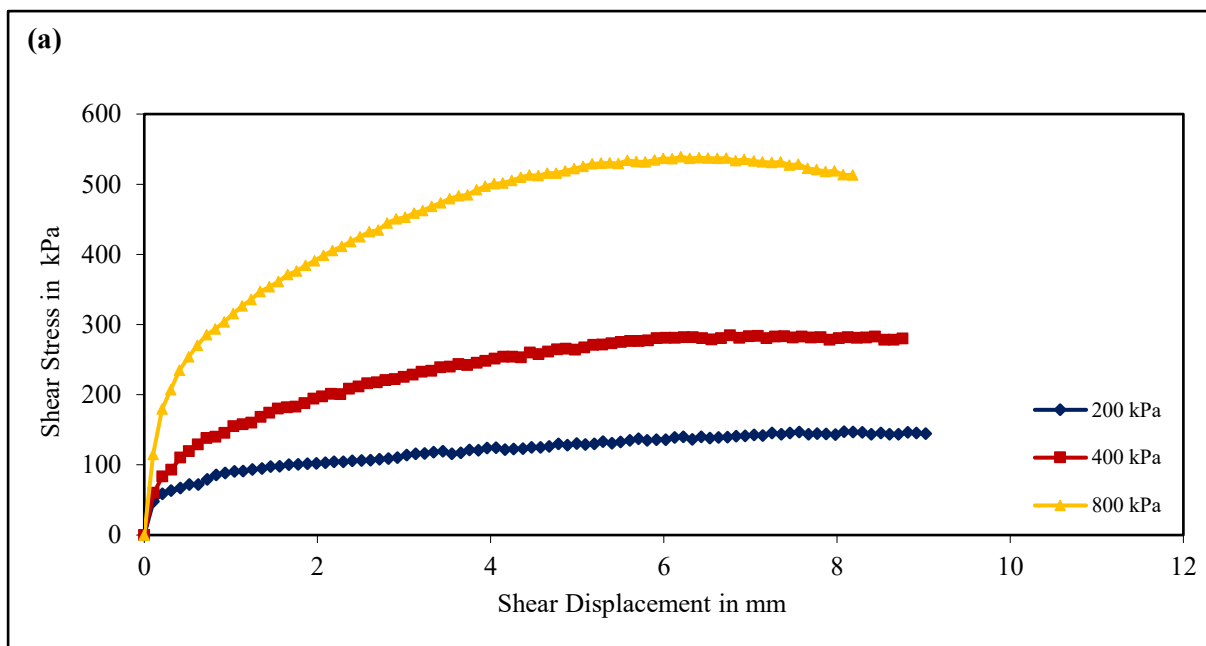
(b)



**Figure 3.9:** (a) Relationship between axial strain and stress and (b) brittle failure mode

### 3.3.4 Consolidated Drained Direct Shear Test

To determine the shear strength of soil materials, direct shear test has been done at different depth 37 m, 39 m and 40 m. It is conducted for cohesionless soil to determine internal angle of friction. The internal angle of friction value varies between 25- 32° for different depth. In Figure 3.10 the stages of direct shear test has been shown and at depth 40 m the phi value is found to be 32°.



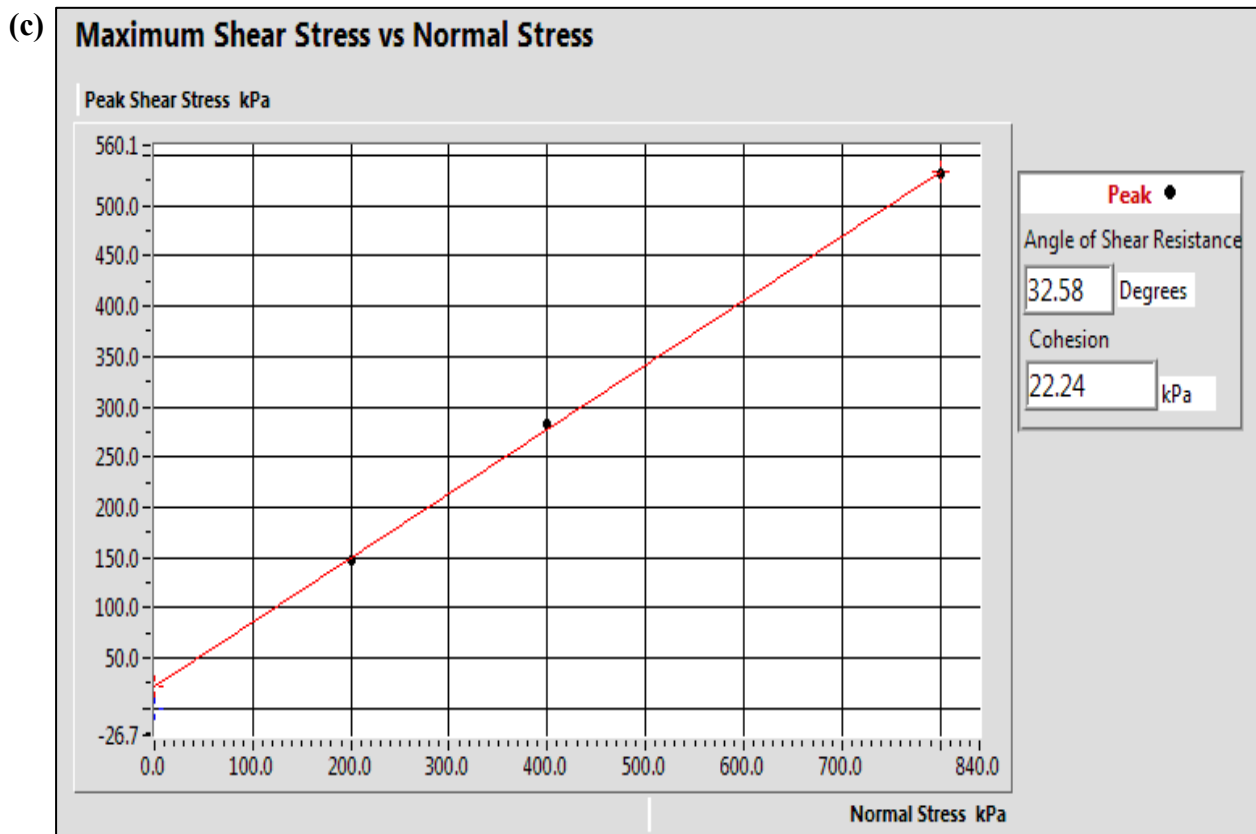
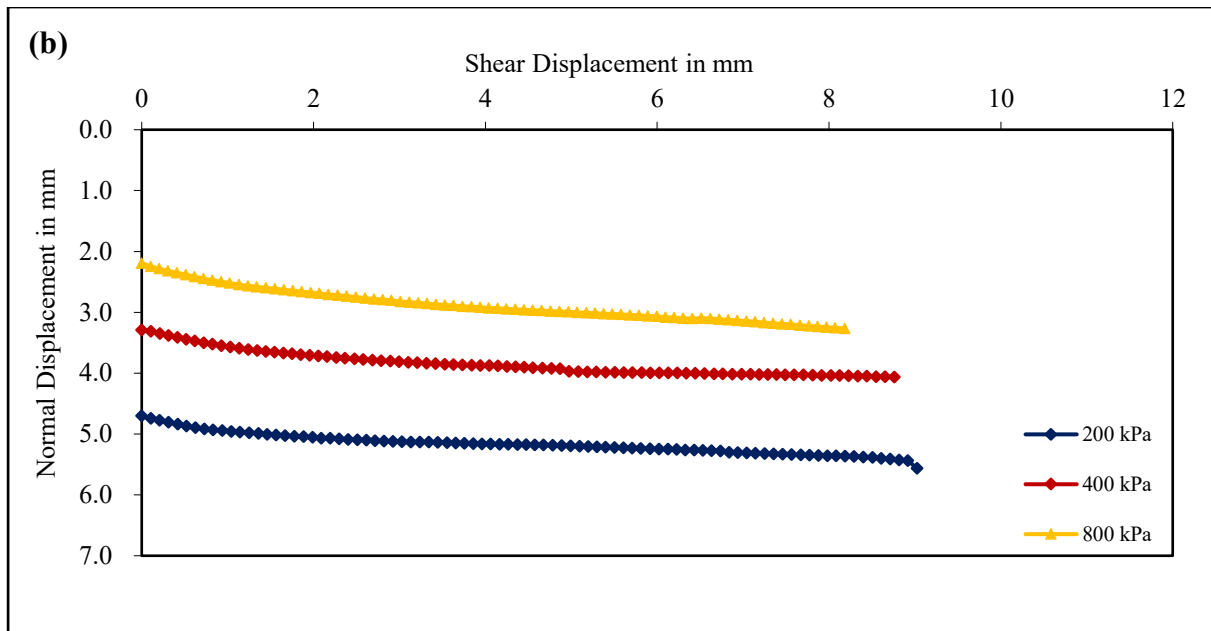
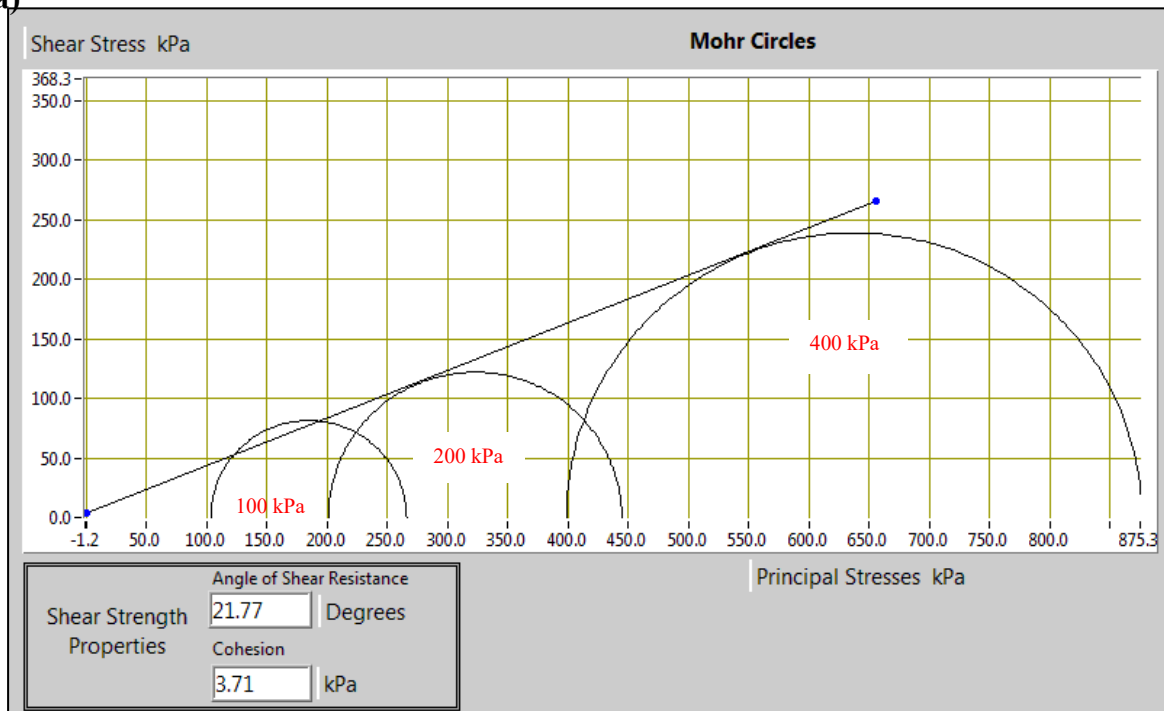


**Figure 3.10:** Direct shear test, relationship between (a) maximum shear stress and normal stress (b) deformation and root time (c) shear stress and horizontal displacement (d) vertical and horizontal displacement

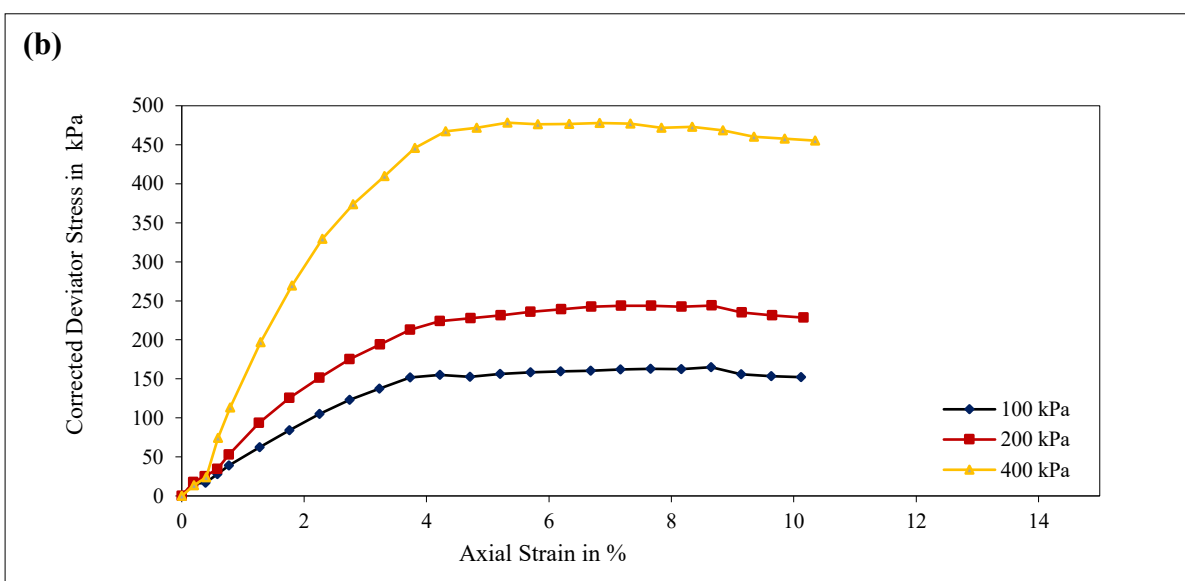
### 3.3.5 Consolidated Drained Triaxial Compression Test

To determine the soil shear strength parameter in drained condition Consolidated Drained (CD) triaxial compression test is an effective way. The CD test has been done at a depth of 11.7 m. The mohr circles obtained from the test is shown in Figure 3.11 (a). From the stress and strain relationship in Figure 3.11 (b) is used to determine stiffness parameters of soil. Figure 3.11 (c) Explains the change of volumetric strain with axial strain. Figure 3.11 (d) shows the shear failure modes of soil samples.

(a)



(b)



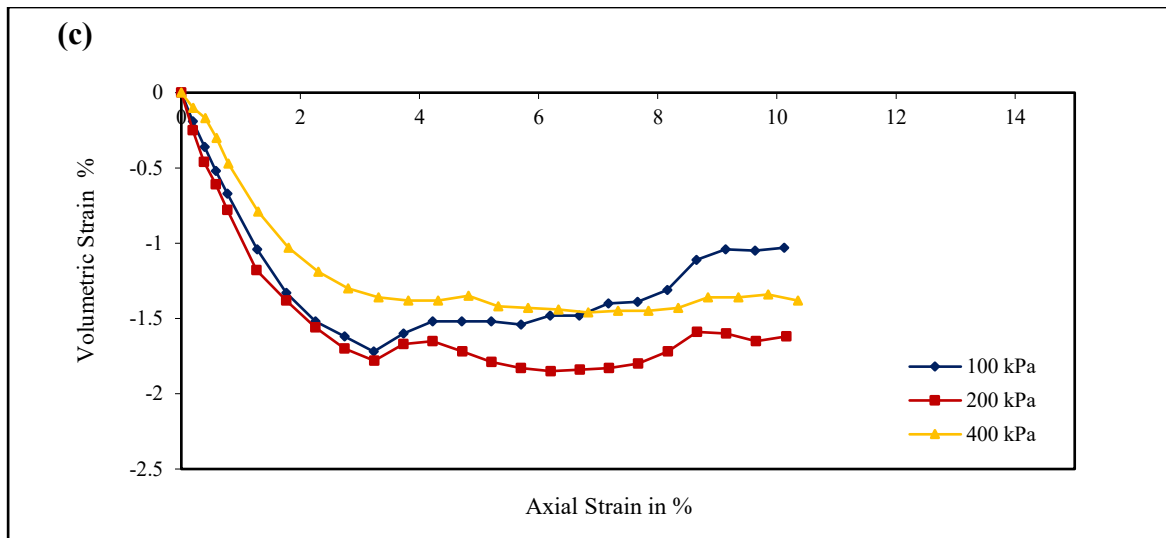


**Figure 3.11:** Relationship between (a) Shear stress and principal stress (b) Deviator stress and axial strain (c) Volumetric strain and axial strain and (d) shear failure modes of soil samples

### 3.3.6 One-Dimensional Compression Test

One dimensional consolidation test has been done at a depth of 10 m with undisturbed soil sample to determine the initial void ratio, compression index. From void ratio to applied pressure graph as shown in Figure 3.12, the void ratio is 0.87 and compression index is 0.261 and swelling index is 0.058 with a preconsolidation pressure of 100 kPa.

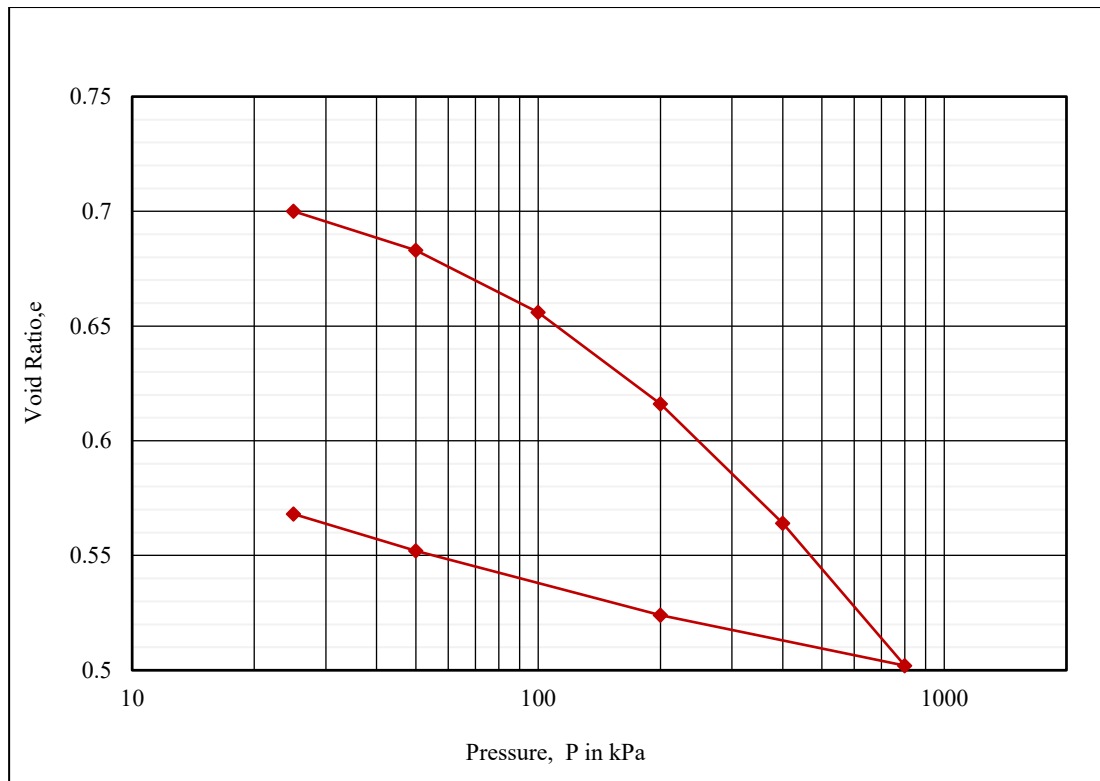


**Figure 3.12:** Relationship between void ratio and applied pressure

**Table 3.2:** SPT and Subsoil Classification

Result Summary			
Depth	SPT range	USCS	Basic soil properties
0 to 4.5	0 to 11	SP	$\gamma = 14 \text{ kN/m}^3$ , $\gamma_{\text{sat}} = 15 \text{ kN/m}^3$ , $G_s = 2.61$ , $w_n = 41.7\%$ , Fines (#200 passing) = 11.0%, $\phi = 26.0^\circ$
4.5 to 37.5	1 to 4	ML	$\gamma = 16 \text{ kN/m}^3$ , $\gamma_{\text{sat}} = 17.5 \text{ kN/m}^3$ , LL = 32-38%, PI = 6 -12%, Fines (#200 passing) = 90-95%, $w_n = 35\%$ , $C_u = 20-24 \text{ kPa}$ .
>37.5	30 to 50	SM	$\gamma = 18 \text{ kN/m}^3$ , $\gamma_{\text{sat}} = 20 \text{ kN/m}^3$ , $G_s = 2.67$ , $w_n = 13-15\%$ , Fines (#200 passing) = 25-44%, $\phi = 33.0^\circ$



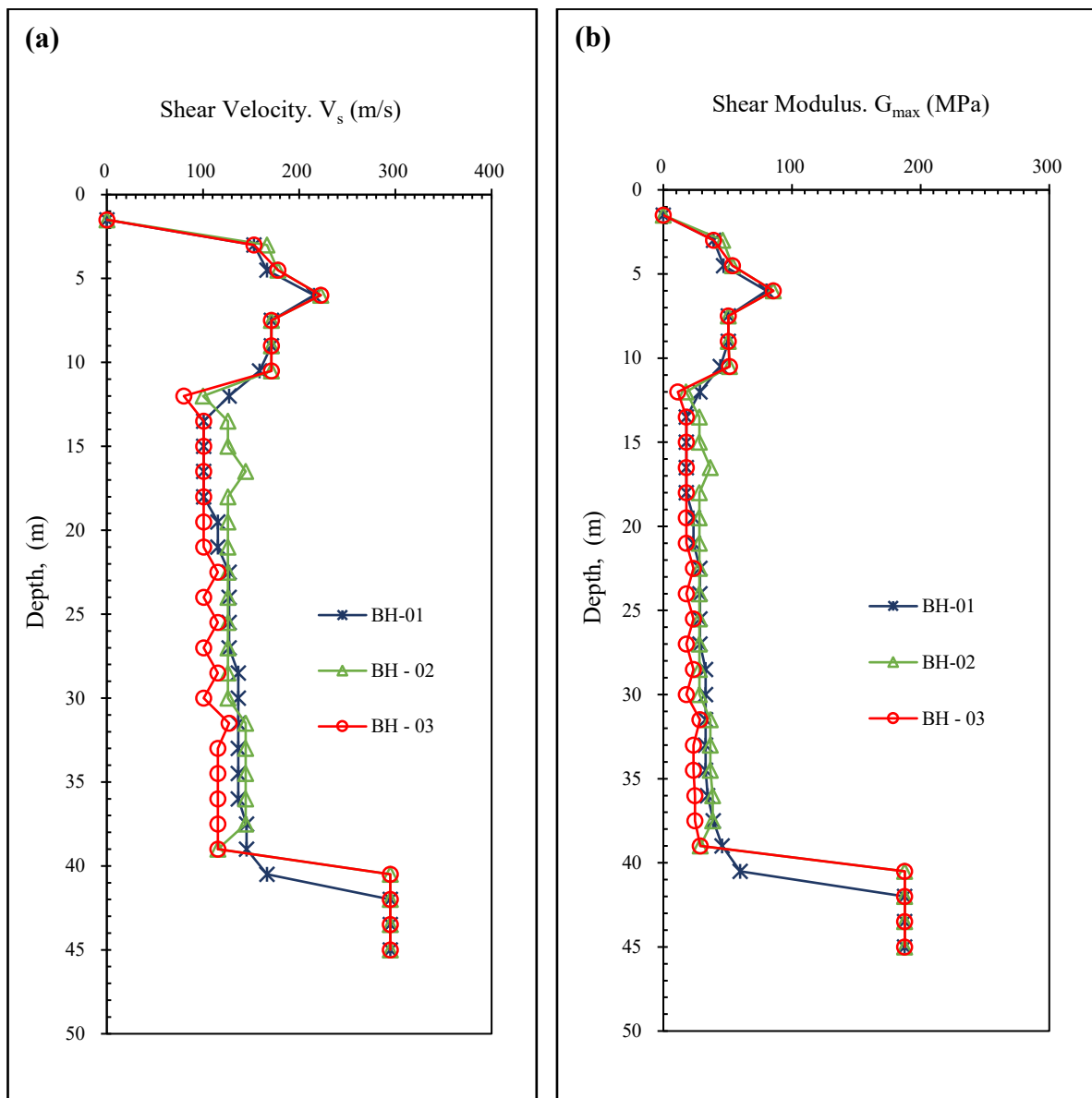


**Figure 3.13:** a) Depth vs Shear wave Velocity b) Depth vs Shear Modulus,  $G_{max}$

The dynamic soil properties like Shear-Wave Velocity ( $V_s$ ) and Small Strain Shear Modulus ( $G_{max}$ ) are correlated from field SPT N values as described in chapter two. In this study, equation suggested by JRA (1980) has been used for calculating of shear wave velocity and shear modulus from SPT N values and presented in Figure 3.13 (a) and (b) respectively. The Figure shows that both the shear wave velocity and shear modulus of the soil increase as the depth of penetration increases though there are some fluctuations.

The minimum shear wave velocity is observed in a layer of 12-37.5 m deep which is 100-130 m/s. The maximum wave velocity is observed to be 300 m/s at a depth 40 m and above. As can be seen from Figure 3.13 (b) that the minimum shear modulus is 18 MPa at a depth of 12 to 37.5 m and the maximum value of the G is 200 MPa which is observed at depth 40 m and above.

### **3.4 Field Test**

The SPC pile is installed in the site by push piling method. Then a static pile load test has been conducted on the installed SPC pile to determine the in-situ pile bearing capacity.

#### **3.4.1 Pile Load Test**

A single circular hollow SPC pile of 450 mm diameter and 110 mm wall thickness is driven through the soil stratum where it has been rested on a dense sand layer at an embedment depth of 42.5 m. To obtain a stable foundation, the pile is penetrated through the soft layers to dense sand layer. The pile is inserted by push piling method with maximum load of 4067 kN. Later on the static pile load test on spun pile is performed according to ASTM D-1143 (ASTM.1994).

The incremental compressive load is applied as 10% of design load until 250 ton design load is reached. The pile is loaded till failure by applying 428 ton load. The applied load is maintained in each case for 1 hr and the load is removed in decrements equal to the loading increments, a 20 min in between gap is provided for decrements. After removing each maximum applied load, reapply the load to each preceding load level in increments equal to 50 % of the design load, allowing 20 min between increments. Applied the additional loads after the design load is reached and maintained till failure occurs. After the maximum required test load has been applied, hold and removed the test load when the pile is failed under maximum load. Site photographs showing push-in test is presented in Figure 3.14 and in Figure 3.15 the pile load setup is shown.



**Figure 3.14:** Push-in test in study area

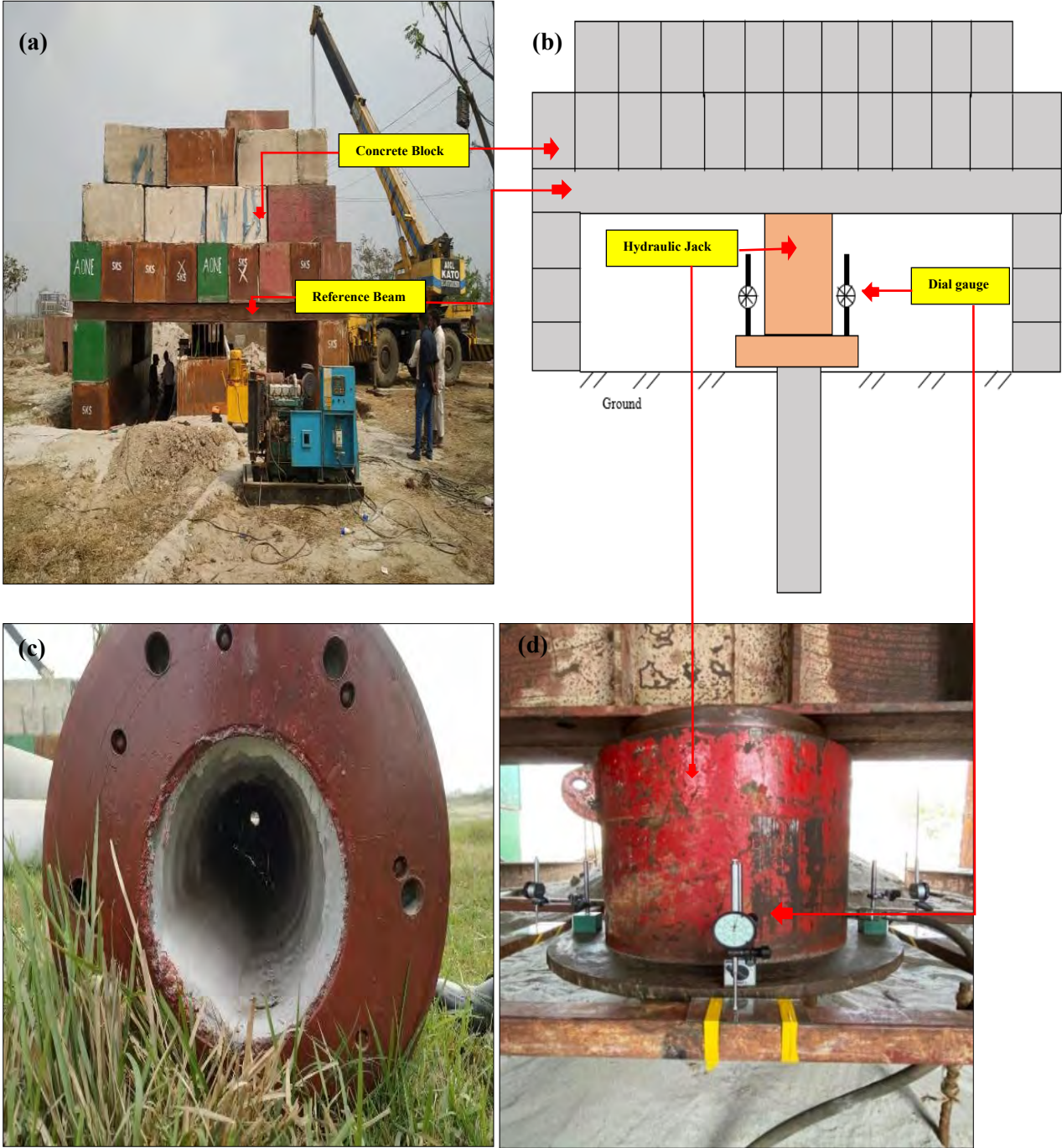


**Figure 3.15:** a) Performing static load test b) Schematic diagram of static load test c) spun pile for driving in soil d) Hydraulic jack and dial gauge setup during the test



### 3.5 Liquefaction Analysis in Jolshiri Site

After determining different soil parameters from field and laboratory test of disturbed and undisturbed samples, the liquefaction analysis has been done after (Seed et al.,1983). The soil parameters like SPT N values, fine contents, unit weight, groundwater table,  $D_{50}$  results have been obtained and used for the liquefaction analysis.

The reclaimed areas are expanding at a faster rate due to industrialization and facilitate the inhabitants. To provide a safe structure, a geotechnical engineer needs to do the liquefaction analysis. In Jolshiri site, the liquefaction analysis is done for identical boreholes from SPT N values and data acquired from soil investigation reports. The cyclic stress ratio is determined using borehole information, total and effective overburden pressure. The SPT test is done at each 1.5 m interval and ended up to 45 metres.

The SPT N values are used to estimate the cyclic resistance ratio. According to Bangladesh National Building Code (BNBC) 2020 the maximum considered earthquake (MCE) for Bangladesh corresponds to 2% probability of exceedance for 50 years of return period. Recent researches and historical data shows that Bangladesh is prone to experience a magnitude of 7.0 or greater earthquake near future. There are four zone coefficient in BNBC-2020 and Dhaka lies in zone-II. So for Dhaka city maximum peak ground acceleration (PGA) at the ground surface and magnitude of earthquake is considered to be 0.20 g and 7.5.

At different depths, the factor of safety against liquefaction is calculated. Figure 3.16 shows the liquefaction assessment curve for three boreholes analysed by the mentioned method above. The curve is shown for different magnitude of earthquake 7.5, 6.5, 6, 5.5 and 5. The three borehole are identical and first layer is loose sandy type of soil. Up-to depth 4.5 metre the factor of safety values lies less than one which indicates strong liquefaction probability at upper layer. The result has also showed compatibility with existing literature for loose sandy or silty soil layers liquefaction analysis.

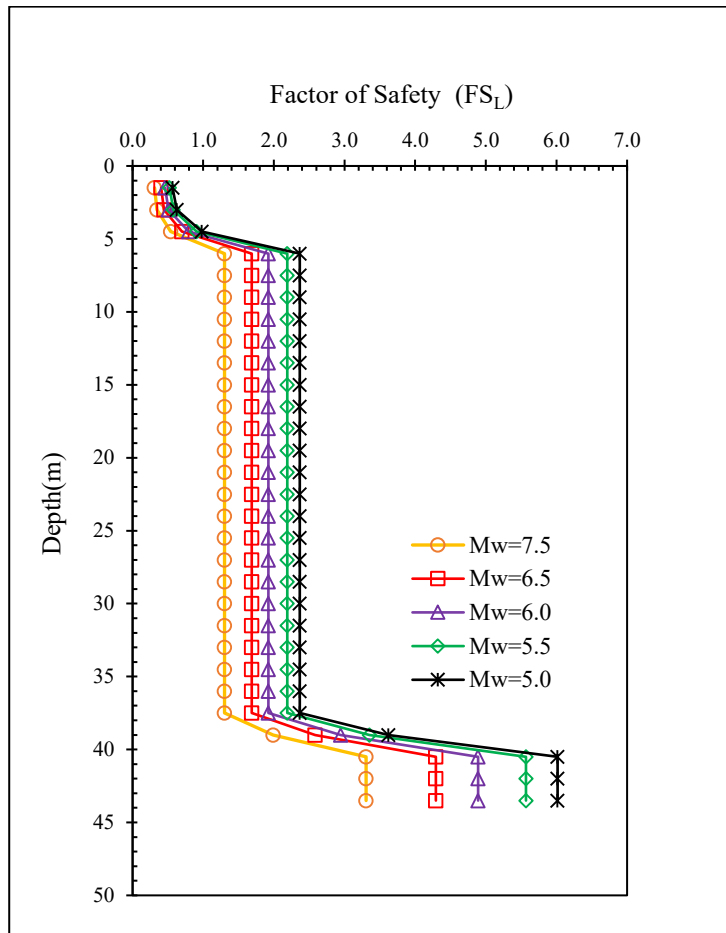


**Figure 3.16:** Comparison of liquefaction assessment

### 3.6 Bearing Capacity Analysis of SPC pile

After collecting the SPT values and data from laboratory test results, the bearing capacity for the test site is evaluated by analytical procedure as described in chapter two. In Figure 3.17 (a) and (b) the bearing capacity with and without considering liquefaction is shown with respect to borehole depth. From Figure 3.18 (a), it is observed that in liquefiable soil the skin friction of pile is reduced considerably for borehole one, two and three around 9.41 %, 8.71 % and 10.15 % respectively. The ultimate bearing capacity is also affected by liquefiable soil characteristics as shown in Figure 3.18 (b). The ultimate pile capacity decreases 3.97% for borehole one and 3.80 %, 4.50% for borehole two and three respectively. So the liquefaction potentiality of any vulnerable site should be taken into consideration to evaluate the actual bearing capacity for designing a safe foundation system.

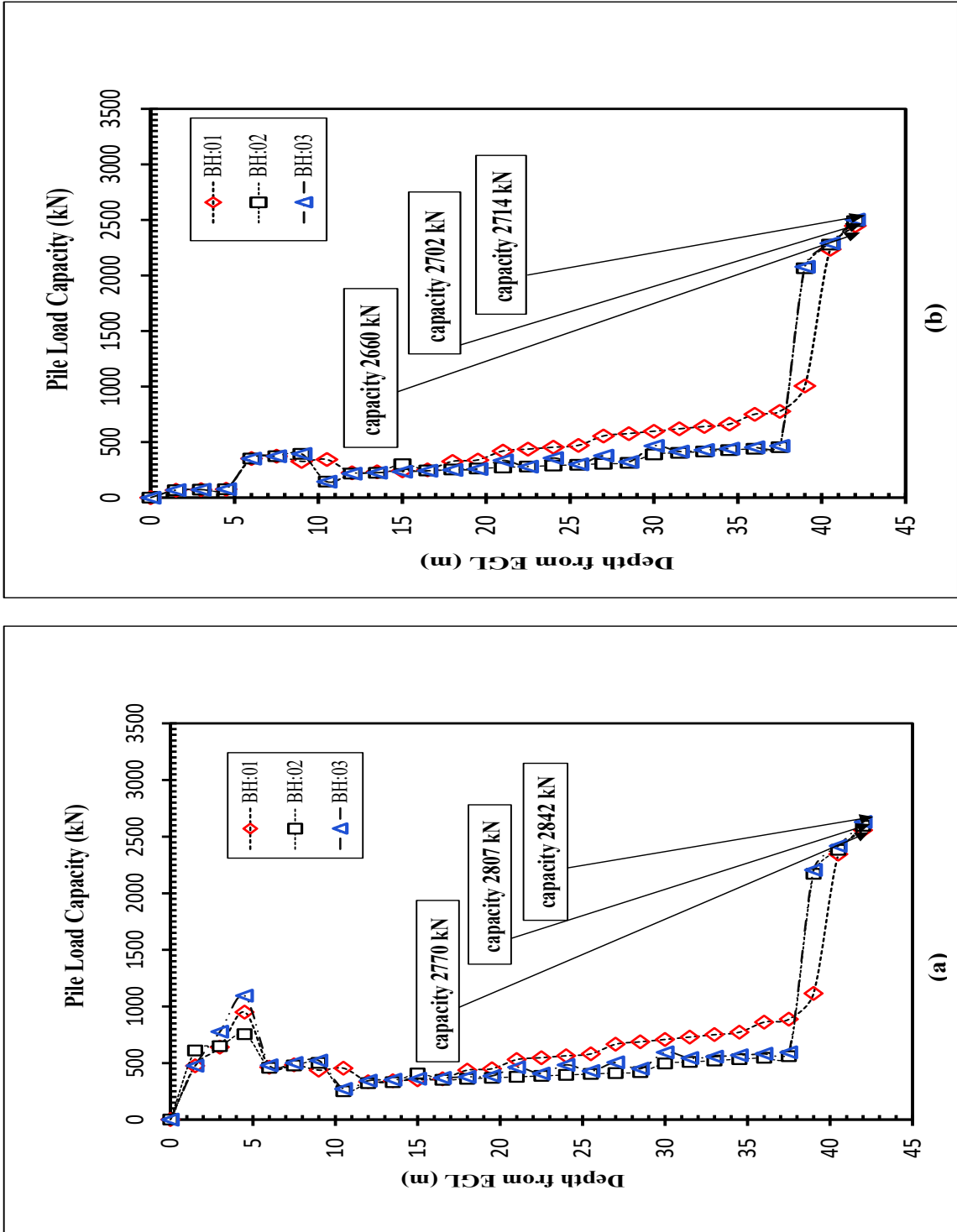


**Figure 3.17:** (a) Bearing capacity without considering liquefaction by analytical method.

(b) Bearing capacity considering liquefaction by analytical method

(a) Comparison of skin friction (with and without liquefaction)

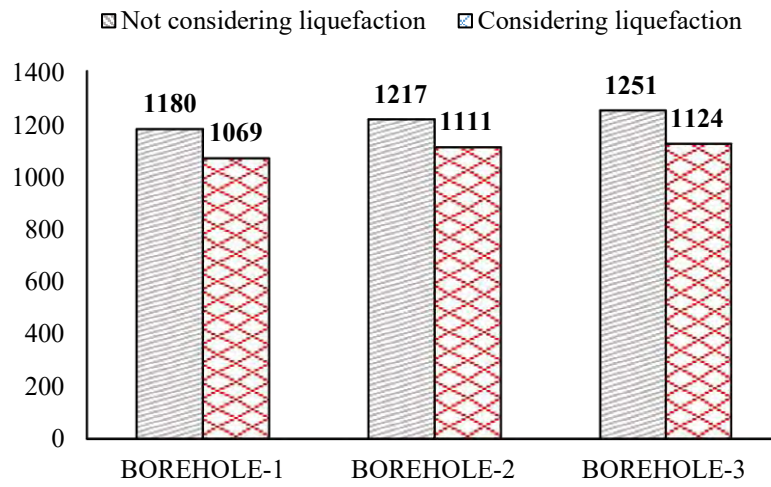


Figure 3.18: (a) Comparison of skin friction considering with and without liquefaction

(b) Comparison of ultimate bearing capacity (with and without liquefaction)

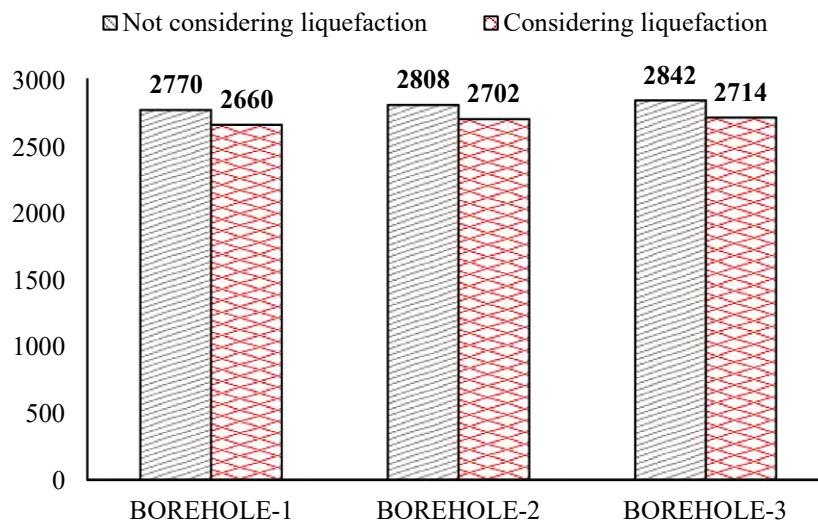
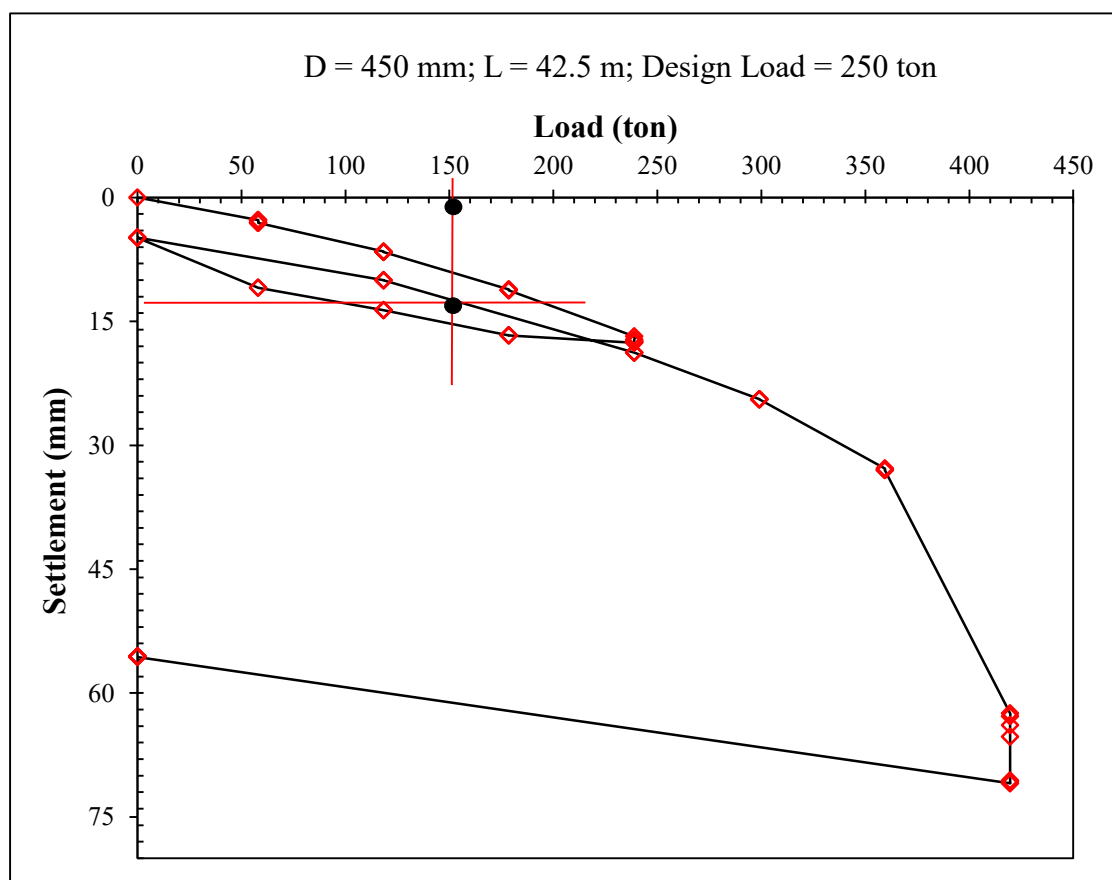


Figure 3.18: (b) comparison of bearing capacity considering with and without liquefaction.



After completion of pile load test, the result has been prepared from the field data. Load-settlement curve of tested SPC pile (450mm dia) is shown in Figure 3.20 . Final result of static load test is presented by following Bangladesh National Building Code (BNBC).

However, for simplicity and as widely adopted practice in Bangladesh, load corresponding to a settlement of 12 mm is considered as design criteria in this study as shown in Figure 3.19. The allowable load from the load-settlement curve is 150 ton corresponding to 12 mm settlement for 450 mm diameter pile with a design load of 250 ton and maximum applied failure load 427.88 ton. Davission offset method is another widely accepted method for load capacity interpretation from pile load test. In this method the ultimate capacity is estimated to be 3790 kN concerning 43.13 mm settlement as shown in Figure 3.20. The shape of curvature method is widely used practice to determine the ultimate bearing capacity from field test data. The tangent from the initial part of the loading curve and the ending part of loading part intersect at a point and that point is considered as the ultimate loading capacity of the pile. Figure 3.21 shows the bearing capacity 3463 kN and settlement is 24.60 mm in shape of curvature method.



**Figure 3.19:** Load vs Settlement plot of conducted load tests

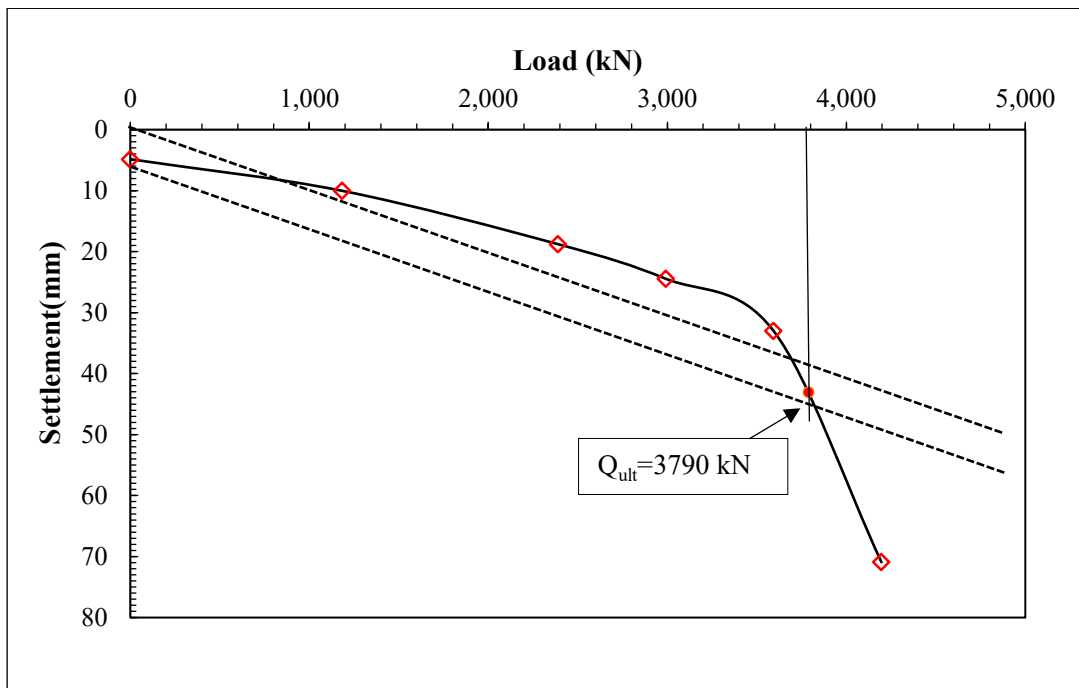


**Figure 3.20:** Load-Settlement curve derived from pile load test by Davisson offset method

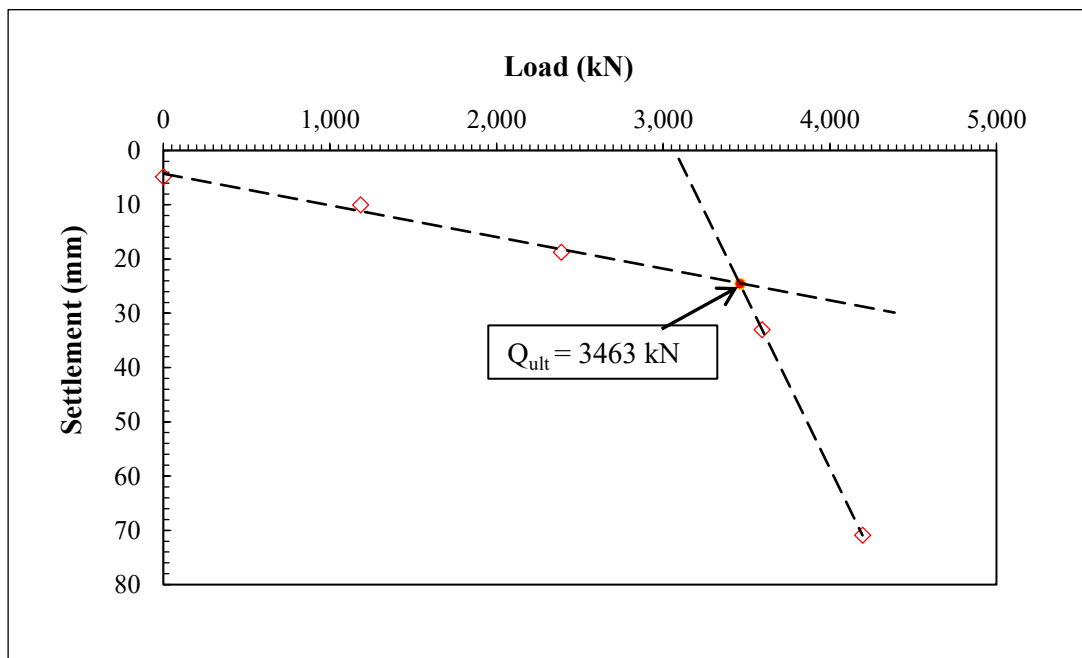


**Figure 3.21:** Load-Settlement curve derived from pile load test by Shape of curvature method

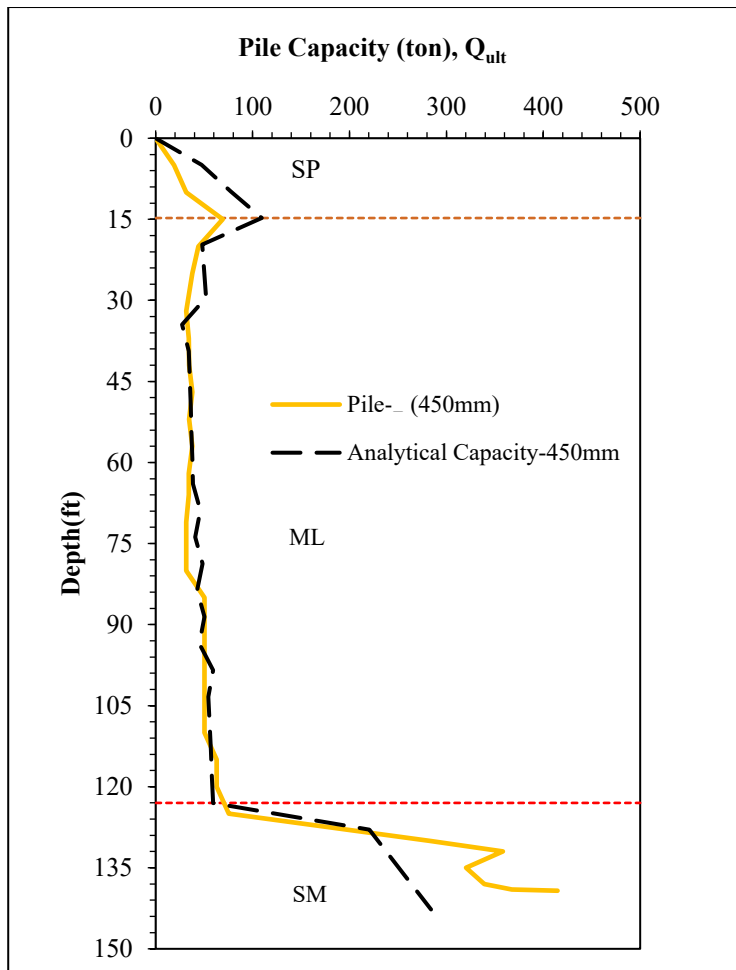


**Figure 3.22:** Comparison of pile bearing capacity determined from Push-in test and analytical method

Analytical bearing capacities of SPC piles are verified through field push-in test at selected site of Jolshiri Abason. Push-in test has been conducted for 450 mm diameter SPC piles with a progressive load at the rate of 1.52 m (5 ft) length. Figure 3.15 shows comparison between analytical capacities and push-in values. Site photographs showing push-in test is presented in Figure 3.14. From Figure 3.22, it is observed that beyond 37.5 m ultimate capacities of 450mm diameter piles yield greater than 100 ton. However, in practice after 37.5 m further driving in to the layer of hard soil (SPT>50) will depend on pile's structural capacity and requirements on pile tip stability.

### 3.7 Summary

This chapter deals with the field test data acquired in investigation site. The bearing capacity determined from both analytical and in-situ pile load test is obtained in this part. From the analysis it can be summarized that:

1. For determining different soil strength parameters, conducting field and laboratory test is the only viable way. With this aim at the very outset, sub soil investigation is performed in the study area and soil samples both disturbed and undisturbed are collected for laboratory tests.
2. The soil boring data obtained from the site is important to classify the soil. From soil investigation it is found that the top 4.5 m is filled with loose sand with a shear wave velocity less than 180 m/s and SPT value less than 15. This layer is susceptible to liquefaction in saturated condition under seismic event.
3. The liquefaction analysis is done to observe the liquefaction susceptibility of the top layer of soil using Seed and Idriss method. It is obtained that the CRR/CSR ratio is less than 1. So in this type of soil SPC pile is installed to increase the bearing capacity and reduce probable pile failure during earthquake.
4. The pile is installed by Push-in method in the site with an ultimate load capacity of 414 ton for 450 mm diameter SPC pile. After that, in situ static pile load test is performed in the site. The design load for the pile is 250 ton and the pile is tested to failure with 427.88 ton load. The ultimate pile bearing capacity is also determined in this chapter by analytical method with and without considering liquefaction phenomenon.
5. The allowable bearing capacity of pile is determined from load-settlement curve obtained from field load test data according to BNBC 2020. This curve is used further to validate the FEM model for numerical investigation. Finally the Push-in test method result is compared with the analytical at the pile tip.

## **CHAPTER 4**

### **NUMERICAL MODELING**

#### **4.1 Introduction**

To evaluate the bearing capacity of pile under static loading condition, the in situ pile load test is the most reliable and accurate method. In this investigation, the study area is filled with loose silty sand type soil which is susceptible to liquefaction if earthquake occurs, so the chance of pile failure during earthquake event is more likely to happen. Though the pile can sustain axial load under design condition but the possibilities of failure under seismic excitation in liquefiable soil should be taken into consideration. The performance of SPC pile is evaluated numerically considering both axial and earthquake loading condition.

In this segment, the results of numerical investigation is presented for SPC pile installed into the study location. The FEM model is calibrated with the field pile load test data. The result of embedded pile deformation is shown using HS soil model. The model parameters are determined from field test results. Also the different stress distribution in soil during earthquake and liquefaction are discussed here. At the end, a comparison is made between axially loaded pile with the earthquake loading.

#### **4.2 FEM Model in PLAXIS 3D**

In this section, modeling assumptions for numerical analysis is described. Soil is modeled by 10 noded element. Drained analysis has been adopted for Hardening Soil (HS) model. Groundwater table is taken at the GL. The soil parameters are determined from SPT N value correlations and laboratory test results. A 42.5 m SPC pile is modeled using embedded beam element with a outer diameter of 450 mm and wall thickness of 110 mm. Each soil layer thickness is taken from the borelog profile collected from the study site and presented in chapter three.

#### **4.3 Derivation of Soil Stiffness Parameters**

In Jolshiri study area, both field and laboratory tests are performed to determine different soil index and strength properties which can act as input parameters for soil modeling in plaxis.

### 4.3.1 Field and Laboratory Tests Performed for Determination of Soil Parameters

Standard penetration test has been conducted in Jolshiri site up-to 45 m depth. SPT N values are recorded at every 1.5 m depth. Both disturbed and undisturbed samples are collected for testing in laboratory. The test procedure is done according to ASTM D 1586. To determine soil index and shear strength properties and to know the actual soil condition in site, performing laboratory test is a must. In this investigation different laboratory tests such as specific gravity test, grain size analysis, Atterberg limit test, CD triaxial test, consolidation test, direct shear test, unconfined compression test etc are carried out.

## 4.4 Modeling Parameters

In this section the input parameters in PLAXIS 3D for both soil and structural element are presented.

### 4.4.1 Soil Modeling Parameters

Hardening Soil (HS) model is advanced model in predicting and simulating behavior of soft soil as well as stiff soil. In hardening soil model yield surface is not fixed in principle stress space but as a result of plastic straining yield surface can develop. This will change the soil stiffness after loading and unloading. After applying primary deviatoric loading, soil shows decreasing stiffness and irreversible plastic strain develops. For HS model the basic idea is to develop hyperbolic relationship between vertical strain and deviatoric stress. It also controls stress dependency level. The parameters requires for HS model are shown in Figure 4.1. HS model uses the theory of plasticity than elasticity theory. In this model the input parameters are;  $m$  the stress dependent stiffness according to power law, plastic straining due to primary deviatoric loading  $E_{50}^{ref}$ , plastic straining due to primary compression  $E_{oed}^{ref}$ , elastic unloading  $E_{ur}^{ref}$  and  $c$ ,  $\phi$ ,  $\psi$  are the failure according to the Mohr-Coulomb failure criterion parameters. The stiffness parameters are determined from triaxial test and consolidation test. In PLAXIS  $K_{0nc}$  is automatically recommended based on Jacky's formula.  $v_{ur}$  and  $R_{int}$  are also recommended values from PLAXIS. The required estimated parameters for HS model is presented in Table 4.1.

Soil - Hardening soil - <NoName>

General Parameters Groundwater Interfaces Initial

Property	Unit	Value
<b>Stiffness</b>		
$E_{50}^{ref}$	kN/m <sup>2</sup>	0.000
$E_{oed}^{ref}$	kN/m <sup>2</sup>	0.000
$E_{ur}^{ref}$	kN/m <sup>2</sup>	0.000
power (m)		0.5000
<b>Alternatives</b>		
Use alternatives		<input type="checkbox"/>
$C_c$		10.00E9
$C_s$		10.00E9
$e_{init}$		0.5000
<b>Strength</b>		
$c'_{ref}$	kN/m <sup>2</sup>	0.000
$\varphi'$ (phi)	°	0.000
$\psi$ (psi)	°	0.000
<b>Advanced</b>		

Next OK Cancel

Figure 4.1: Parameters for HS model

**Table 4.1:** Material properties for the soil layers

Parameters	Unit	Loose sand	Clayey silt	Silty sand
Unstaturated unit weight ( $\gamma_{\text{unsat}}$ )	kN/m <sup>3</sup>	16	16	18
Sturated unit weight ( $\gamma_{\text{sat}}$ )	kN/m <sup>3</sup>	17	17.5	20
Secant stiffness modulus ( $E_{50}^{\text{ref}}$ )	kN/m <sup>2</sup>	10000	15000	38000
Oedometer modulus ( $E_{\text{oed}}^{\text{ref}}$ )	kN/m <sup>2</sup>	10000	15000	38000
Unloading/reloading stiffness ( $E_{\text{ur}}^{\text{ref}}$ )	kN/m <sup>2</sup>	30000	45000	114000
Poisson's ratio, $\nu$		0.3	0.3	0.3
Cohesion, $c$		0	15	0
Angle of friction, $\phi$		23	25	36
Dilation Angle, $\Psi$		0	0	0
Unloading/reloading poisson's ratio, $\nu_{\text{ur}}$		0.2	0.3	0.25
Power for stress-level dependency of stiffness, $m$		0.5	0.5	0.5
$K_0$ value for normally consolidated factor, $K_{0\text{nc}}$		0.531	0.577	0.412
Interface factor, $R_{\text{int}}$		0.7	0.9	0.9

#### 4.4.2 Embedded Pile Modeling Parameters

The finite element modeling is done in PLAXIS 3D and validated with the static pile load test conducted on site. The soil is modeled using HS model parameters and SPC pile is modeled as embedded beam element in PLAXIS. The SPC pile is loaded under different axial load during pile load test and reached to the ultimate load capacity. In PLAXIS the bearing capacity of pile is the input parameter for embedded pile rather than the result of finite element calculation. The embedded pile input parameters are determined from pile load test. As embedded pile is



considered as beam element so the parameters are presented in terms of Young modulus  $E$  and the unit weight  $\gamma$  of pile material. For modeling different geometric properties of pile, predefined shapes (masive circular pile, circular tube, square pile) with pile diameter and wall thickness are provided. The properties of pile soil interaction is defined by skin resistance and base resistance. In Table-4.2 the required properties of embedded pile are given.

**Table 4.2:** Required parameters of the embedded pile

Parameters	Name	Value	Unit
Predefined beam type	Circular tube	-	-
Diameter	Diameter	0.450	m
Wall thickness	Thickness	0.110	m
Young's modulus	$E$	$32.88 \cdot 10^6$	$\text{kN/m}^2$
Unit weight	$\gamma$	24	$\text{kN/m}^3$
Skin resistance	Type	Linear	-
Skin resistance at the beginning of the embedded beam	$T_{\text{top,start,max}}$	20	$\text{kN/m}$
Skin resistance at the end of the embedded beam	$T_{\text{bot,end,max}}$	100	$\text{kN/m}$
Base resistance	$F_{\text{max}}$	1600	$\text{kN}$

#### 4.5 Numerical Modeling

The FEM model is developed for both axial and earthquake loading condition using same parameters stated in Table 4.1 and 4.2. The soil profiles are modeled by consulting the borelog collected from site to the depth of borelog up-to 45 m. Each layer has different characteristics according to several tests performed. At first a borehole is located at (0,0,0) point. For model perimeter 20 m in x direction and 20 meter in y direction are taken as model width. The model depth is taken as 45 m in z direction as shown Figure 4.2. The water table is assumed at the existing ground level. The pile is located at the middle of the soil perimeter as shown in Figure 4.3 (a). In this stage axial load is provided as a point load at the top of the pile. After completing

the soil and structural modeling, the finite element meshing is done. Figure 4.3 (b) shows the connectivity plot of the model after meshing stage. The stage construction phases of PLAXIS for axially loaded pile are given below in Table 4.3. In Table 4.4 the break down of loading and unloading stages are given.

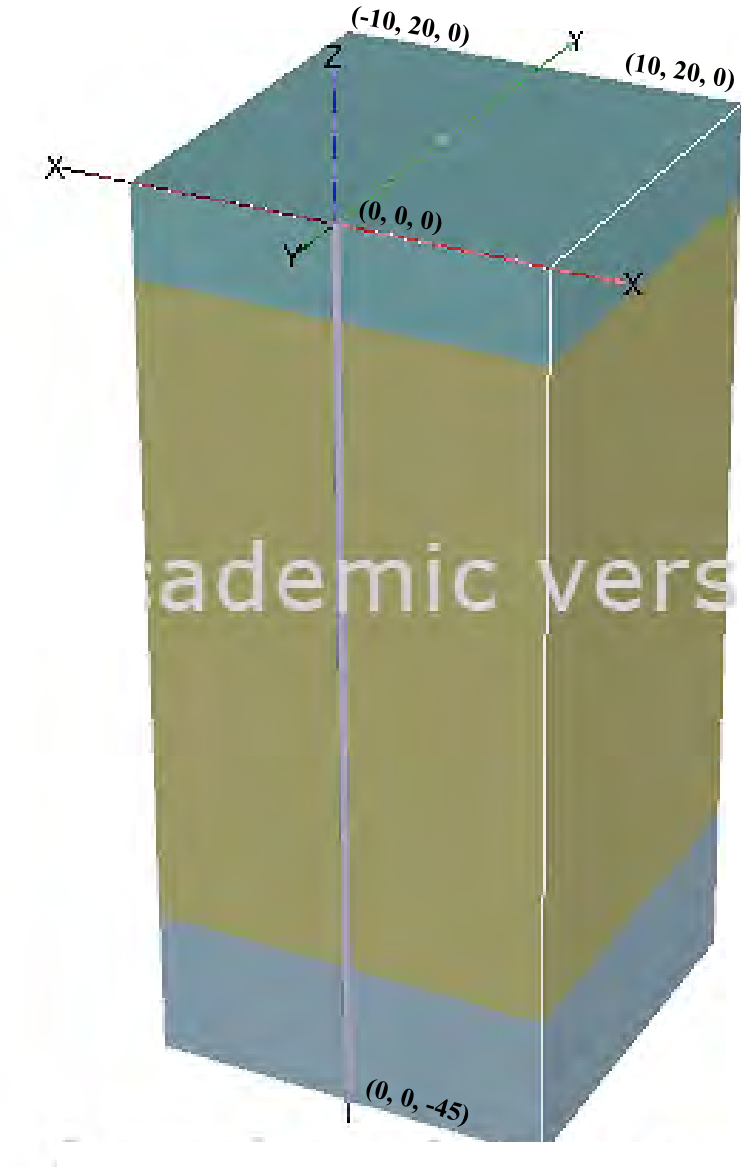


**Figure 4.2:** FEM model developed in PLAXIS 3D

**Table 4.3:** Stage construction phases for compressive loading

Phase	Analysis type	Elements	Activated
Initial	K <sub>0</sub>	Soil volume	√
		Embedded pile element	x
		Point load	x
Pile construction	Plastic	Soil volume	√
		Embedded pile element	√
		Point load	x
Loading stage	Plastic	Soil volume	√
		Embedded pile element	√
		Point load	√
		Deformation in z direction	√
Unloading stage	Plastic	Soil volume	√
		Embedded pile element	√
		Point load (design load in reverse order)	√
		Deformation in z direction	√

**Table 4.4:** Stage construction phases for incremental loading and unloading stages

Phase	Analysis type	Incremental loading and unloading stages
Loading stage	Plastic	L = 0
		L = 590 kN
		L = 1202 kN
		L = 1815 kN
		L = 2490 kN
Unloading stage	Plastic	UL = 1815 kN
		UL = 1202 kN
		UL = 590 kN
		UL = 0

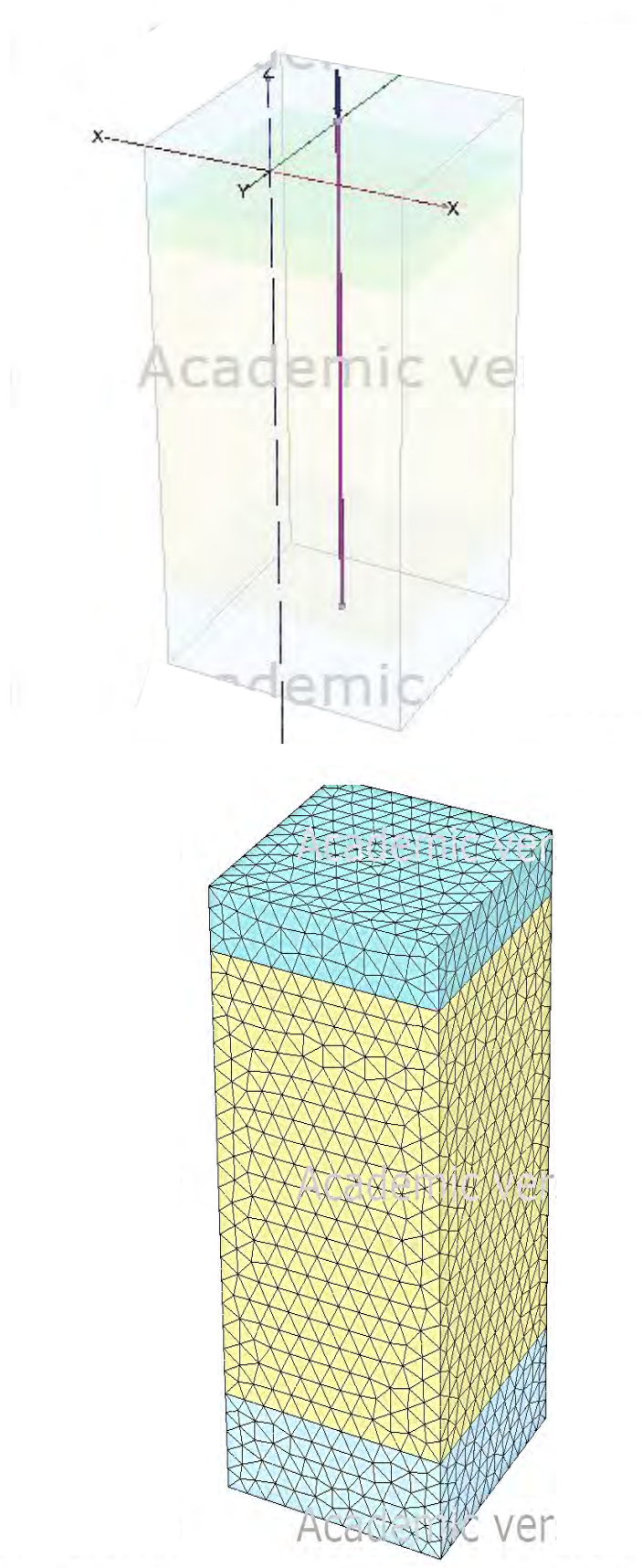


**Figure 4.3:** (a) Axially loaded embedded pile and (b) connectivity plot

#### 4.5.1 Validation with Field Pile Load Test Data

The pile load test is simulated in PLAXIS 3D and the maximum settlement from the analysis is 18.47 mm which is very close to the maximum settlement of field test 17.60 mm as shown in Figure 4.4. The simulated result shows good agreement with the field pile load test results under static loading condition. Therefore, this calibrated model can be used for further analysis.

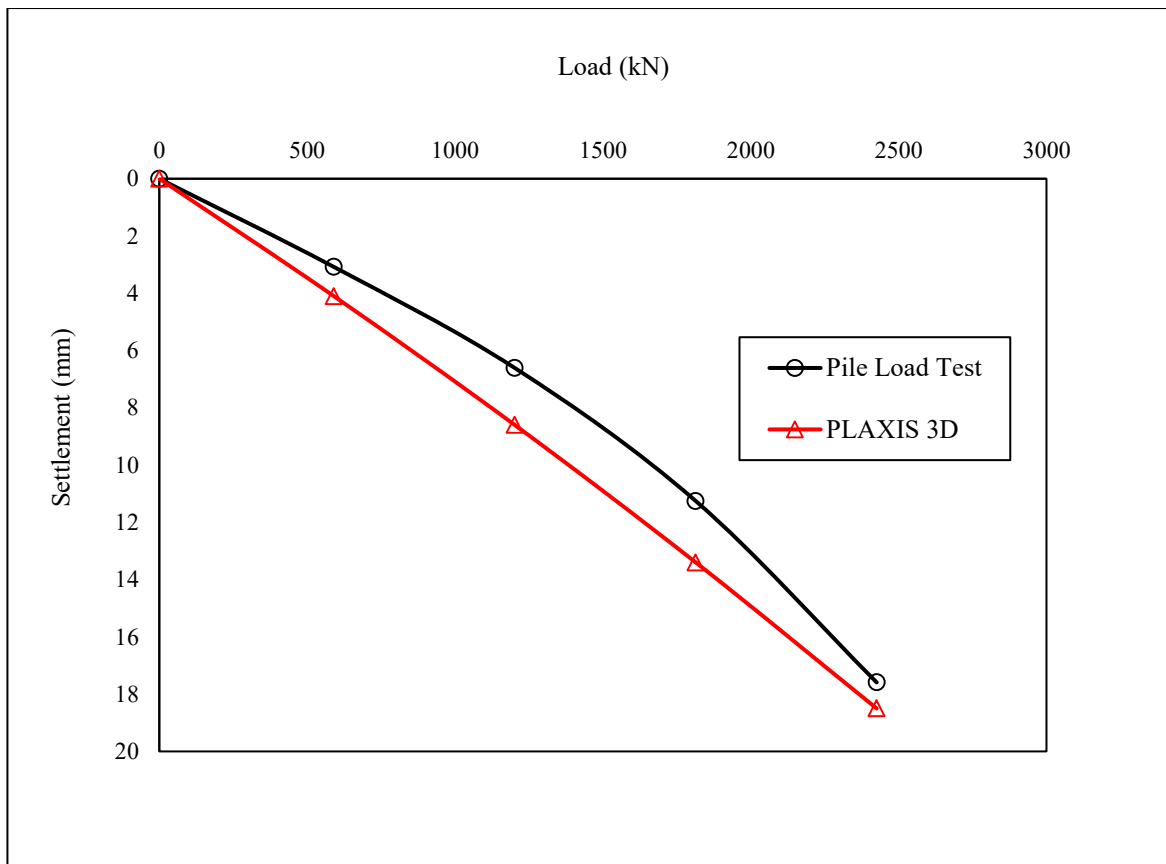


**Figure 4.4:** Comparison of PLAXIS 3D obtained results with field measured result

#### 4.5.2 Pile Deflection under Axial Loading

After completing the numerical model, the pile is analysed under different incremental loading condition similar to the field condition as shown in Table 4.4. At different loading stages pile exhibits displacement in both lateral and vertical direction. In PLAXIS displacement are shown in three direction i.e.  $U_x$ ,  $U_y$ ,  $U_z$  as well as total displacement is also depicted in form of graph or contour plot.  $U_x$ ,  $U_y$  displays displacement in lateral direction and  $U_z$  in vertical direction.

Figure 4.5 shows the axial load distribution along the pile length. The vertical load is applied at pile head at different stages and the result shows that with increasing depth the axial load decreases. Figure 4.6 shows the three dimensional view of displacement contour of pile in z direction around the pile from the modeling results from compression loading. The displacement field is concentrated around the pile with a pile head displacement of 18.47 mm. Figure 4.7 shows the top view of pile displacement. The pile shows tolerable displacement under design load 2500 kN.

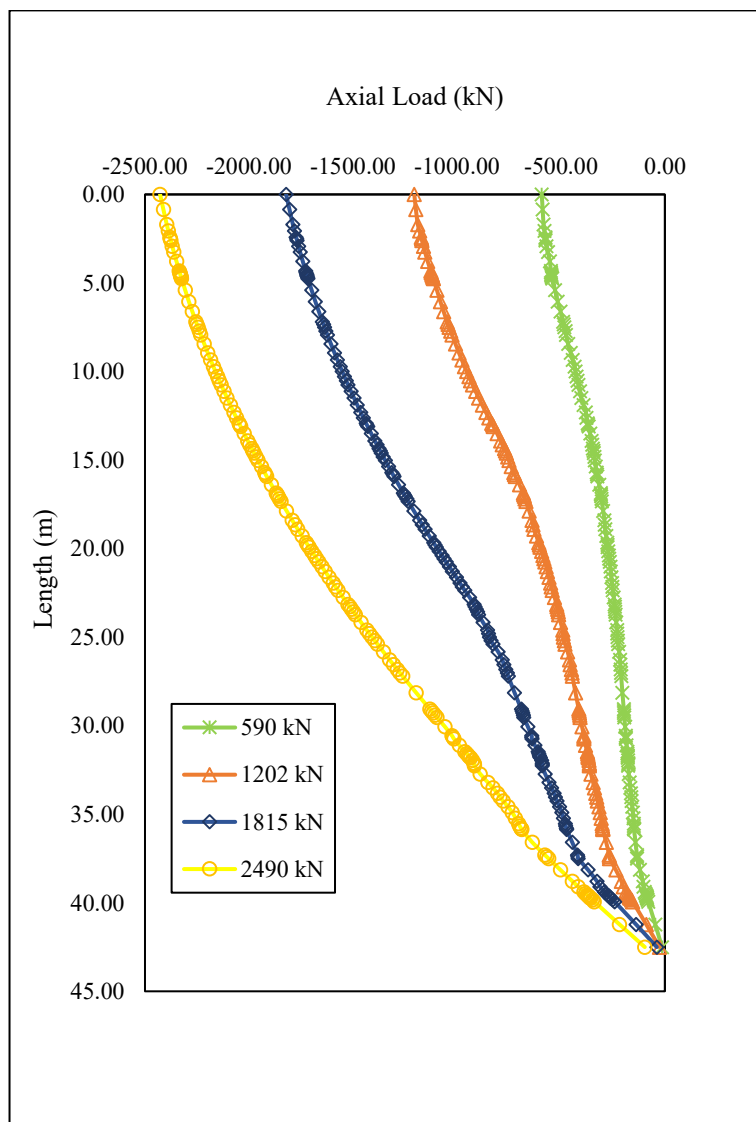


**Figure 4.5:** Relationship between pile depth and axial load

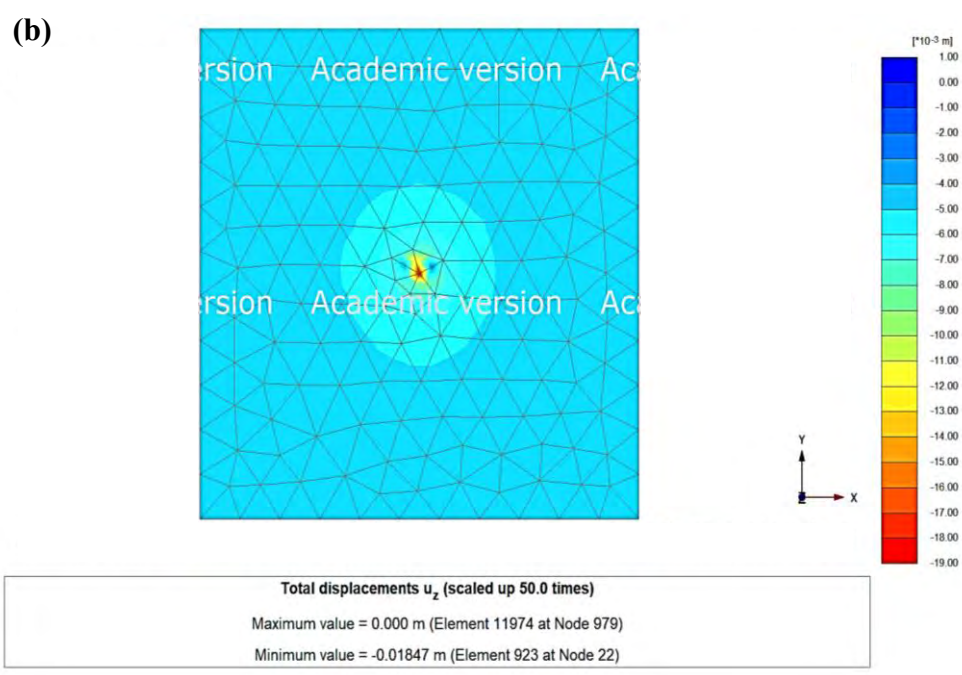
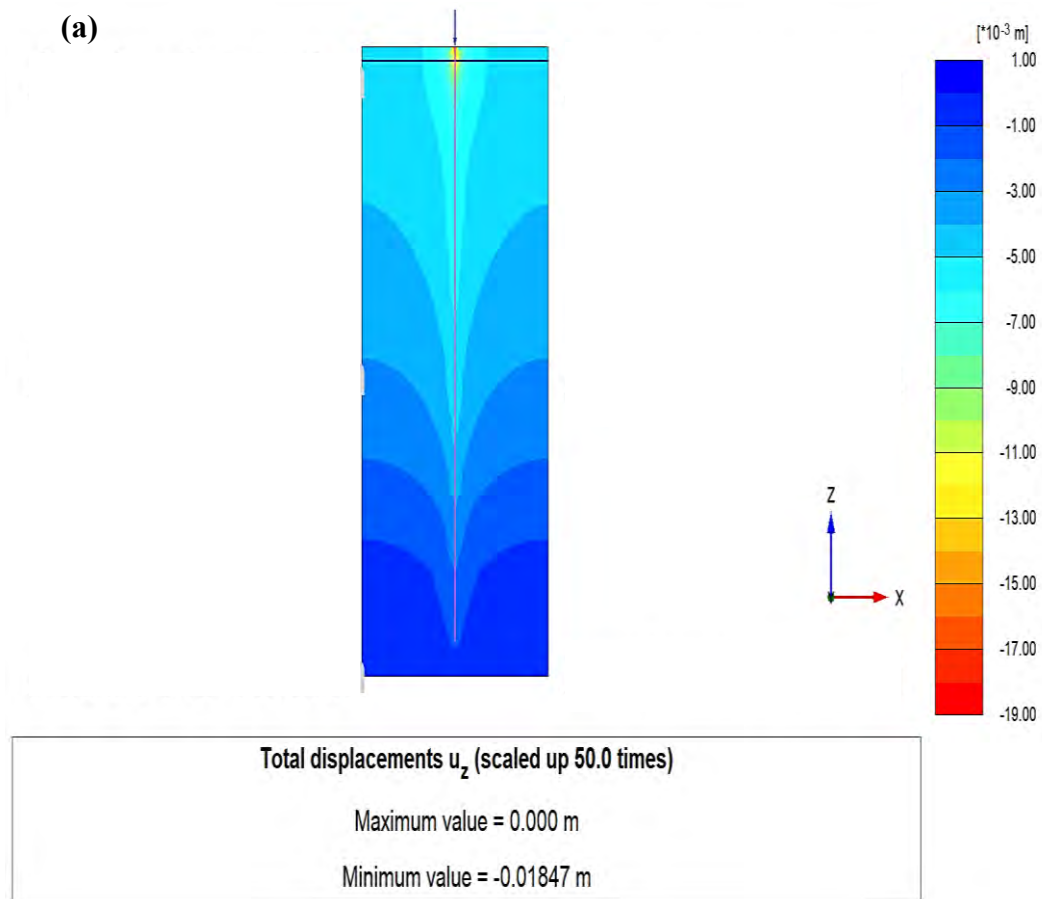


**Figure 4.6:** a) Displacement field around pile b) Top view of displacement contour

### 4.5.3 Stress Distribution

The Principle total stress in soil skeleton is shown in Figure 4.7 at 42.5 m depth. The maximum stress generated due to axial loading is 647 kN/m<sup>2</sup>. The stress field is concentrated around the pile and it is represented as red color. The yellow field shows stress distribution in soil particles. The total strain contour at the top of the pile in z direction is presented in Figure 4.8 and the maximum strain is 0.016. The stress strain relationship of a particular point at bottom end is displayed in Figure 4.9. It seems that mostly the strain develops in soil element as the result of plastic strain.

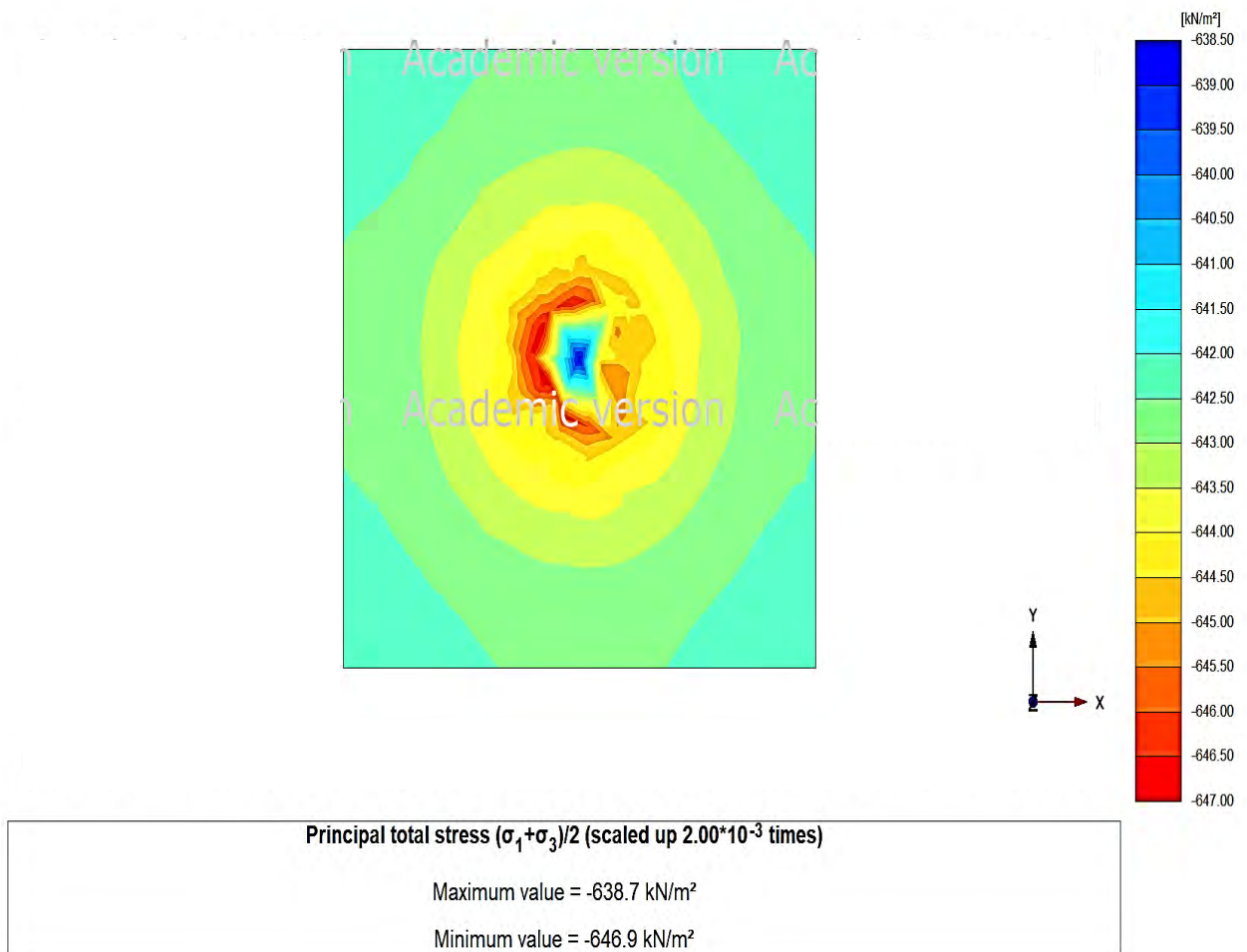
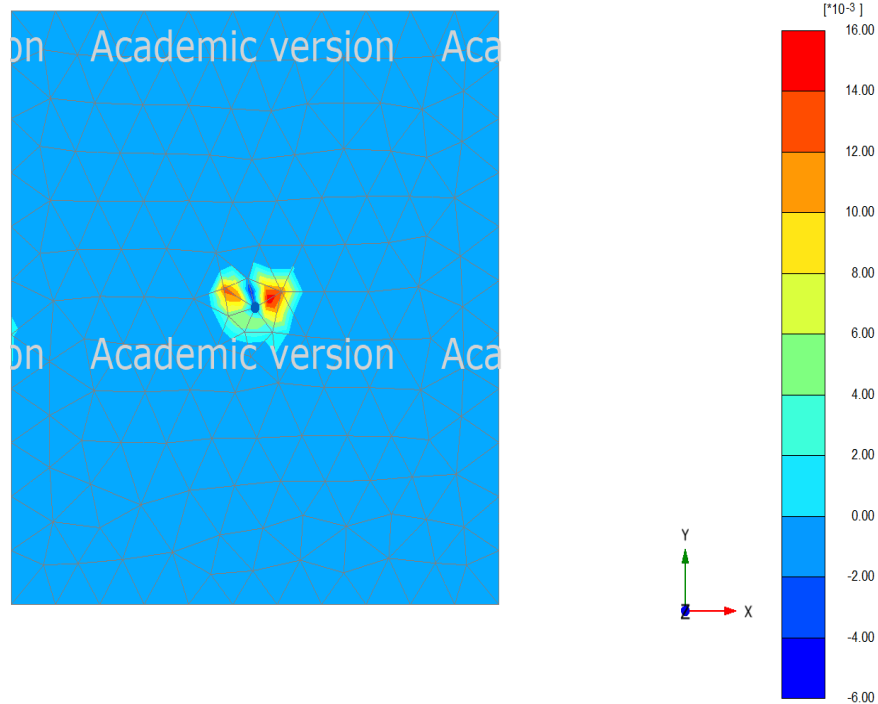


**Figure 4.7:** Total principle stress at surrounding soil at pile bottom





**Total cartesian strain  $\epsilon_{zz}$  (scaled up 50.0 times)**  
 Maximum value = 0.01579 (Element 923 at Node 7722)  
 Minimum value =  $-5.775 \cdot 10^{-3}$  (Element 923 at Node 22642)

**Figure 4.8: Total strain in z direction**

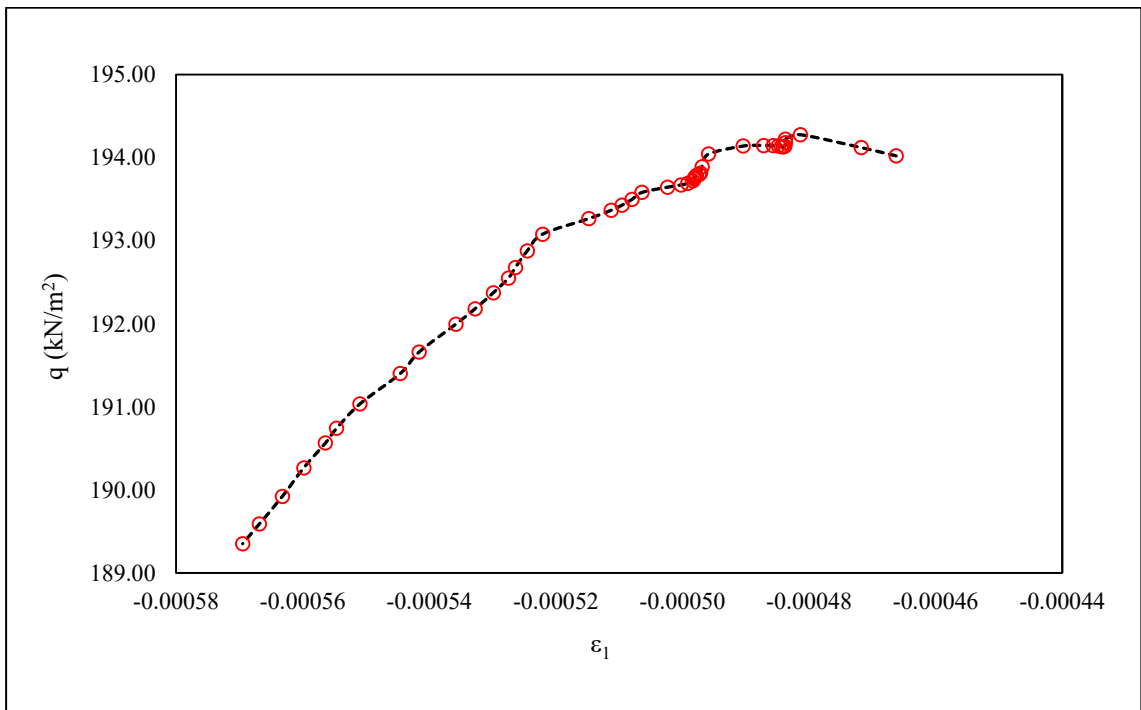


**Figure 4.9: Stress-strain relationship**

## 4.6 Parametric Study

The numerical model can be influenced by pile diameter, length and mesh size that can affect the pile response in soil body. The parameters can make differences in terms of accuracy and efficiency of the computation. Influence of different pile diameter, length and mesh sizes is also investigated through parametric analysis.

### 4.6.1 Influence of Mesh Size

For performing finite element calculation, a fully defined geometry is divided into finite elements. This combinations of finite element is called mesh. Mesh coarseness is considered to have significant effect on calculated results. Fine meshing is important to get accurate result in any analysis but it takes longer time for calculation. The mesh generation process includes soil stratigraphy, structure, loads and boundary. The element distribution depending on relative element size factor ( $r_e$ ), there are five global levels in PLAXIS as as shown in Table 4.5.

**Table 4.5:** Element size factor with element distribution

Element Distribution	$r_e$
Very Coarse	2
Coarse	1.5
Medium	1.0
Fine	0.7
Very Fine	0.5

In this study, three mesh sizes have been used to see the sensitivity of mesh sizes on results obtained in the analysis. Figure 4.10 (a), (b) and (c) shows the fine, medium and coarse mesh connectivity plot respectively. For the current study fine mesh element has been used for both vertical and earthquake loading conditions. Figure 4.11 shows that the full loading stage is completed and  $M_{stage}$  value reaches to 1 which means all the out-of-balance forces are omitted during each stage calculation process. In the end, ultimate displacement is found to be very close for fine and medium mesh sizes on the top of the pile, 18.47 mm and 18.35 mm respectively at ultimate load. For coarse mesh the axial displacement is 17.54 mm as shown in Figure 4.12. Figure 4.13 displays the moment generated under different meshing condition. It is evident from these above plotted graph that effect of meshing variation on the output results is

significant in case of moment generation. The deviation among the result are very close to each other in terms of displacement.

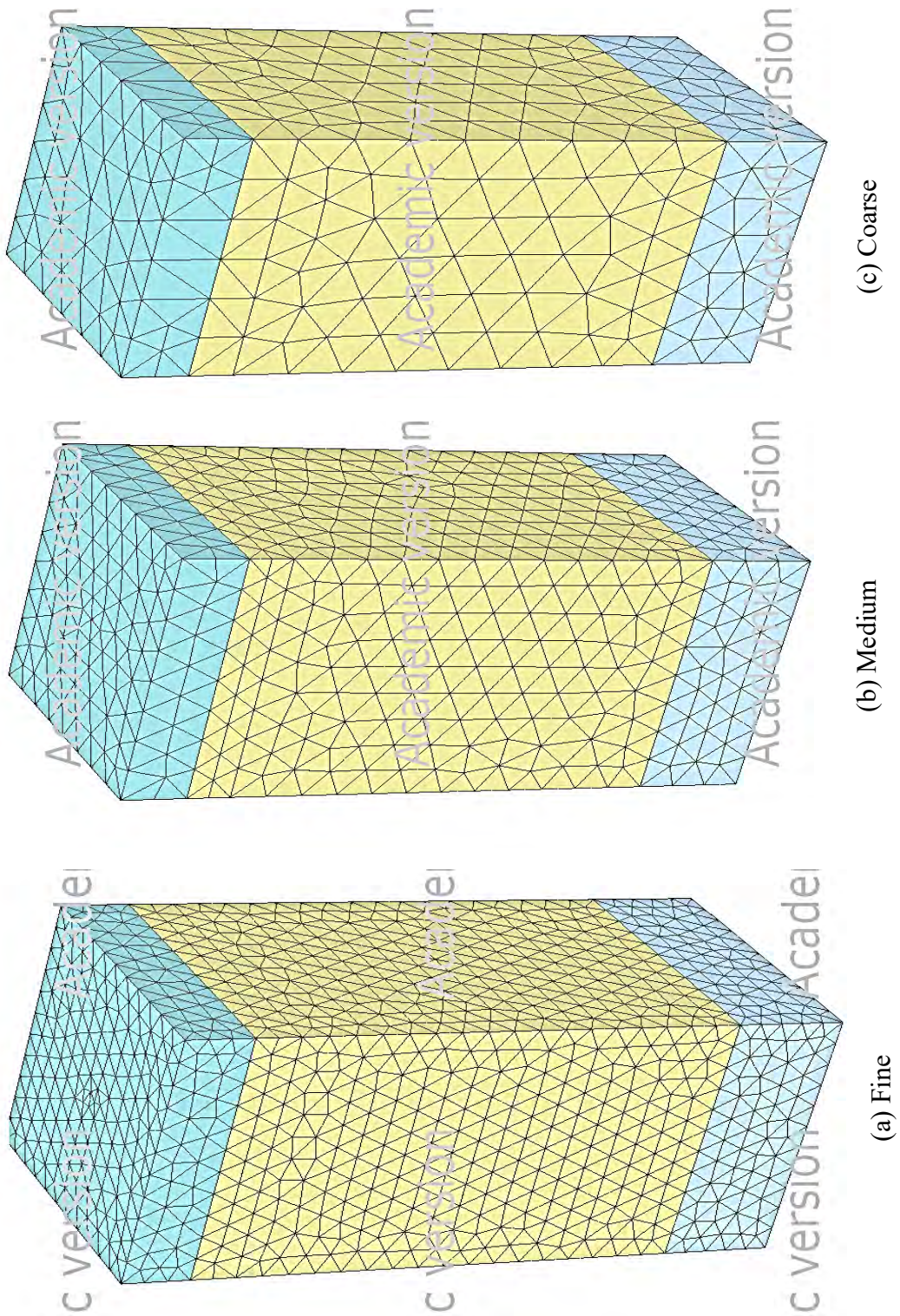


**Figure 4.10:** mesh element connectivity plot

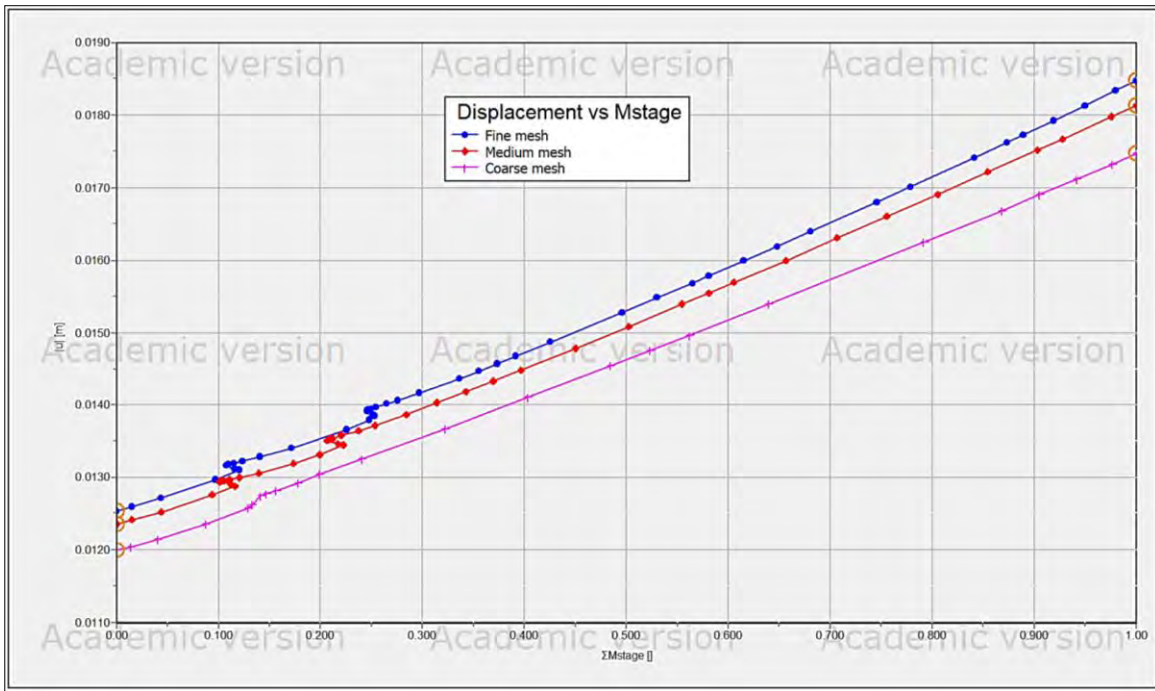


**Figure 4.11:** Total displacement of pile with respect to full loading stage for different mesh condition

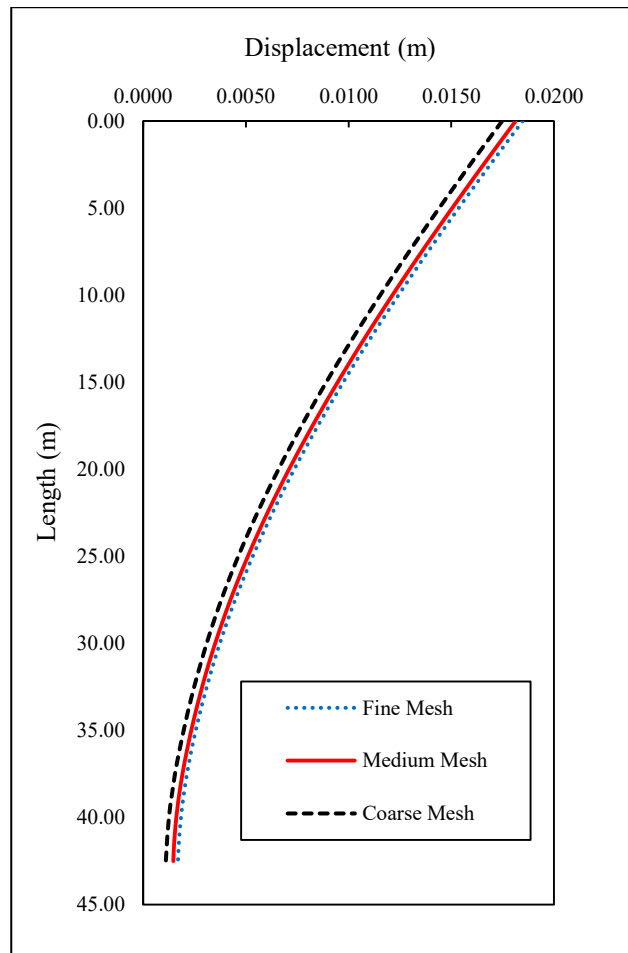


**Figure 4.12:** Distribution of displacement with pile depth for different mesh condition

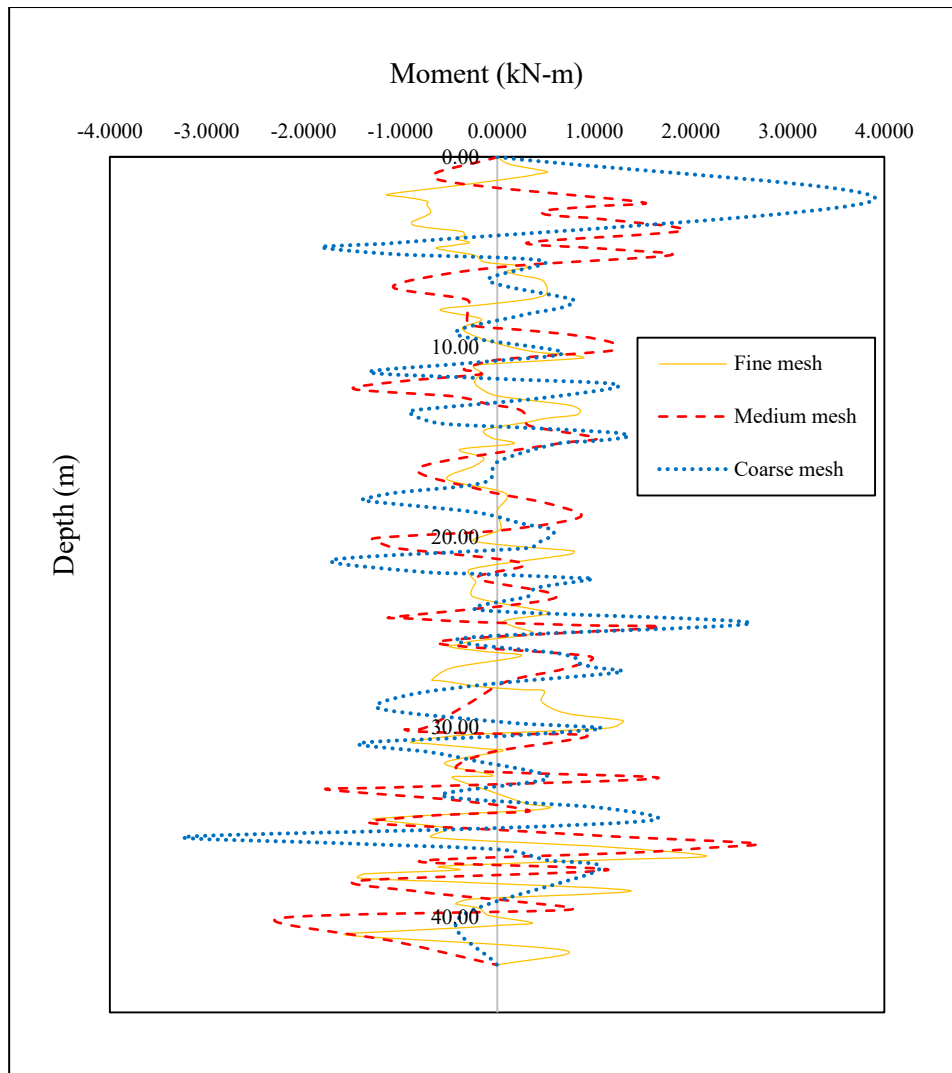


**Figure 4.13:** Comparison of moment for different mesh size

#### 4.6.2 Effect of Pile Length

To achieve adequate bearing capacity, a pile tip needs to be placed in dense stratum of soil. In this study the different soil layers from borelog shows that up-to 37.5 m depth soil is clayey silt. After that the dense sand layer is found with SPT value 50. The required pile depth is 42.5 m for this area. To observe the effect of pile length on displacement, three pile depths 35 m, 42.5 m and 50 m are selected. By using pile length 35 m, pile shows higher displacement about 24.20 mm. But when pile lengths are 42.5 and 50 m, the pile shows almost similar displacement 18.47 mm and 18.56 mm respectively which are lower than the displacement related to 35 m pile length as shown in Figure 4.14. It can be seen that increase in pile length can reduce pile displacement significantly.



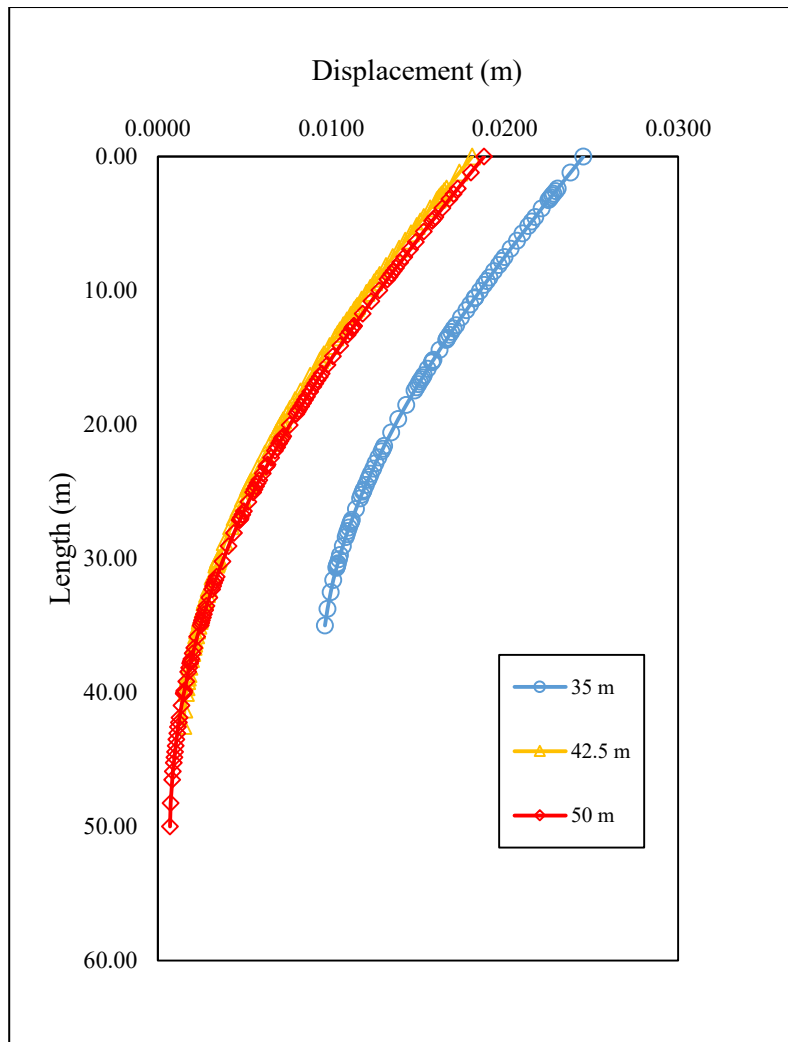


**Figure 4.14:** Distribution of displacement with pile depth for different pile length

### 4.6.3 Effect of Pile Diameter

Effect of pile diameter on axially loaded pile is investigated by considering three different pile diameters and same wall thickness in this analysis, i.e 400, 450 and 500 mm. Wall thickness of the hollow pile is assumed to be 110 mm in all cases. This variation shows that pile with larger diameter results in lower displacement of pile at the top whereas small diameter pile causes larger displacement, see Figure 4.15. The maximum displacement of pile occurs at the top in loose sandy soil. For D 400 and 450 mm the displacements are 24.02 and 18.47 mm. For D = 500 mm the displacement is 16.50 mm. That portrays that piles with larger diameters offers more resistance to the soil movements, resulting in a higher load carrying capacity of pile.

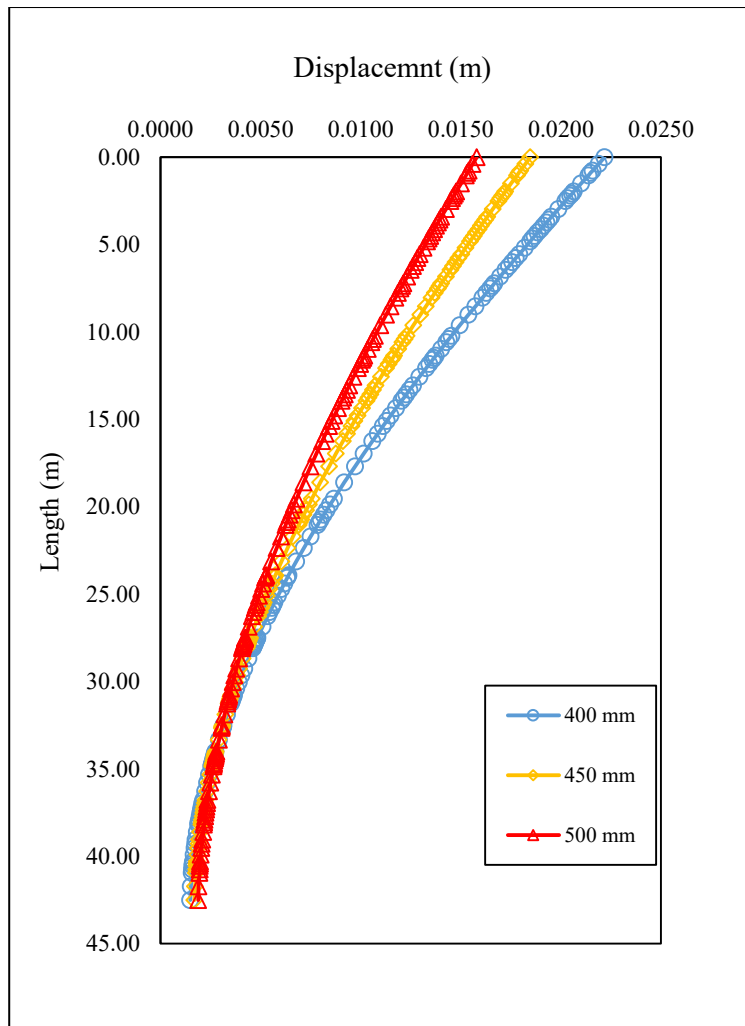


**Figure 4.15:** Distribution of displacement with pile depth for different pile diameter

#### 4.7 Earthquake Analysis

For earthquake analysis, the free field site response has been carried out along a 1D linear elastic frequency domain. In this study, PLAXIS 3D finite element software is used to conduct this analysis. For the current study HS model is used for modeling soil element according to soil investigation done in the study site previously. The earthquake load is applied at the bottom of the FEM model as prescribed displacement. In dynamic loading condition, using HS model generates plastic strain with increased preconsolidation stress in soil. Under this condition damping is defined by Rayleigh damping. The stage construction phases in PLAXIS 3D for earthquake loading condition are given below in Table 4.6.

**Table 4.6:** Stage construction phases for earthquake analysis

Phase	Analysis type	Elements	Activated
Initial	K <sub>0</sub>	Soil volume	√
		Embedded pile element	x
		Point load	x
Pile construction	Plastic	Soil volume	√
		Embedded pile element	√
		Point load	x
Loading stage	Plastic	Soil volume	√
		Embedded pile element	√
		Point load (design load)	√
		Deformation in z direction	√
Earthquake loading stage	Dynamic	Soil volume	√
		Embedded pile element	√
		Prescribed surface displacement (input earthquake loading)	√
		Deformation in x direction	√
		Boundary condition for dynamic	√

#### 4.7.1 Dynamic Soil Behavior

Constitutive model presents in PLAXIS needs to be validated for seismic analysis before implementation. Every constitutive model can be used for modeling material behavior. But due to some limitations each model cannot simulate seismic behavior. During an earthquake, soil is subjected to cyclic shear loading showing a nonlinear dissipative behavior. The total amount of damping is introduced through frequency dependent Rayleigh formula. Which is considered in HS model as previously discussed. Generally HS and hardening soil with small strain (HSSM) models are recognized for using in earthquake analysis. Here in this study, Hardening Soil model with the same soil properties have been used for seismic analysis as shown in Table-4.1 with assigning 5% Rayleigh damping as shown in Figure 4.16.



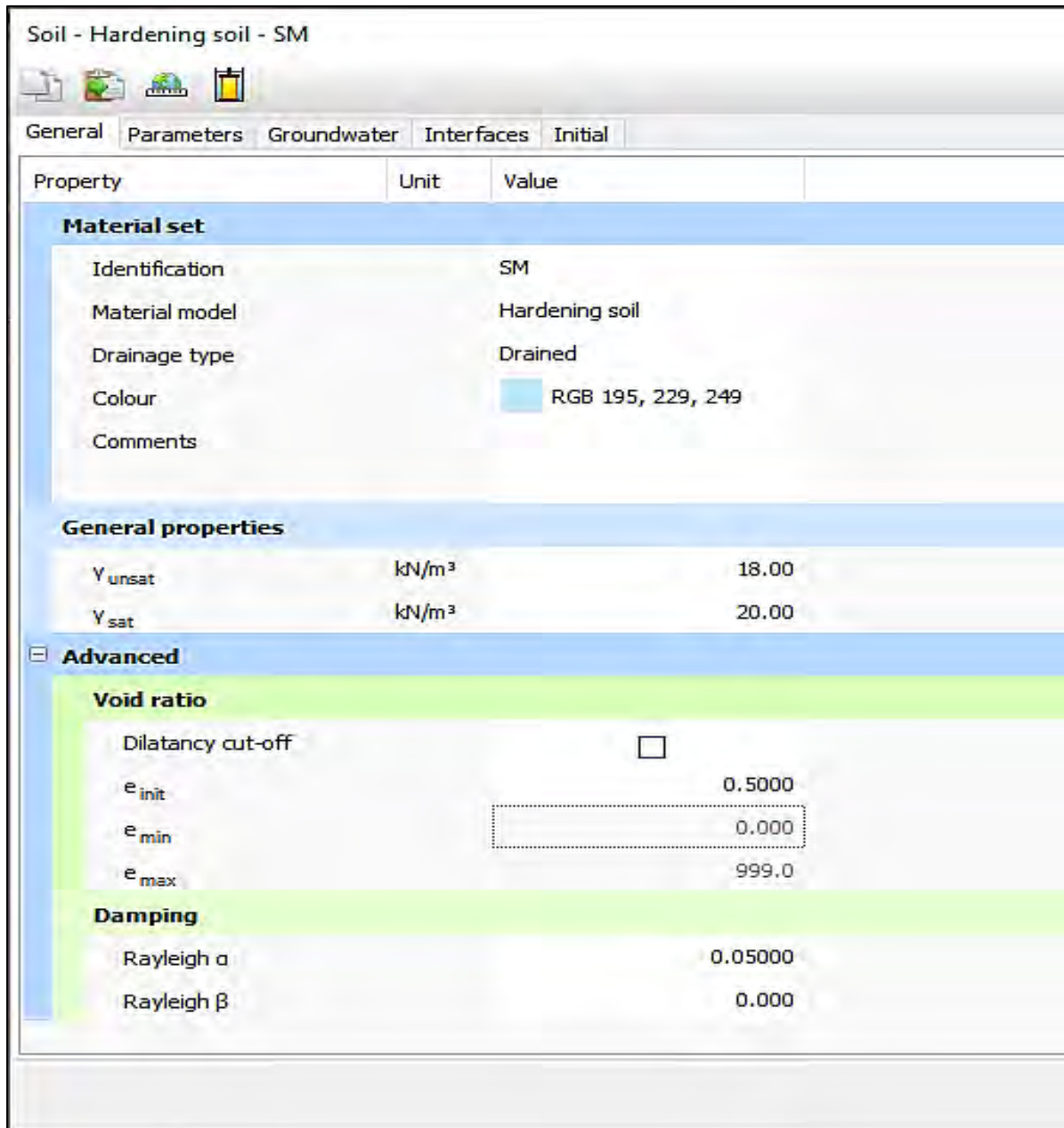
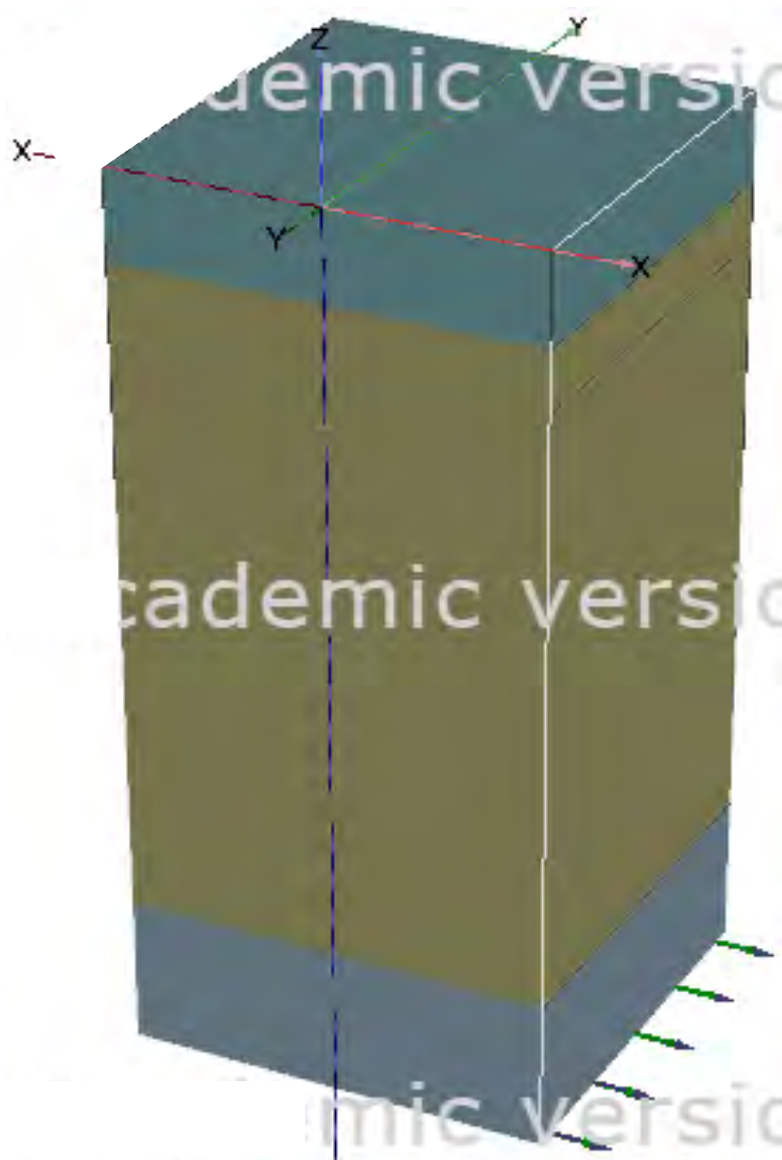


Figure 4.16: Assigned Rayleigh damping for soil

#### 4.7.2 Boundary Condition

A proper boundary condition is important for analyzing pile accurately. The overall dimension of the model is same as the axially loaded pile model. Earthquake load is applied in the model as uniform prescribed displacement in x direction as shown in Figure 4.17. The deformation is free in  $X_{min}$  and  $X_{max}$  direction. In  $Y_{min,max}$  and  $Z_{min,max}$  direction the deformation is kept fixed. To introduce the soil strength reduction due to soil movement, an interface surface with strength reduction at the bottom surface is added. For input seismic motion the boundaries in x

direction are kept free. The free field boundary condition for lateral deformation keeps the boundary free for motion to move at the sides and also absorbs the reflected secondary waves. In Y direction it is none as no absorbant boundary condition is applied. In  $Z_{min}$  compliant base is assigned and  $Z_{max}$  is none for unabsorbing bedrock. A Compliant base boundary for bottom boundary ensures the reflection of waves from above layers are absorbed and thus direct earthquake accelerogram can be applied directly.



**Figure 4.17:** 3-D view of boundary condition

### 4.7.3 Earthquake Input Signal

In this analysis 1995 Kobe and 1989 Loma Prieta earthquake motions are used. These two motions have different characteristics. Kobe earthquake is a severe one with a magnitude  $M_w=7.2$  and  $PGA = 0.75 g$ . Loma Prieta has a magnitude  $M_w= 6.8$  and  $PGA = 0.36 g$ . The acceleration time histories of 40 s duration are presented in Figure 4.18 a and b. These records are applied in the horizontal direction at all bottom node of the model. They are scaled into same acceleration 0.15 g for Dhaka zone. In order to reduce the calculation time only 5 s of Kobe earthquake and 5 s of Loma prieta earthquake are applied. Figure 4.19 shows the Kobe earthquake acceleration data input in PLAXIS 3D for earthquake analysis.

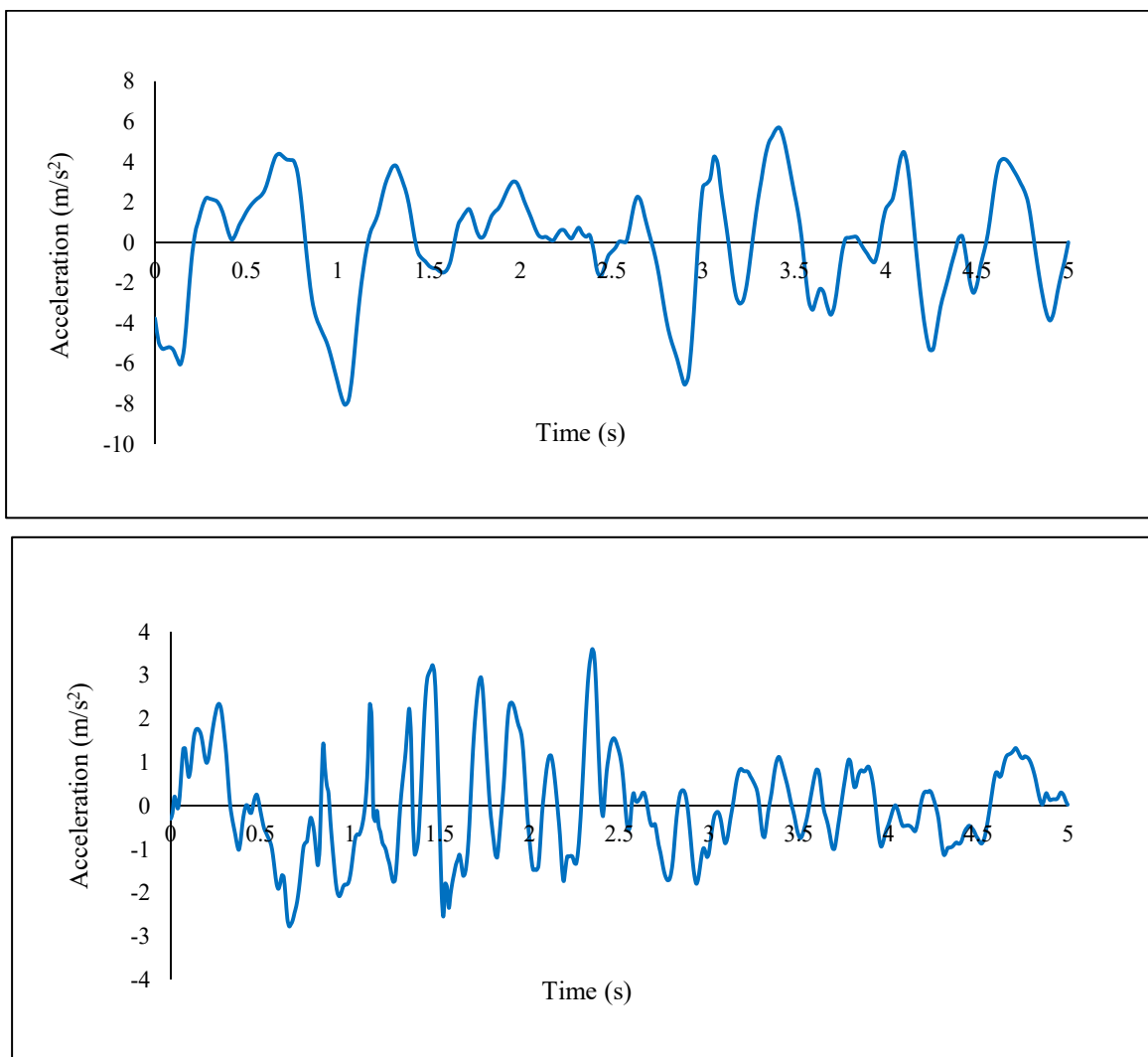


**Figure 4.18:** Original earthquake frequency (a) 1995 Kobe (b) 1989 Loma Prieta.

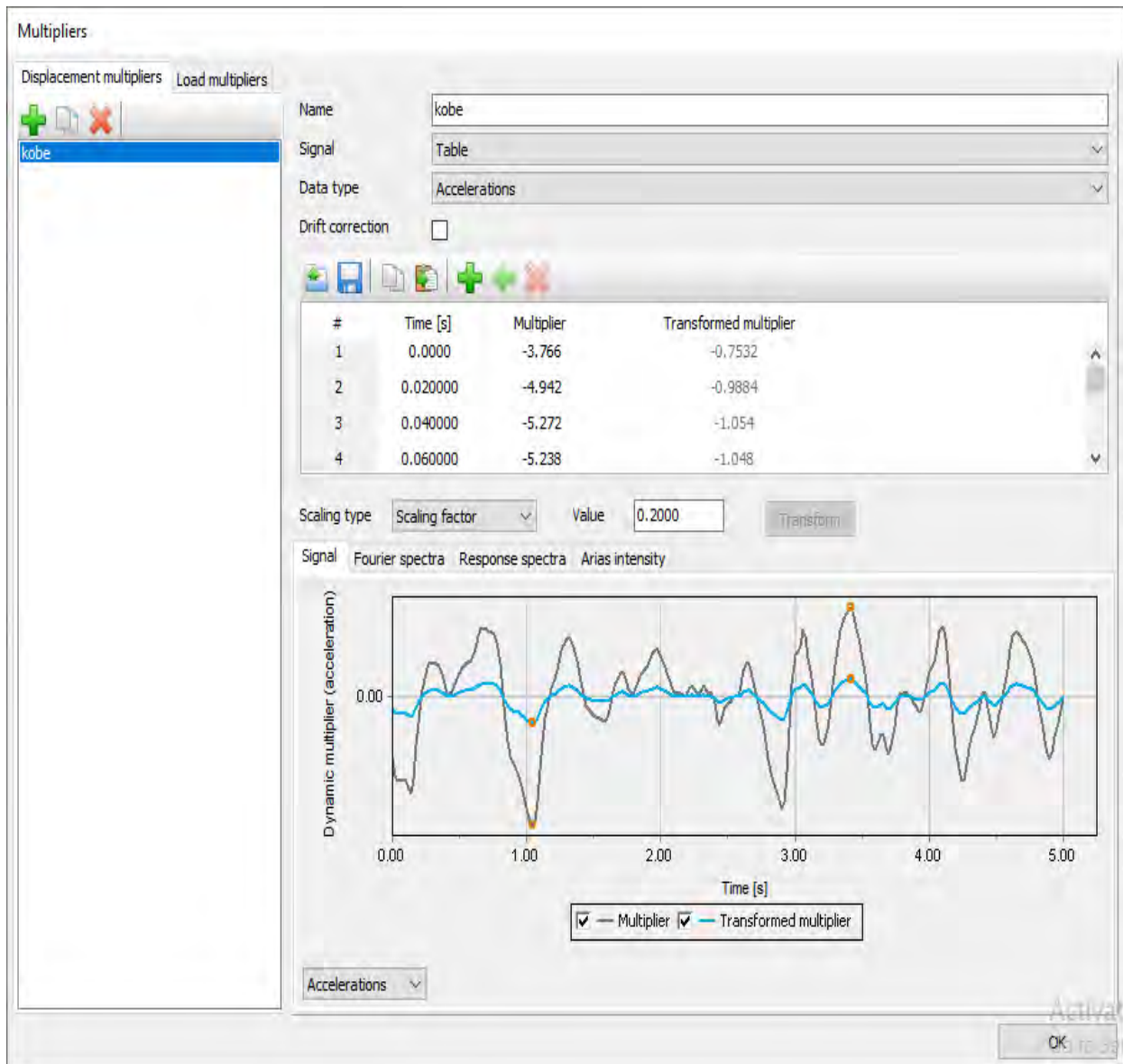
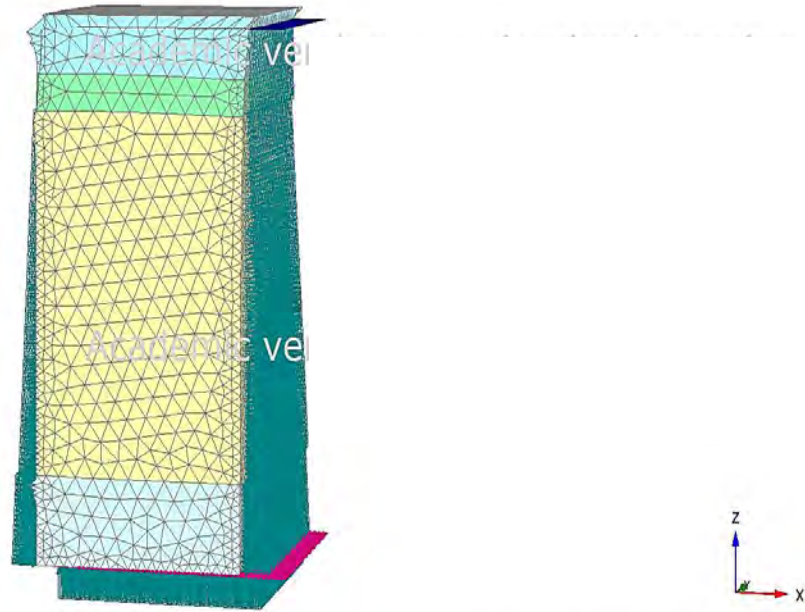


**Figure 4.19:** Kobe earthquake input signal

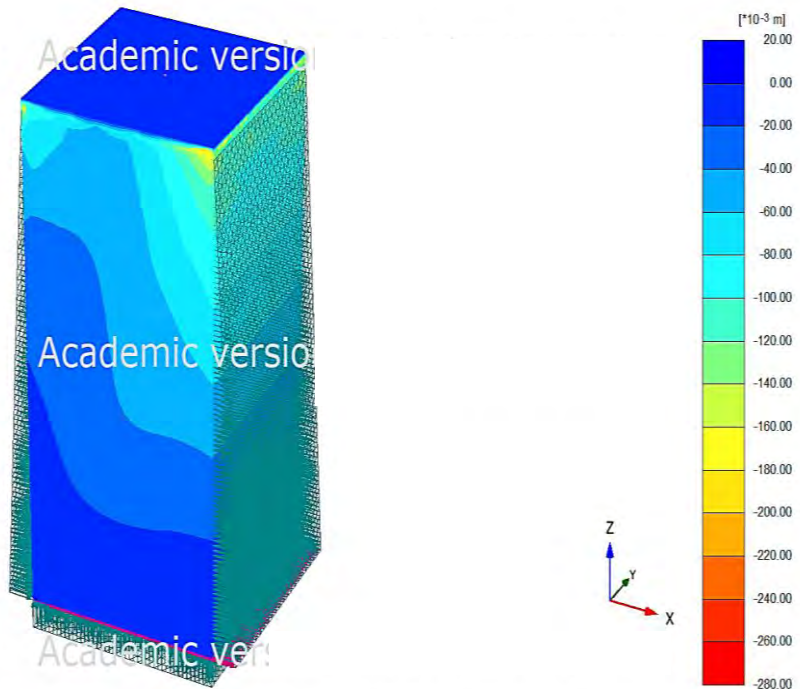
#### 4.8 Pile Deformation under Earthquake Loading

The deformed shape of soil body after a seismic activity can be observed in Figure 4.20. It is seen that the top soil layer is displaced in x direction relating more than the other soil layers as the top layer is loose sandy soil. The vertical and lateral deformation of soil are illustrated in Figure 4.21 and 4.22. It is found that majority of the vertical deformation are concentrated at the boundaries but in case of lateral deformation, it is spread all over the soil body, see Figure 4.22 and 4.23.



Deformed mesh  $|u|$  (scaled up 5.00 times) (Time 5.000 s)  
 Maximum value = 1.051 m (at Node 31858)

**Figure 4.20:** Soil deformation due to earthquake loading (Kobe)



Total displacements  $u_z$  (scaled up 5.00 times) (Time 5.000 s)  
 Maximum value =  $0.3141 \cdot 10^{-3}$  m (Element 22498 at Node 8016)  
 Minimum value = -0.2750 m (Element 776 at Node 60108)

**Figure 4.21:** Vertical displacement of soil under earthquake loading



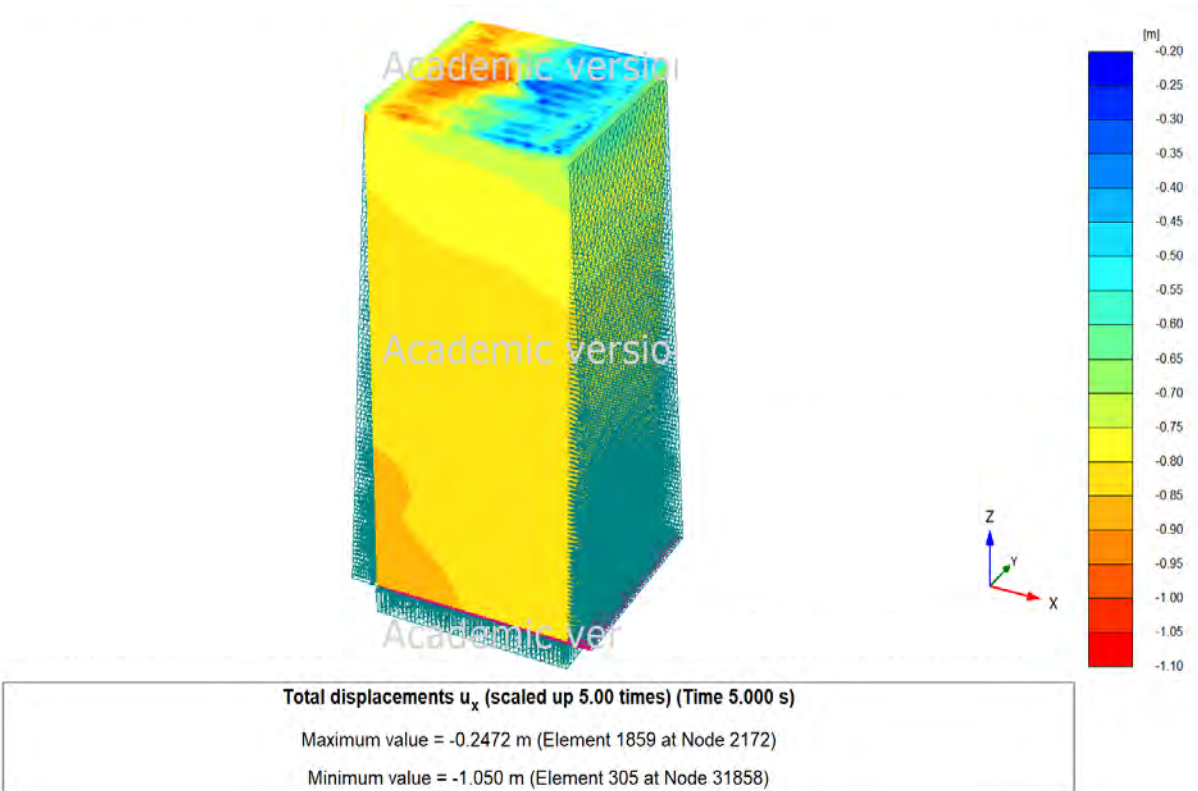


**Figure 4.22:** Lateral displacement of soil under earthquake loading

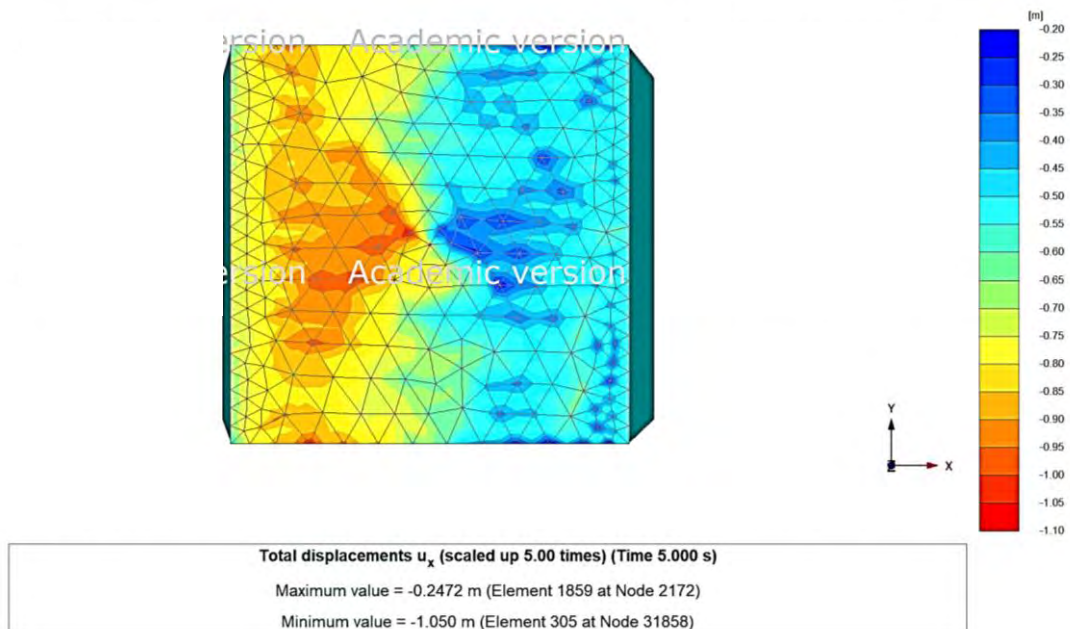


**Figure 4.23:** Top view of lateral displacement of soil under earthquake loading

The displacement in pile occurred due to earthquake loading is compared with the displacement occurred only under axial loading over the length of pile. The displacement at the top of the pile is significantly increased for earthquake loading condition than the axial load. In case of Loma Prieta earthquake, the pile top displacement is increased by 8.5 times than axial load and for Kobe earthquake loading it is reported to be increased by 40 times as shown in Figure 4.24. This phenomenon explains that during seismic action a pile can experience excessive lateral deformation and tends to fail. But during axial loading condition the pile can sustain the load with a minimum settlement. So seismic assesment should be taken into account even the pile can sustain the compressive load.

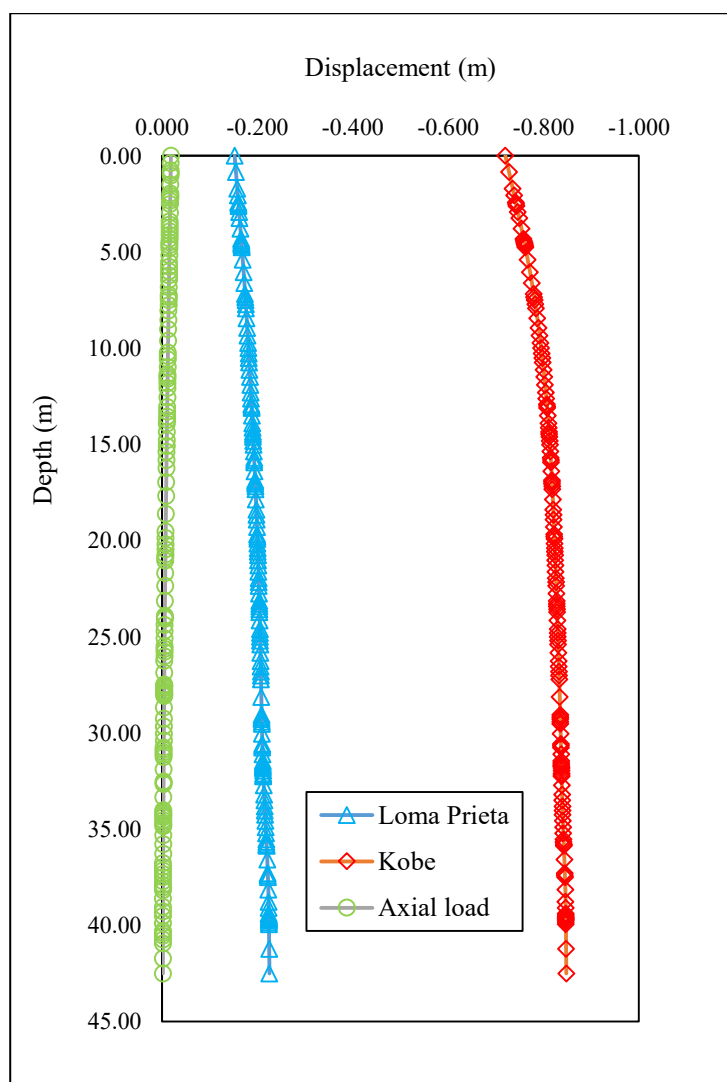


**Figure 4.24:** Displacement comparison of pile under both axial and earthquake loading

Earthquake load produces internal forces in the structure which causes stresses in foundation system and propagates to the soil. These spectrums describe the maximum response of foundation system for a specified earthquake ground motion and 5% of damping. The PSA value with respect to the natural period of vibration of structure allows to calculate the maximum shear stress at the base of the structure. In Figure 4.25 spectral acceleration for Kobe earthquake is compared at three different depth of soil body for damping ratio  $\xi = 5\%$ . At top layer of soil there is loose sand which is susceptible to liquefaction during earthquake. This liquefiable layer magnifies the response spectra as shown in Figure 4.25 with blue color. The red and cyan color spectral acceleration represents the mid and bottom layer respectively. The PSA for these two layers are relatively lower than the top layer as these layers have stiffer soil properties. The predominant period can be determined from PSA graph, which is 0.25 s. Figure 4.26 shows the magnitude of acceleration in x direction of Kobe earthquake at three different soil depth. It is evident that at the top layer the acceleration is amplified.

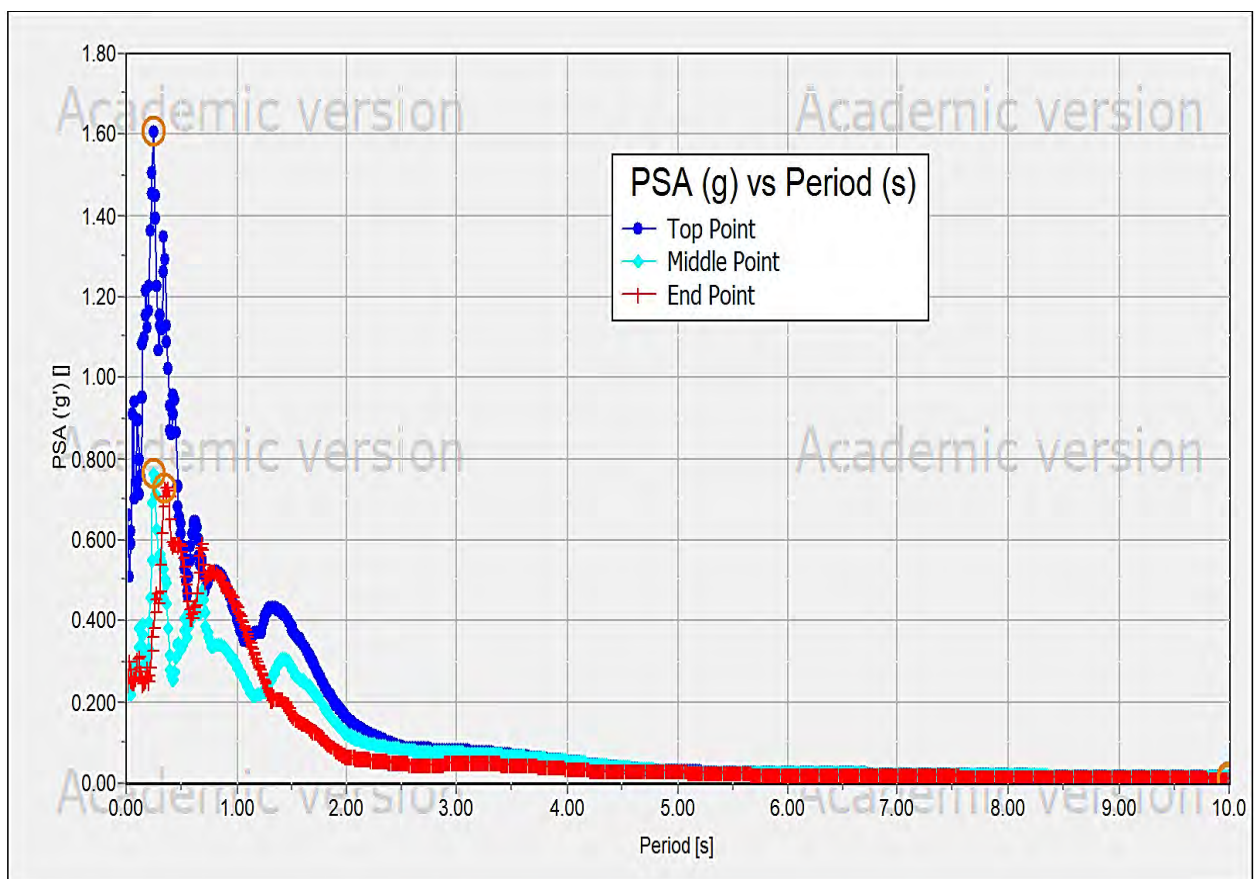


**Figure 4.25:** Acceleration response spectrum of analysed model for Kobe earthquake at different depth



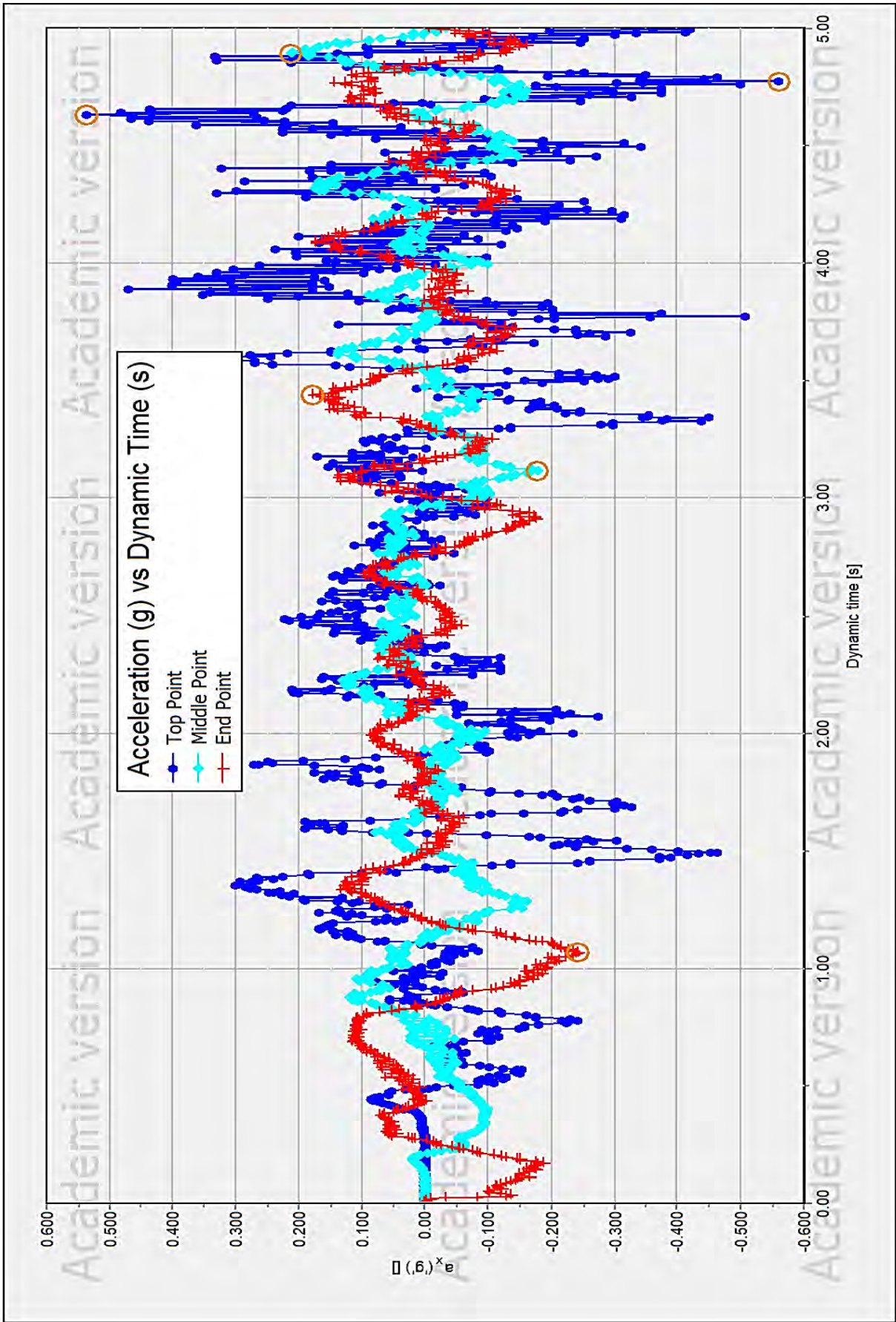


**Figure 4.26:** Earthquake acceleration at different depth of soil

The ratio of acceleration response at the top to the response at the bottom is reported in Figure 4.27. It shows that the top point is amplified to 131 ratio with respect to bottom point under given earthquake loading.

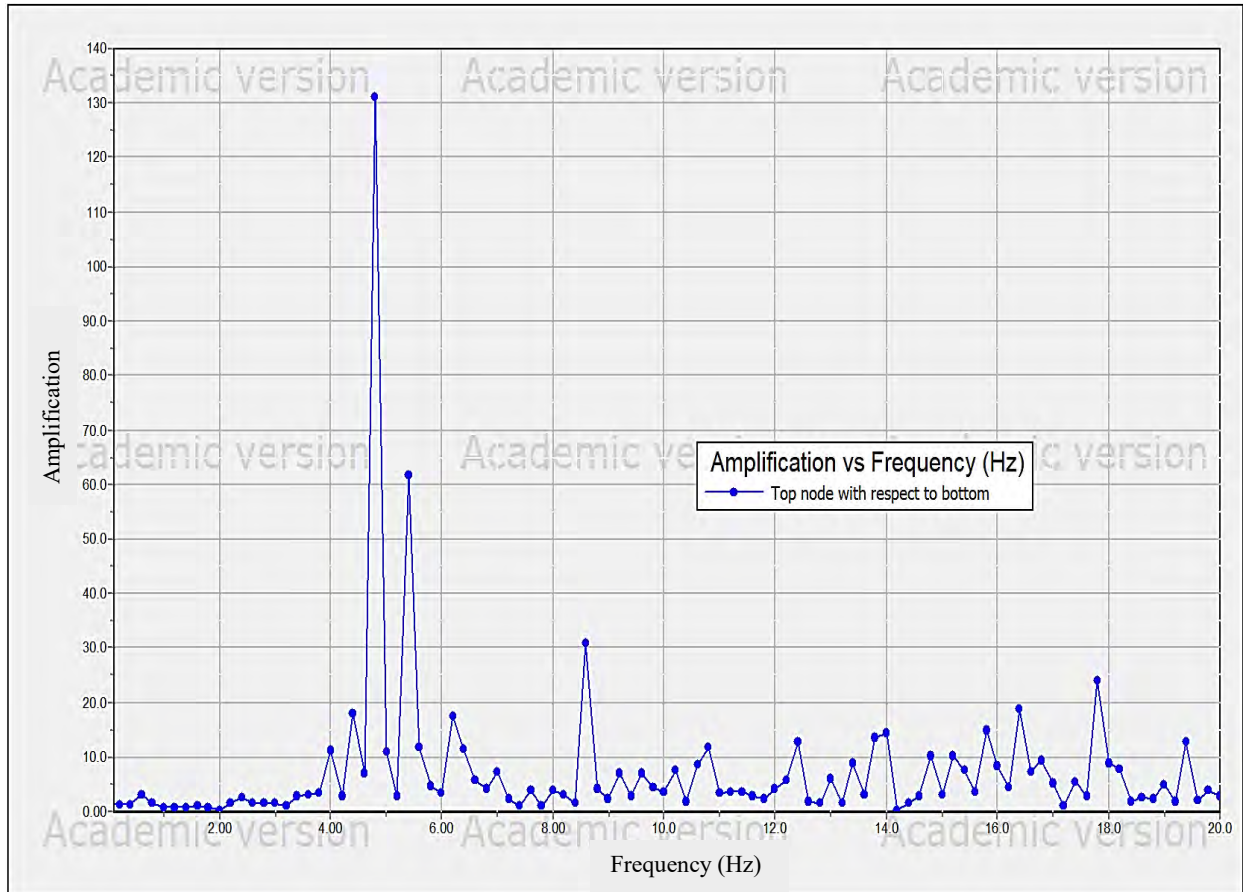


**Figure 4.27:** Amplification spectrum

The maximum strain develops at top and bottom stress point in soil element are shown in Figure 4.28 and 4.29 for Kobe and Loma Prieta earthquake. It is seen that at top the strain value of Kobe earthquake is 7.6 times greater than Loma Prieta whereas at bottom point it is 1.6 times higher with respect to Loma Prieta earthquake. It is clear that the seismic excitation causes large deformation at top level by magnifying the response spectrum. Large magnitude earthquake can develop higher strain in soil body.

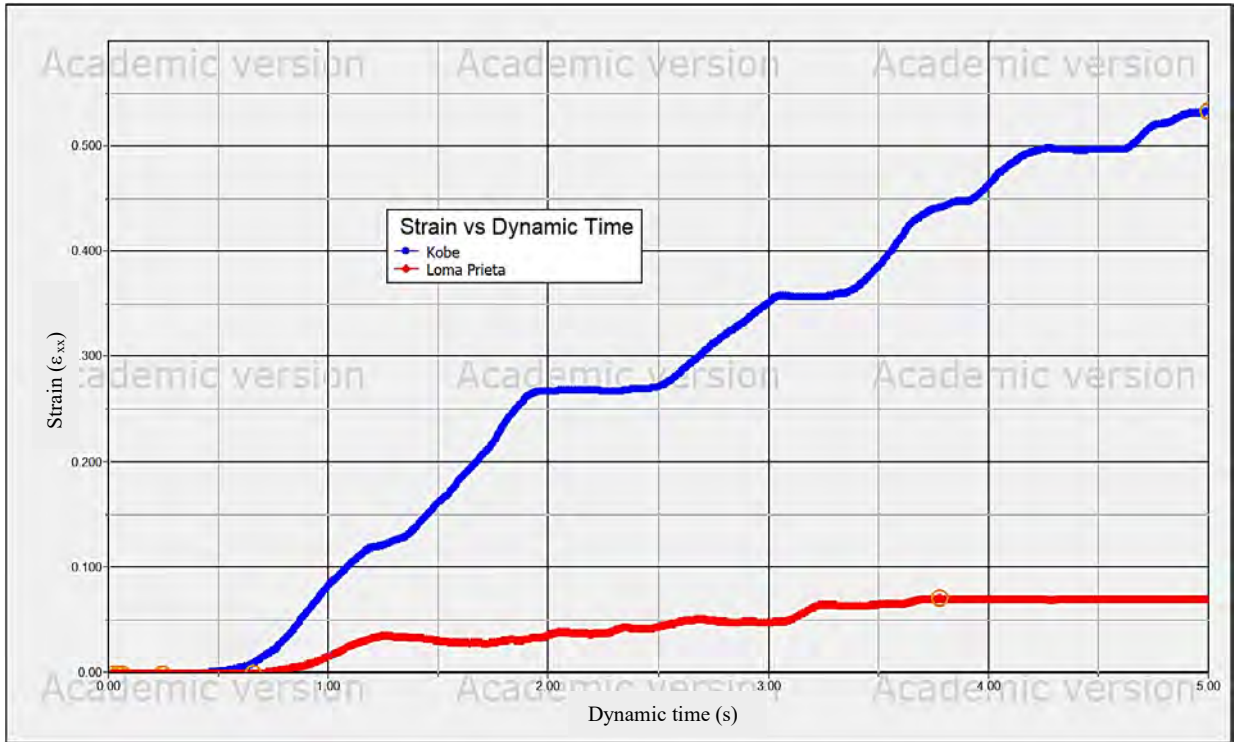


**Figure 4.28:** Maximum strain at top of soil profile for earthquake loading

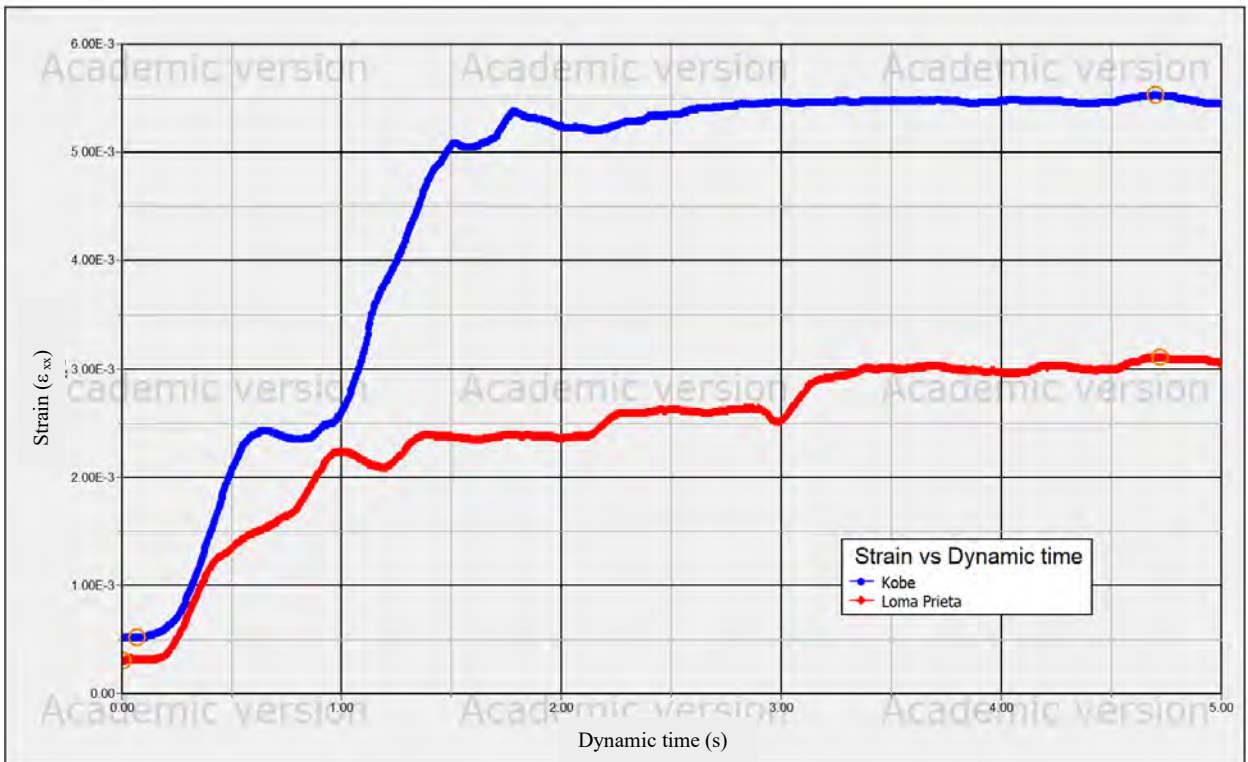


**Figure 4.29:** Maximum strain at bottom of soil profile for earthquake loading



Maximum shear stress  $\tau_{\max}$  in the soil at the bottom of the pile is shown in Figure 4.30. At maximum shear stress the Mohr's circle is expanded to touch coulomb failure envelop. The max value of shear stress is 146 kN/m<sup>2</sup>. It is 7.2 % higher than the shear stress under axial loading, see Figure 4.31. Total stress increases about 8.5 % for seismic activity than only axial loading condition at the bottom of pile as shown in Figure 4.32.

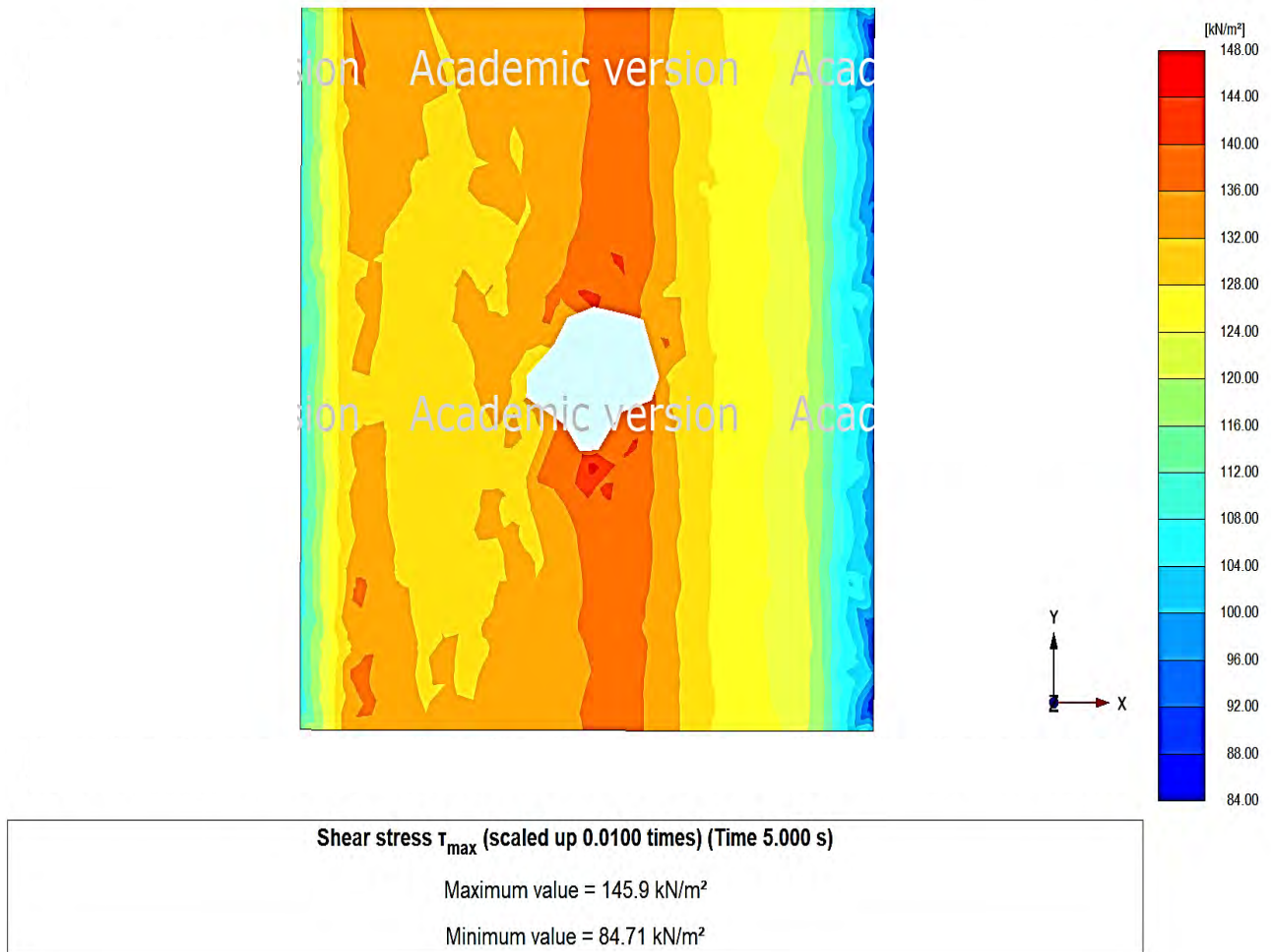


**Figure 4.30:** Maximum shear stress under earthquake loading

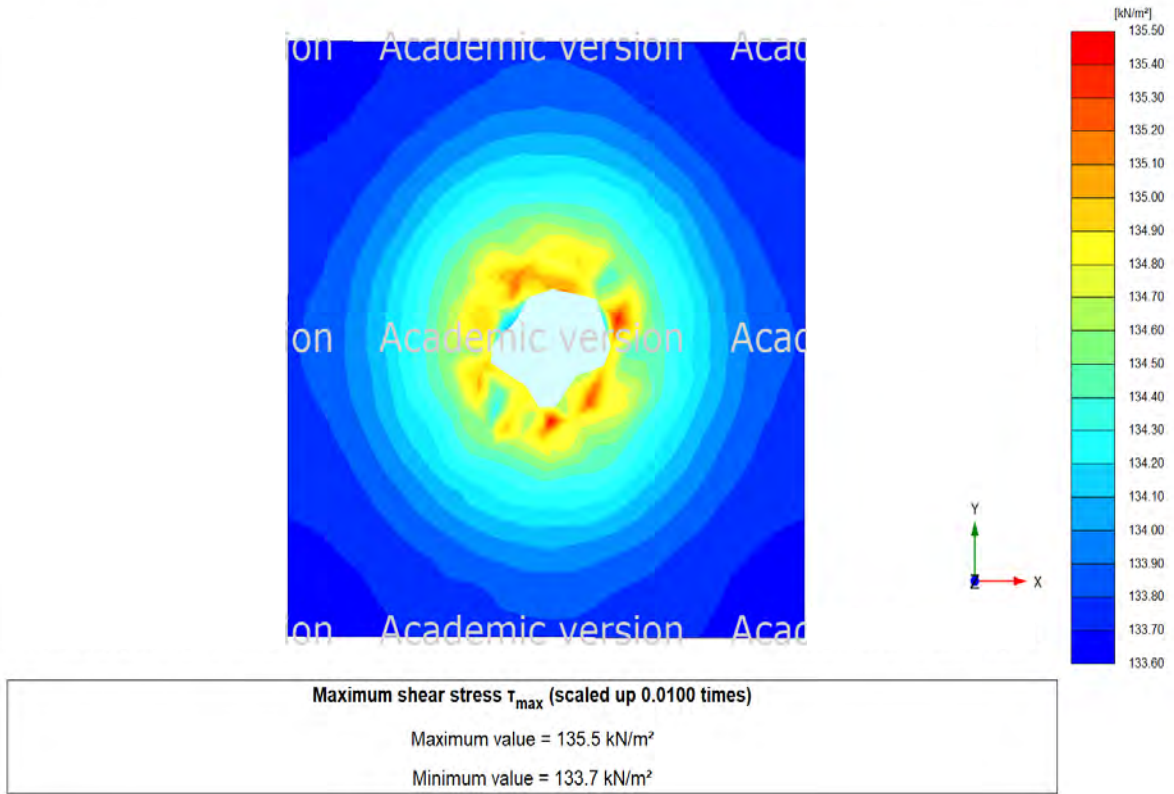


**Figure 4.31:** Maximum shear stress under maximum axial loading

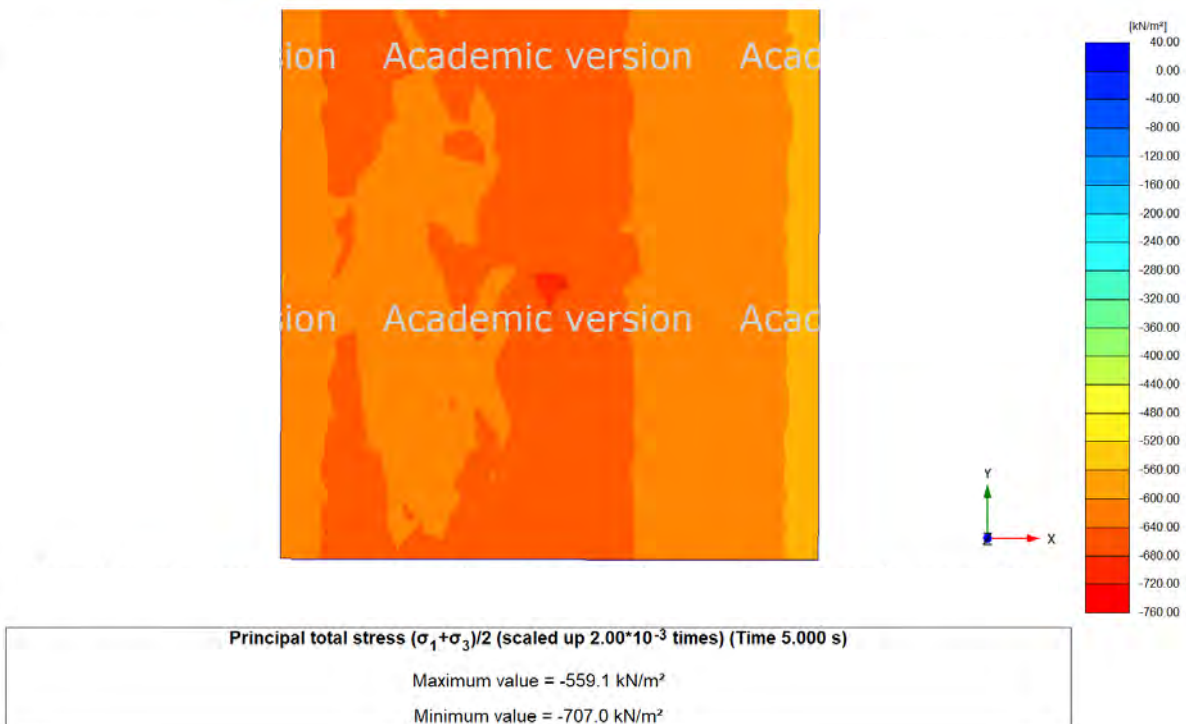


**Figure 4.32:** Principle total stress under earthquake loading

## 4.9 Liquefaction Analysis

During earthquake seismic wave propagation, it not only causes damage to structure but also initiate other phenomenon like landslides and soil liquefaction. So liquefaction should also be considered while performing site response analysis in loose cohesionless soil. To evaluate the liquefaction potentiality, the triggering factor for liquefaction is to be identified. The triggering factors depend on the earthquake magnitude, duration and peak ground acceleration. To understand the possibility of liquefaction in a specific site nonlinear dynamic analysis can be done. In PLAXIS 3D hardening soil model is not able to capture the liquefaction phenomenon. The UBC3D-PLM is a nonlinear elastic-plastic model that is capable of capturing seismic liquefaction behavior of sands and silty sands. The model can accumulate strain and pore pressure of sandy soil that can capture the onset of liquefaction. the Initialy UBC3DPLM implementation in PLAXIS was developed by Tsegaye (2010).

### 4.9.1 Liquefiable Sand Layer Parameters

The parameters for UBC3D-PLM can be determined from laboratory tests under cyclic loading but if it is not possible then data can be extracted from in-situ tests like SPT N value and CPT. There are some corelation proposed by Beaty and Byrne (1998) which can be used to determine required parameters from corrected SPT N value. The correlations are presented below:

$$K_G^e = 21.7 \times 20 \times ((N_1)_{60})^{0.333} \quad (4.1)$$

Here  $K_G^e$  is the elastic shear modulus

$$K_B^e = K_G^e \times 0.7 \quad (4.2)$$

Here  $K_B^e$  is the elastic bulk modulus

$$K_G^p = K_G^e \times ((N_1)_{60})^2 \times 0.003 + 100.0 \quad (4.3)$$

Where  $K_G^p$  is the plastic shear modulus

$$\varphi_{pi} = \varphi_{cv} + \frac{(N_1)_{60}}{10} \quad (4.4)$$

$$\varphi_p = \varphi_{pi} + \max(0.0, \frac{(N_1)_{60} - 15}{5}) \quad (4.5)$$

Where  $\varphi_{pi}$  and  $\varphi_{cv}$  are peak friction angle and constant volume friction angle

$$R_f = 1.1 \times ((N_1)_{60})^{-0.15} \quad (4.6)$$

$R_f$  is the failure ratio

In this study, during earthquake analysis the liquefaction phenomenon is not considered and only HS model is used for soil modeling. In this segment earthquake analysis is done considering liquefaction phenomenon with undrained behavior in loose sandy type soil using UBC3D-PLM model. The liquefiable sand layers parameters are shown in Table 4.7

**Table 4.7:** Input parameters of liquefied sand layer of UBC3D-PLM model

Parameters	Symbol	Unit	Value applied in model
Unit weight	$\gamma_{\text{unsat}}$	kN/m <sup>3</sup>	16
Saturated unit weight	$\gamma_{\text{sat}}$	kN/m <sup>3</sup>	17
Poisson's ratio	$\nu$	-	0.3
Constant volume friction angle	$\phi_{\text{cv}}$	(°)	22
Peak friction angle	$\phi_{\text{p}}$	(°)	23
Cohesion	$c$	kPa	0
Elastic shear modulus	$K_G^e$	-	1019.0
Elastic bulk modulus	$K_B^e$	-	713.0
Plastic shear modulus	$K_G^p$	-	617.0
Elastic shear modulus index	$n_e$	-	0.5
Elastic bulk modulus Index	$m_e$	-	0.5
Plastic shear modulus index	$n_p$	-	0.5
Failure ratio	$R_f$	-	0.74
Atmospheric pressure	$P_A$	-	100
Tension cut-off	$\sigma_t$	kPa	0.00
Densification factor	$f_{\text{dens}}$	-	0.45
Corrected SPT value	$(N_1)_{60}$	-	13.0
Post liquefaction Factor	$f_{\text{Epost}}$	-	0.20

Figure 4.33 shows the deformation in soil element at top layer due to liquefaction. It is noted that UBC3D-PLM model can describe the liquefaction phenomenon in loose sandy soil which tends to liquefy at the moment of earthquake loading. There are some other state parameters that can confirm the liquefaction event using UBC3D-PLM model. In PLAXIS liquefaction can be explained by excess pore water pressure ratio  $r_u$ . It is the ratio between excess pore pressure and initial effective vertical stress at the depth.

$$r_u = 1 - \frac{\sigma'_v}{\sigma'_{v0}} \quad (4.7)$$

Here  $\sigma'_v$  is the vertical stress at the end of dynamic calculation and  $\sigma'_{v0}$  is the initial vertical effective stress earlier seismic activity. If  $r_u$  is equal to 1 then the layer is in complete liquefied state. If a layer has  $r_u$  value equal or greater than 0.7 then the layer will be defined as liquefied. In the analysis the maximum excess pore pressure ratio  $r_u$  is about 0.99 ~ 1 as shown in Figure-4.34 and 4.35 for both Kobe and Loma Prieta earthquake is equal to 1.

It is obtained that if a soil layer is loose sandy soil or silty soil it can liquefy during seismic event due to generation of excessive pore pressure. The maximum pore pressure generated during earthquake in the liquefied layer is 1178 kN/m<sup>2</sup> and 1048 kN/m<sup>2</sup> for Kobe and Loma Prieta earthquake as shown in Figure 4.36. It shows that larger the peak acceleration the larger the pore pressure generates. During liquefaction, the relative displacement at pile head increases about 30 to 60 % for both Kobe and Loma Prieta earthquakes as shown in Figure 4.37. It is observed from the deformed shape of pile that the displacement profile puts the pile in bending. It can also be seen that the nonliquefiable layers of the soil begin to displace laterally with respect to the liquefiable layer.



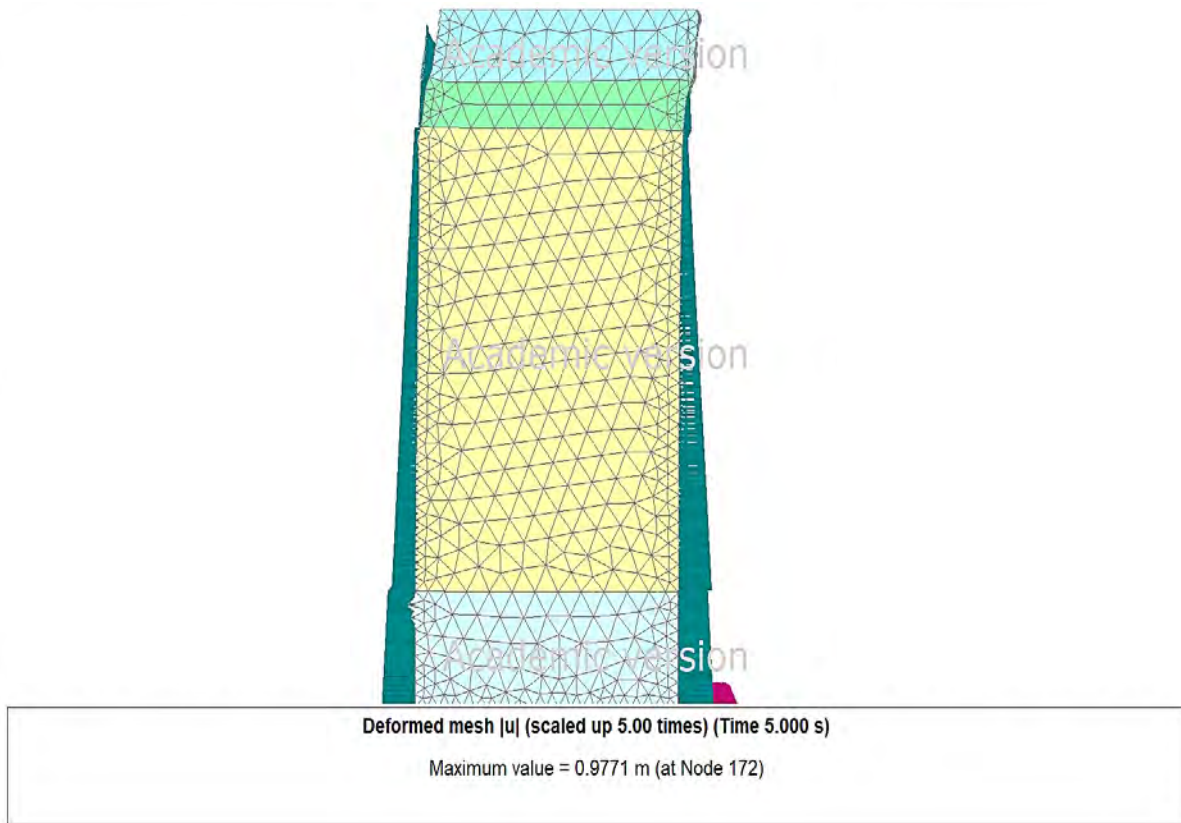


**Figure 4.33:** Deformation at the top soil layer due to liquefaction

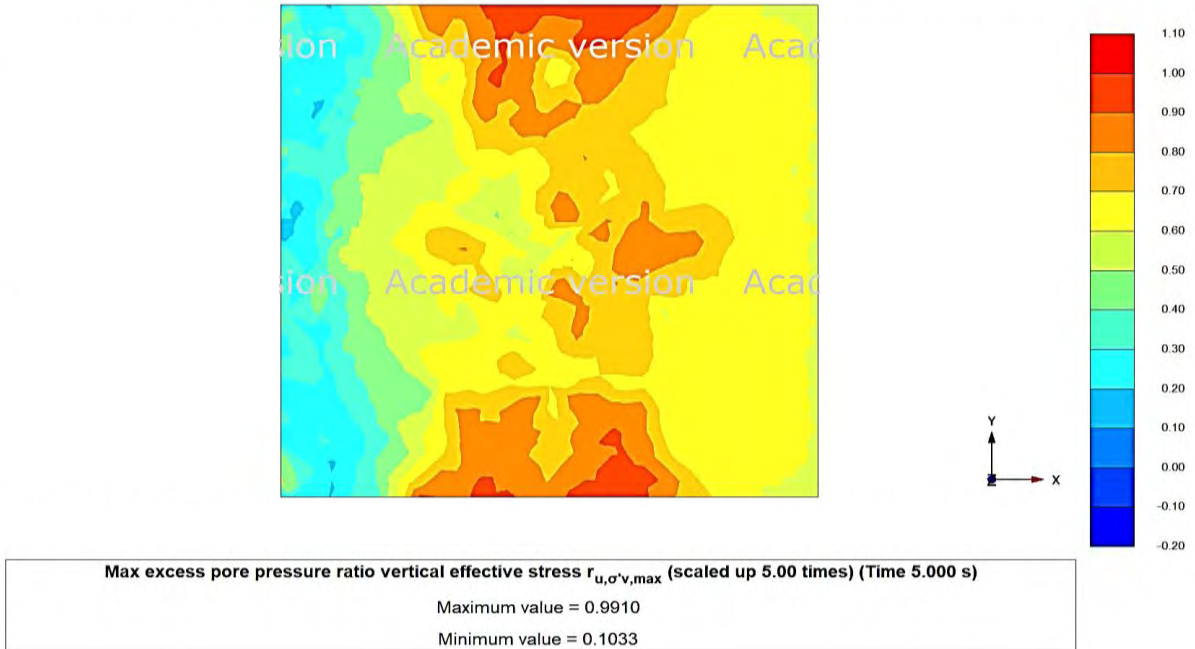


**Figure 4.34:** Maximum pore pressure ratio at top soil layer for Kobe earthquake

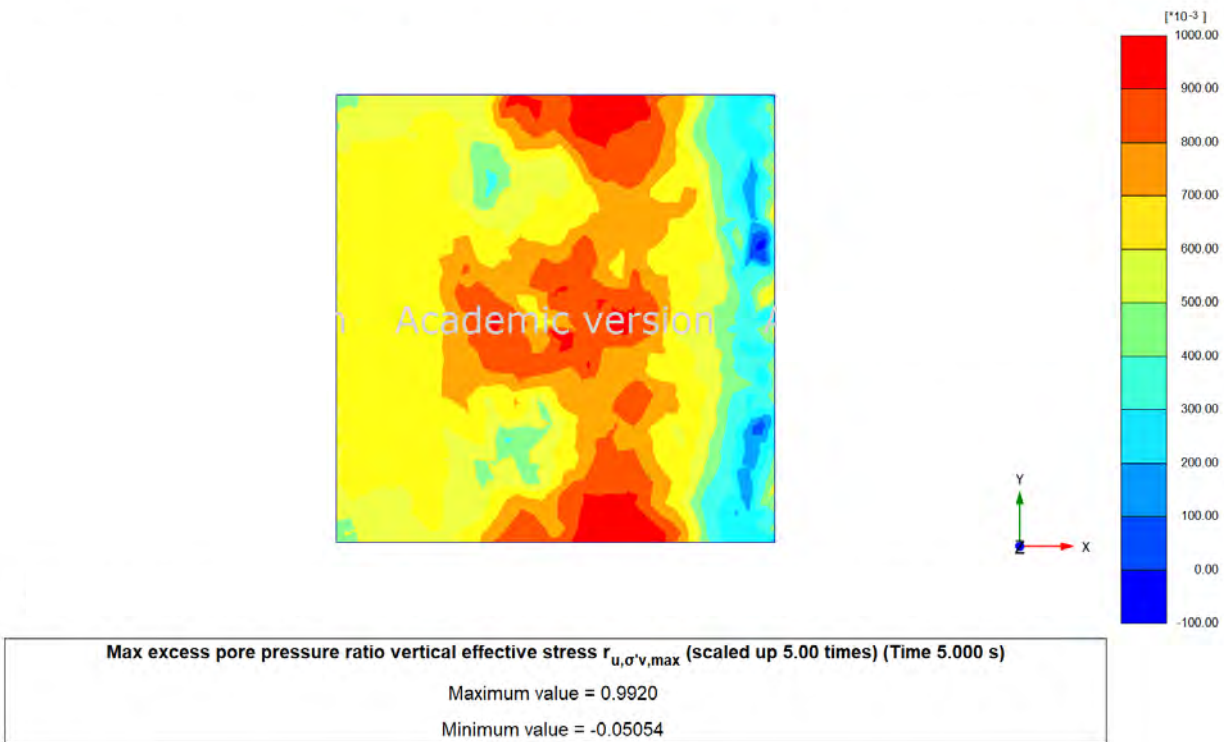


**Figure 4.35:** Maximum pore pressure ratio at top soil layer for Loma Prieta earthquake

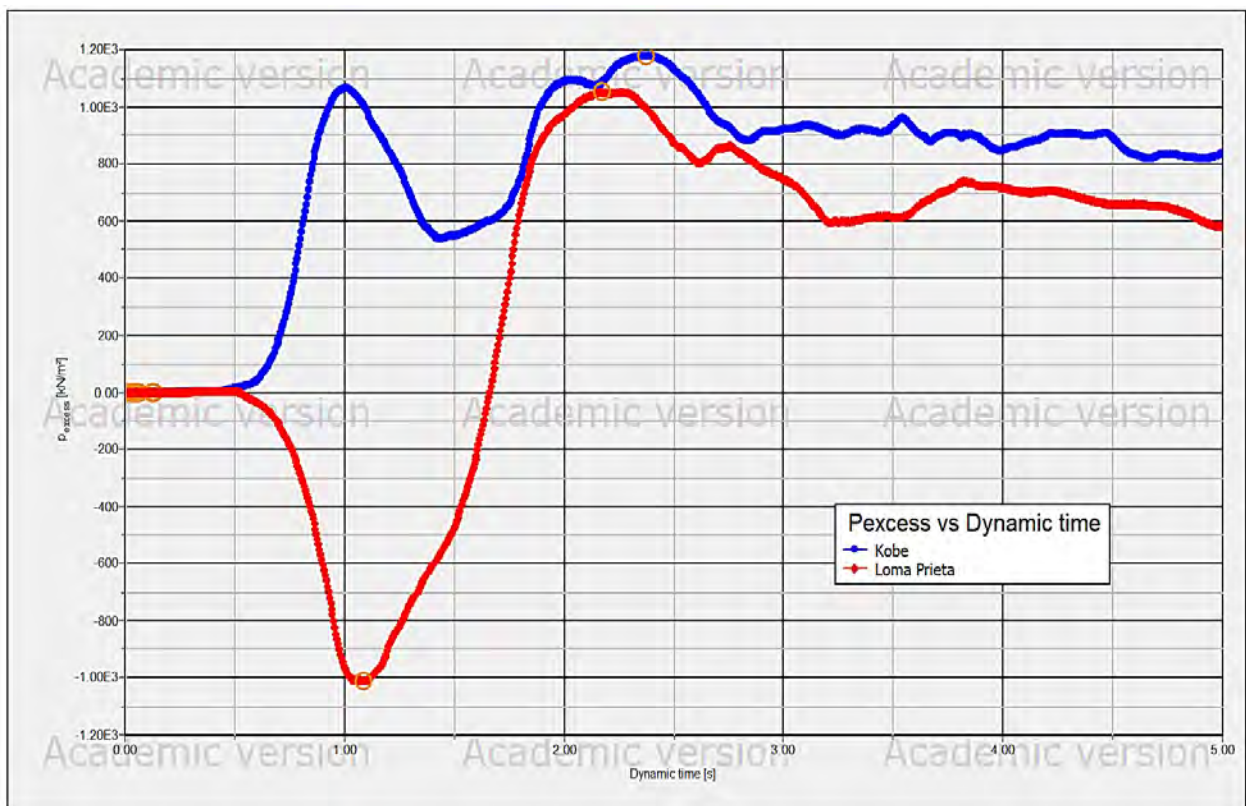


**Figure 4.36:** Maximum excess pore water pressure generated during Kobe and Loma Prieta earthquake

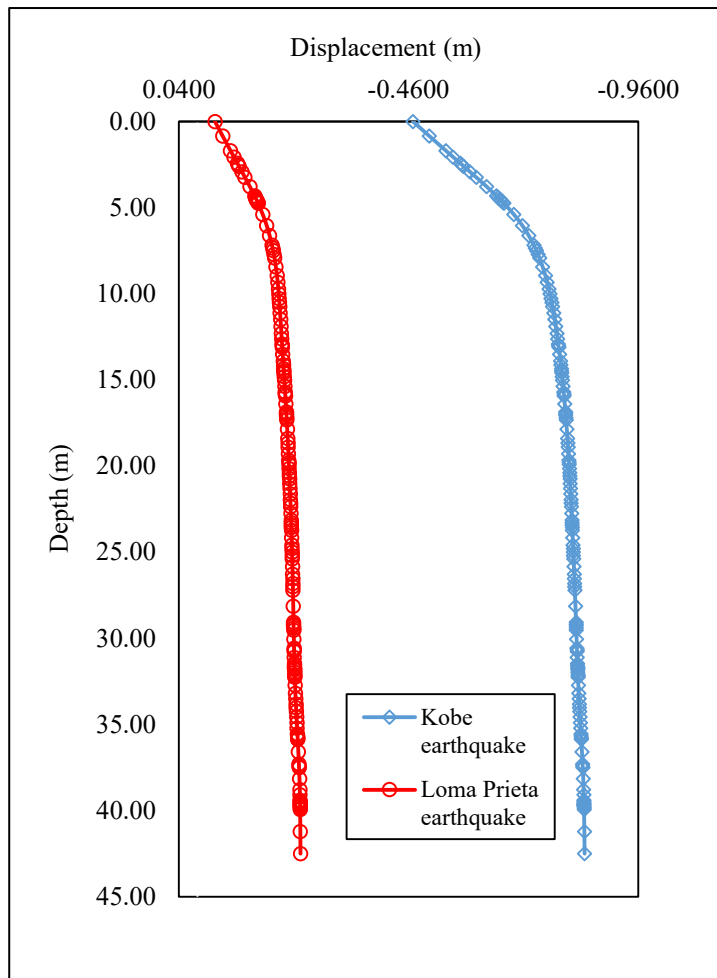


**Figure 4.37:** Displacement comparison of pile under earthquake loading

#### 4.10 Soil Improvement Impact on Liquefiable Soil

The presence of liquefiable soil layer in any site can immensely influence the pile response both in deflection and bending moment especially when subjected to increased magnitude. During seismic action there is possibilities to develop large amount of moment that cannot be resisted by pile. If only earthquake is considered then the observed maximum moment is 42 kN-m and 10 kN-m for Kobe and Loma Prieta earthquake respectively, see Figure 4.38. From the sectional analysis it is found that the maximum moment carrying capacity of 450 mm dia SPC pile is 180 kN-m, see Table 3.1. In this study area as there is fill soil upto 5 m so while liquefaction event is taken into account, the maximum bending moment is found to be 478 kN-m for Kobe earthquake and 242 kN-m for Loma Prieta earthquake. It is 11 times and 26 times higher than the moment found without considering liquefaction, see Figure 4.39. The maximum

bending moment is found at the interface of liquefiable and non-liquefiable soil layers which agrees with the existing literatures. However, location of maximum bending moment also depends on pile head condition. The bending moment demand for fixed head pile is greater than free headed pile.

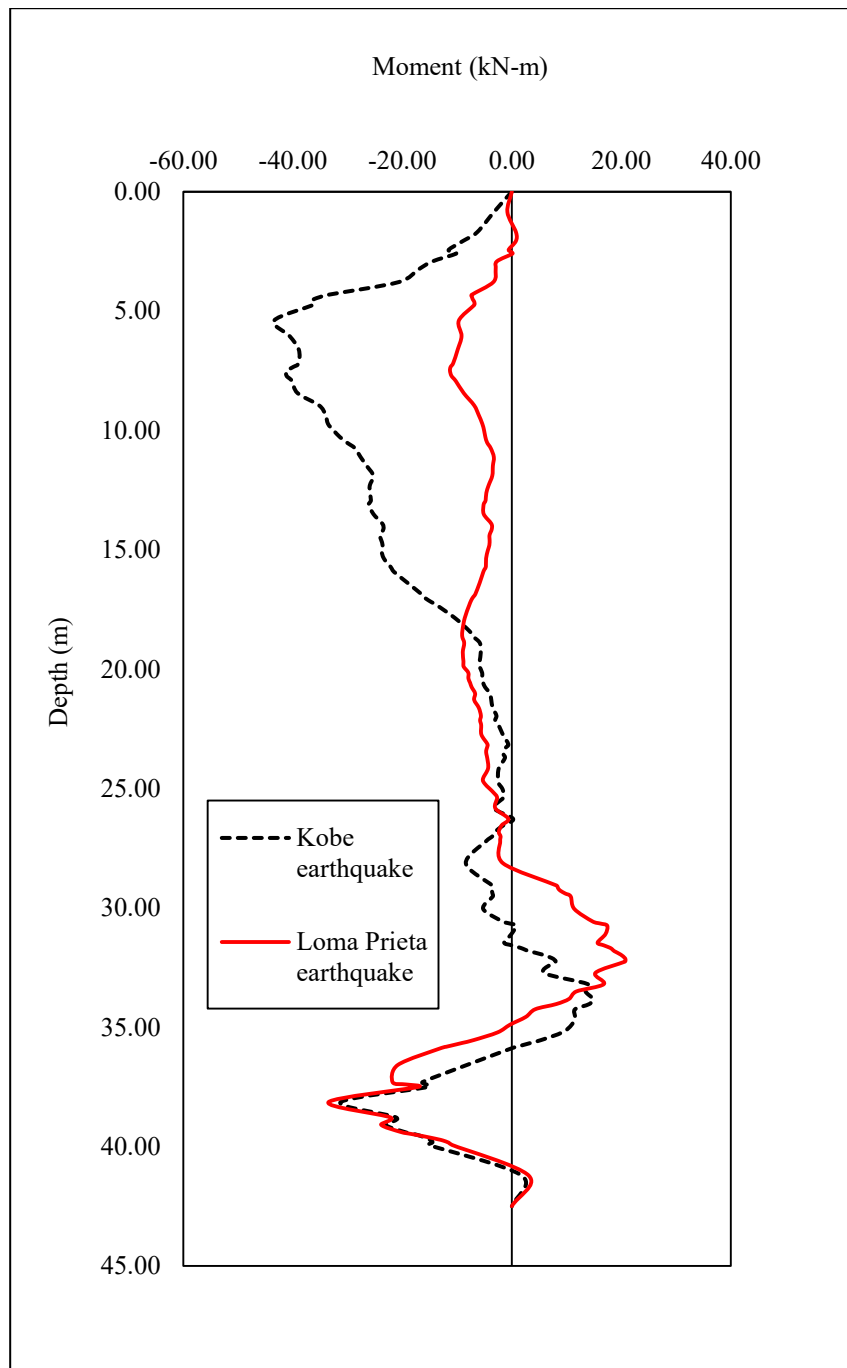


**Figure 4.38:** Comparison of moment developed under earthquake loading condition

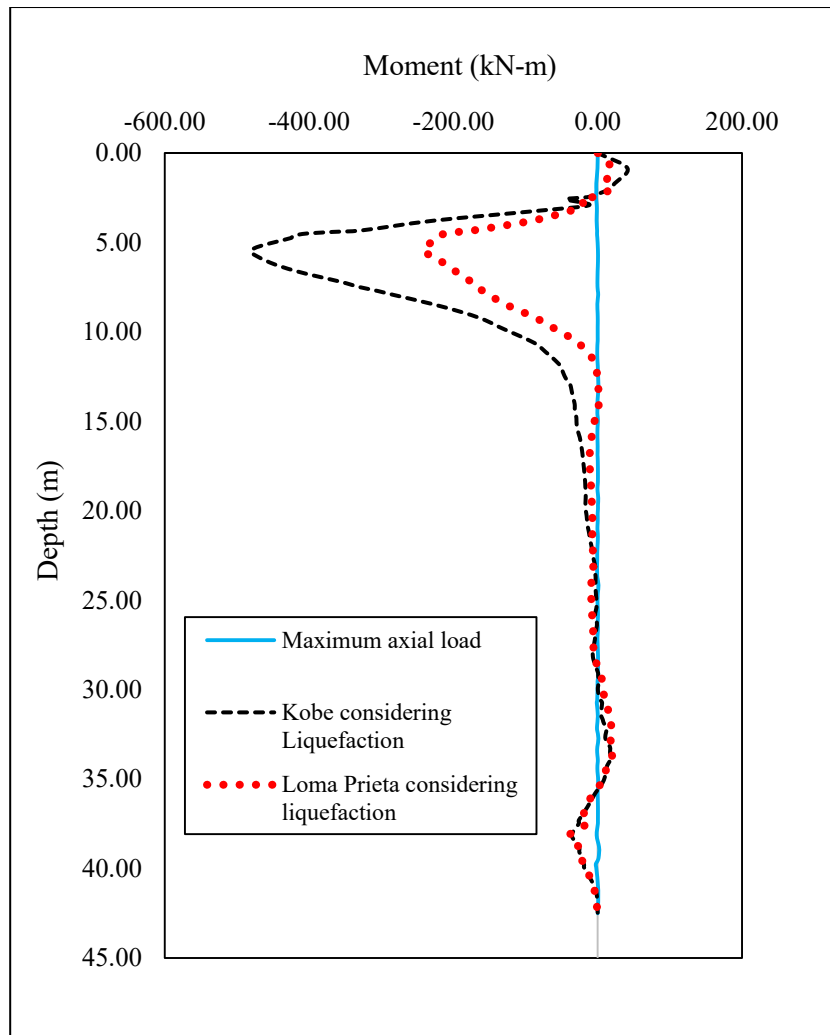


**Figure 4.39:** Comparison of moment developed both considering and without considering liquefaction

With generation of large force due to the lateral movement of the liquefiable and non-liquefiable layer has the potential to induce large bending moments in the piles leading to failure. Lateral load can cause pile failure due to change in flexural stiffness and capacity. So up-to a certain depth the soil needs to be improved so that the generated moment can be reduced. Soil in liquefied site showed larger stiffness degradation and piles showed larger bending moment than piles in non-liquefied site. In this study two cases are considered for soil improvement. Up-to depth 5 m and 15 m the soil is improved to see the moment capacity of pile. The soil improvement is simulated by increasing soil strength parameters used in UBC3D-PLM model and HS model. For soil improvement only up-to 5 m, the first loose sand layer is improved and analyzed using UBC3D-PLM model considering drained behavior. In case of 15 m soil improvement strength parameters of soil layer up-to 15 m is increased and analyzed with

UBC3D-PLM and HS model to observe the improved soil behavior. The improved soil parameters for first 5 m soil improvement is presented in Table 4.8. Keeping the first layer as the same properties given in Table 4.8, material properties of remaining 10 m soil is improved as shown in Table 4.9.

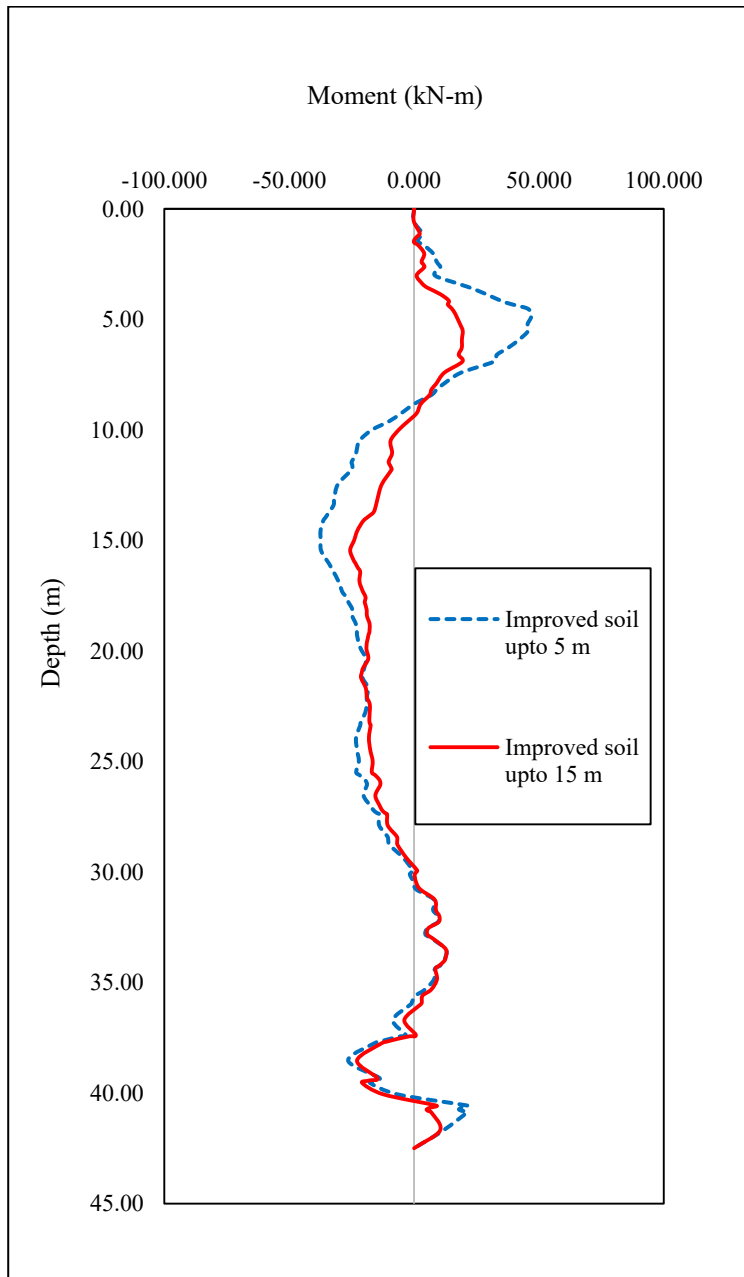
**Table 4.8:** Material properties for soil improvement up-to 5 m

Parameters	Symbol	Unit	Value applied in model
Unit weight	$\gamma_{\text{unsat}}$	kN/m <sup>3</sup>	17
Saturated unit weight	$\gamma_{\text{sat}}$	kN/m <sup>3</sup>	18
Poisson's ratio	$\nu$	-	0.3
Constant volume friction angle	$\phi_{\text{cv}}$	(°)	30
Peak friction angle	$\phi_{\text{p}}$	(°)	33
Cohesion	$c$	kPa	0
Elastic shear modulus	$K_{\text{G}}^{\text{e}}$	-	1316.0
Elastic bulk modulus	$K_{\text{B}}^{\text{e}}$	-	921.0
Plastic shear modulus	$K_{\text{G}}^{\text{p}}$	-	3195.0
Elastic shear modulus index	$n_{\text{e}}$	-	0.5
Elastic bulk modulus Index	$m_{\text{e}}$	-	0.5
Plastic shear modulus index	$n_{\text{p}}$	-	0.5
Failure ratio	$R_{\text{f}}$	-	0.9
Atmospheric pressure	$P_{\text{A}}$	-	100
Tension cut-off	$\sigma_{\text{t}}$	kPa	0.00
Densification factor	$f_{\text{dens}}$	-	1.0
Corrected SPT value	$(N_1)_{60}$	-	28.0
Post liquefaction Factor	$f_{\text{Epost}}$	-	1.0

**Table 4.9:** Material properties for soil improvement up-to 15 m

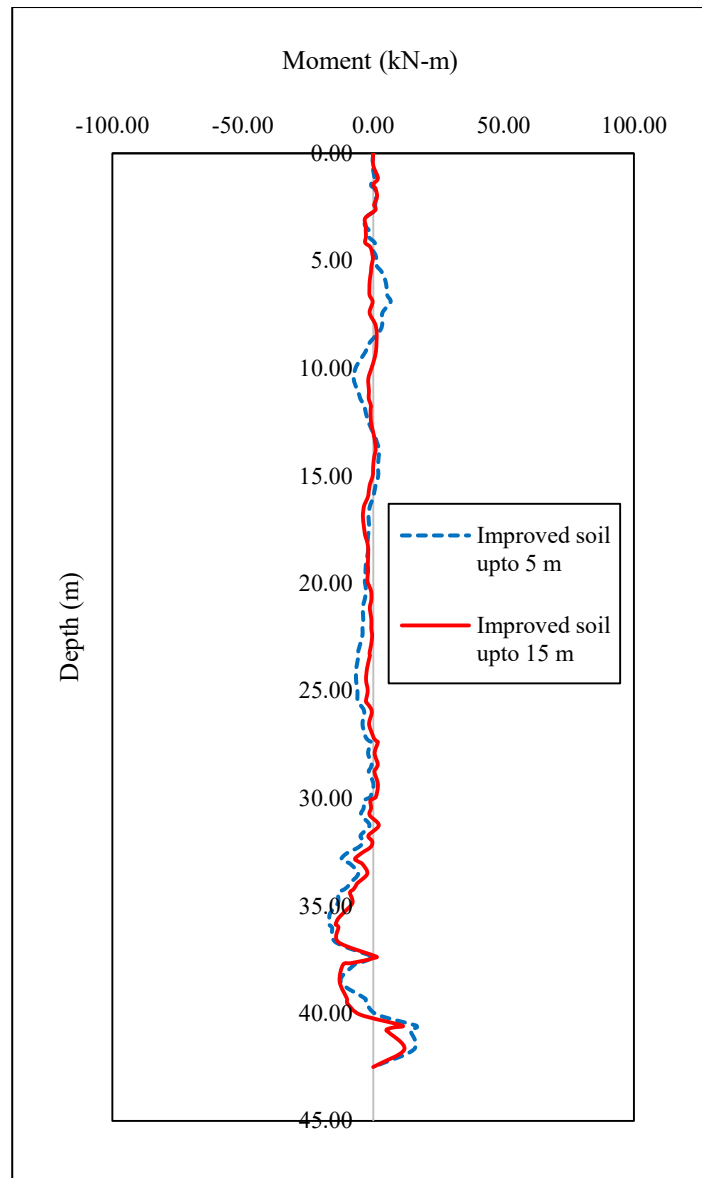
Parameters	Unit	Clayey silt (10 m)
Unstaturated unit weight ( $\gamma_{\text{unsat}}$ )	kN/m <sup>3</sup>	17
Sturated unit weight ( $\gamma_{\text{sat}}$ )	kN/m <sup>3</sup>	18.5
Secant stiffness modulus ( $E_{50}^{\text{ref}}$ )	kN/m <sup>2</sup>	20000
Oedometer modulus ( $E_{\text{oed}}^{\text{ref}}$ )	kN/m <sup>2</sup>	20000
Unloading/reloading stiffness ( $E_{\text{ur}}^{\text{ref}}$ )	kN/m <sup>2</sup>	60000
Poisson's ratio, $\nu$		0.3
Cohesion, $c$		25
Angle of friction, $\phi$		28
Dilation Angle, $\Psi$		0
Unloading/reloading poisson's ratio, $\nu_{\text{ur}}$		0.3
Power for stress-level dependency of stiffness, $m$		0.5
$K_0$ value for normally consolidated factor, $K_{0\text{nc}}$		0.577
Interface factor, $R_{\text{int}}$		0.9

Figure 4.40 and 4.41 shows that if the soil layer is improved only up to 5 m then moment in pile is reduced to a certain limit 45 kN-m and 6 kN-m for Kobe and Loma Prieta earthquake respectively which is within the pile moment capacity but if up to 15 m soil can be improved then it comes to 20 kN-m and 3 kN-m. It is significantly smaller under earthquake loading.



**Figure 4.40:** Comparison of moment reduction after soil improvement for Kobe earthquake





**Figure 4.41:** Comparison of moment reduction after soil improvement for Loma Prieta earthquake

In Figure 4.42, a comparison is made among moment generated during earthquake without considering liquefaction, considering liquefaction phenomenon and soil improvement. Due to soil improvement the moment in pile decreases to 96% and 100% at the interface of filled soil and clayey silt soil for Kobe and Loma Prieta earthquake respectively than the unimproved soil. Again, it can be observed that soil improvement up-to 15 m depth can reduce moment considerably than improved soil up-to 5 m depth. However, it can be concluded that soil improvement technique can enhance the pile flexural capacity under earthquake loading. Mostly spun pile damages occurs due to flexural failure. So soil improvement technique can minimize the chance of pile collapse and probability of liquefaction as well.

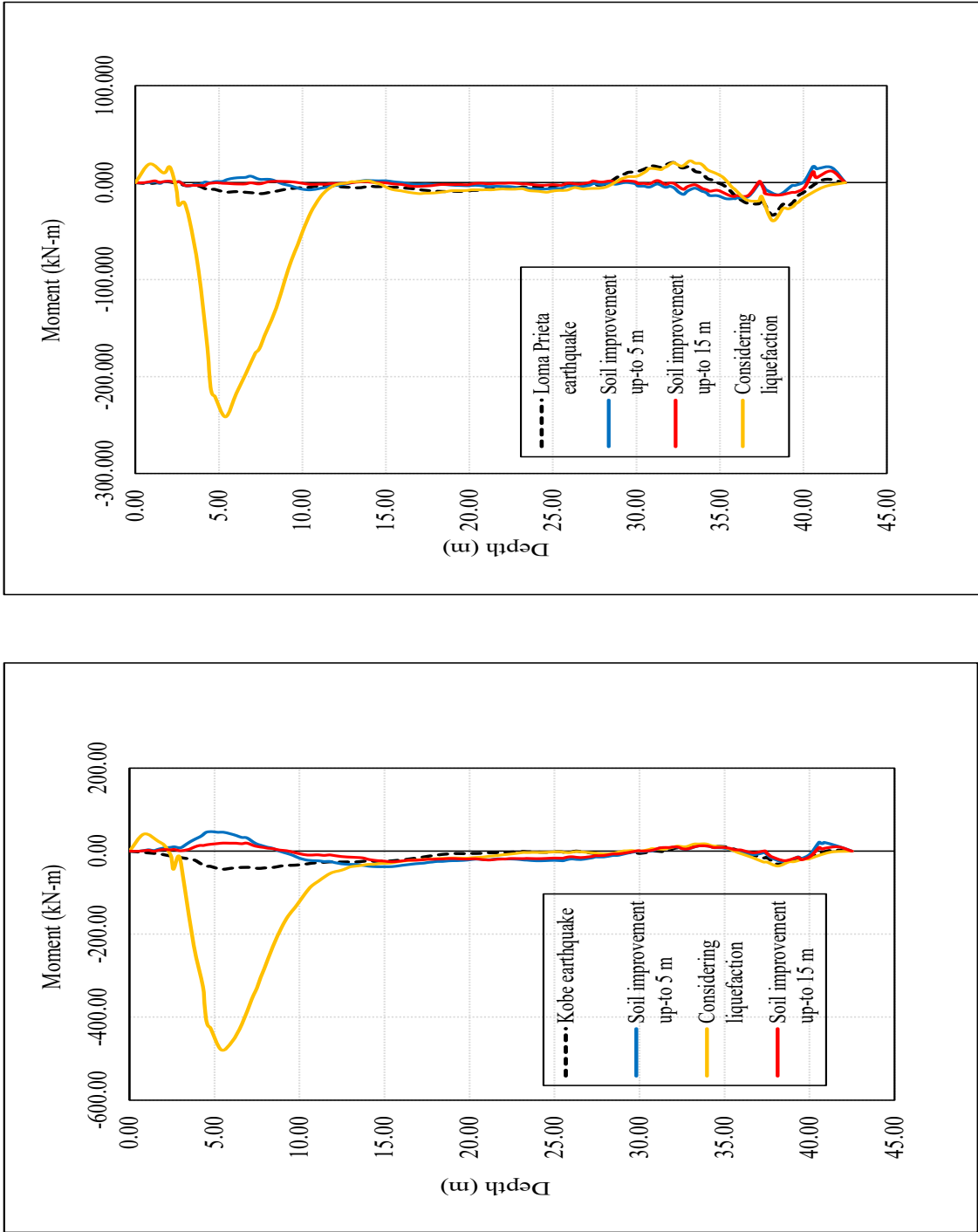


**Figure 4.42:** Comparison of moment considering liquefaction, withoutout liquefaction and soil improvement for (a) Kobe (b) Loma Prieta earthquake

## 4.11 Summary

This chapter explains the finite element modeling analysis of SPC pile under both axial and earthquake loading condition. The analysis can be summarized as follows:

1. For practical application and model validation a realistic soil constitutive soil model needs to be chosen which can simulate the nonlinear and stress dependent characteristics of soil. For FEM model HS model is chosen for simulate soil behavior. For structural component like pile embedded beam element is chosen. The input parameters are determined from laboratory test results and empirical correlations. The static pile load test result is validated with the FEM model using the soil and structural modeling parameters in PLAXIS 3D for Jolshiri site.
2. The parametric study is conducted to observe the influencing effect of pile diameter, length and mesh size of model on the simulated results under static loading condition.
3. The pile response under earthquake loading is simulated. The stage construction steps are presented for the analysis in PLAXIS 3D. Two seismic signal, Kobe and Loma Prieta are used as input earthquake loading to observe pile displacement, stress and strain distribution in soil body.
4. Liquefaction phenomenon has been simulated using UBC3D-PLM model in PLAXIS 3D during earthquake event. The top layer is susceptible to liquefaction effect due to excess pore water pressure generation. The maximum pore pressure ratio and pile displacement are determined for Kobe and Loma Prieta during liquefaction.
5. The large moment generation during liquefaction can lead the pile to collapse due to flexural failure. Liquefaction can trigger the pile to produce larger moment than the moment generated during seismic event without liquefaction occurrence. Soil improvement effect on the liquefiable layer is observed at the end of this chapter to reduce large moment generation and pile failure.

## CHAPTER 5

### CONCLUSIONS AND RECOMMENDATIONS

#### 5.1 Conclusions

This research investigates the axial and seismic performance of SPC piles in the reclaimed area of Jolshiri, Bangladesh. It is a new attempt to install SPC pile in liquefiable soil in Bangladesh. The Hardening Soil (HS) model has been used in the finite element model in PLAXIS 3D for earthquake analysis. Later, prediction of liquefaction phenomenon has been made during earthquake event using UBC3D-PLM model.

In previous chapters performance of SPC pile under static load has been determined by performing an in-situ pile load test. Model validation has been done with field results and the influence of various critical factors on pile and soil are investigated through parametric studies. These studies have given insight into the complex soil-structure interaction problem encountered in the field and their practical implications in design and analysis for constructing SPC pile in reclaimed soil in context of Bangladesh. The conclusions are summarized below to give a more comprehensive idea:

1. From field the tests, it is found that the top 4.5 m layer filled up with the loose silty sand has a SPT N value below 11 and shear wave velocity below 180 m/s. A hard stratum starts from 37.5 m with SPT value of 50 and shear wave velocity below 300 m/s. From the soil classification, it is observed that in Jolshiri site the top layer of soil is highly susceptible to liquefaction phenomenon.
2. The factor of safety is found less than 1 for the first layer for different earthquake magnitudes according to Seed and Idriss method. It can be concluded that loose sandy layer is vulnerable during earthquake event and there is possibility of liquefaction occurrence.
3. From Push-in test, the pile capacity for the 450 mm diameter pile is found to be 414 ton. From static pile load test, the load-settlement curve is obtained. According to BNBC 2020, the allowable load is observed to be 150 ton from the test. The analytical investigation of the pile capacity shows that with considering the liquefaction phenomenon in the site, the pile skin friction is reduced considerably for boreholes one,

two and three around 9.41 %, 8.71 % and 10.15 % respectively. The ultimate pile capacity decreases 3.97% for borehole one and 3.80 %, 4.50% for borehole two and three respectively due to the liquefaction effect.

4. The load-settlement curve acquired from the field and PLAXIS 3D have showed good agreement and this model is used for further analysis. Under axial loading condition, it is found that the pile does not fail under design load but when it is increased to 200% then the failure has been observed within the pile. Under design load, maximum pile displacement observed is 18.47 mm. The stress distribution in the soil around the pile bottom is found to be 647 kN/m<sup>2</sup>.
5. From parametric studies, it can be observed that different mesh size does not affect the pile displacement significantly. But in the case of moment generation, a little variation is observed. Three pile length has been varied 35 m, 42.5 m and 50 m. It can be summarized that an increase in pile length can reduce pile displacement. Again, varied pile diameter 400, 450 and 500 mm have been used and found that larger pile diameter can also reduce the pile displacement significantly.
6. The pile has showed larger displacement under earthquake loading. The displacement is increased about 8.5 times and 40 times for Kobe and Loma Prieta earthquake respectively than the axial loading condition. At top, the strain in soil for Kobe earthquake is 7.6 times greater than Loma Prieta earthquake. Moreover, total and shear stress have increased about 7.2% and 8.5% in case of Kobe earthquake respectively than axial loading. It can be deduced that the earthquake loading can increase the lateral deformation and stresses of both pile and soil elements than the axial loading.
7. From liquefaction analysis, it is found that the maximum excess pore pressure ratio  $r_u$  is about 0.99 ~ 1 for the loose sandy top layer. This means the layer has been completely liquefied during an earthquake. Under this condition, the pile could not sustain the design load and failed under 250 ton load. Larger pore pressure has been generated with the increased acceleration. As a result, pile has showed larger displacement about 30-60 % higher than non-liquefied condition. With the displacement of top layers having liquefiable soil, the bottom nonliquefiable soil also starts to displace.

8. During liquefaction, maximum bending moment is found to be 11 and 26 times higher for Kobe and Loma Prieta earthquake respectively than the moment during non-liquefiable condition. It is more than the design moment capacity of the pile. The maximum bending moment is generated at the interface of the liquefied and non-liquefied soil layer. As a remedial measures, 5 m and 15 m top soil has been improved to see the effect on the moment capacity of the pile. After doing analysis with the improved soil parameters, it is found that the moment has been reduced and lies within the design capacity. In this case, soil improvement up-to 15 m depth is more effective than improvement up-to 5 m.
9. The above analysis and results have showed that SPC pile works efficiently under axial loading but under the earthquake loading, the pile settlement is excessive for the soil type observed at the Jolshiri. Moreover, when liquefaction phenomenon is considered then soil may fail before the pile fails and increased moment at the interface can cause flexural failure of pile. Therefore, SPC pile can be used in the study site under static loading condition but caution is needed to use them in terms of liquefaction occurrence. Also, engineers can do more parametric study to improve the pile design and soil improvement technique can be taken into consideration for better dynamic response of SPC pile.

## **5.2 Recommendations for Future Work**

With the development of researches and complex problem, it is become a necessary to conduct numerical analysis to confirm critical issues in routine design process. PLAXIS is an advance geotechnical software that is very popular worldwide for its powerful and user friendly finite element package. Therefore, PLAXIS 3D is a suitable software for engineers to evaluate interactions between soil and structural elements with accuracy. Advance constitutive model like UBC3D-PLM, HS model and HS small model are very popular to capture earthquake and liquefaction phenomenon but due to lack of field test data, obtaining required input parameters and the model calibration has become an issue for researchers. Following aspects should be taken into account for future research works:

1. For determining input parameters soil sample should be collected from each layer of soil profile if possible as correlations established elsewhere may be useful for

preliminary study but model where more accuracy needed can find it difficult to match the best results.

2. Field test data is required for dynamic load test calibration. Despite of being costly it is recommended to conduct such test to simulate the dynamic response of pile in a specific site and validate the finite element model with the field test data. The instruments to be installed at the specific location to monitor the pile deflection in seismic acceleration.
3. HS model can predict better pile and soil response in seismic motion. In contrast to the HS model, the HS small model shows hysteresis in cyclic loading. When applied in dynamic calculation, the hysteretic behavior of HS small model leads to damping. HS small model uses the same parameters like HS model except two parameters i.e. small-strain shear modulus and shear strain at 70%. So HS small can be used for seismic analysis in PLAXIS for more accurate simulation but it requires field verification.
4. As precast pile SPC pile showed better performance under static loading condition but other option of driven pile can be compared for the specific site under both axial and lateral loading.
5. Different combination of group pile condition is recommended to simulate with respect to deflection, moment capacity and group efficiency in earthquake loading. Again, different pile head condition can show distinct dynamic response, so both fixed and free head pile condition can be considered for dynamic analysis.
6. The shear resistance capacity of SPC pile can be evaluated for both single and group pile arrangement to observe the sustainability of pile under shear failure.



## REFERENCES

- Abdoun, T., and Dobry, R. (2002). Evaluation of pile foundation response to lateral spreading. *Soil Dynamics and Earthquake Engineering*, 22(9-12), 1051-1058.
- Abdoun, T., Dobry, R., O'Rourke, T. D., and Goh, S. (2003). Pile response to lateral spreads: centrifuge modeling. *Journal of geotechnical and geoenvironmental engineering*, 129(10), 869-878.
- Akiyama, M., Abe, S., Aoki, N., and Suzuki, M. (2012). Flexural test of precast high-strength reinforced concrete pile prestressed with unbonded bars arranged at the center of the cross-section. *Engineering Structures*, 34, 259-270.
- Al-abboodi, I., and Sabbagh, T. T. (2019). Numerical modelling of passively loaded pile groups. *Geotechnical and Geological Engineering*, 37(4), 2747-2761.
- Al-Abboodi, I., Toma-Sabbagh, T., and Al-Jazaairry, A. (2015). Modelling the response of single passive piles subjected to lateral soil movement using PLAXIS. *International Journal of Engineering Research and Technology*, 4(3), 176-180.
- Al-Qayssi, M. R., Al-Wakel, S. F., and Abdulwahhab, I. G. (2001). Three-Dimensional Analysis for the Effect of Piles Geometry and Arrangement on the Dynamic Response of Piled Raft Foundation. *Journal of Engineering and Sustainable Development*, 22(5).
- Amorosi, A., Boldini, D., and Di Lernia, A. (2016). Seismic ground response at Lotung: Hysteretic elasto-plastic-based 3D analyses. *Soil Dynamics and Earthquake Engineering*, 85, 44-61.
- Ansary, M. A., Rahman, S., Murad, E. M., Chowdhury, S., and Shuvra, D. (2010). *Proposed time history and response spectrum for Dhaka, Chittagong and Sylhet cities*. Paper presented at the Proceedings, 3rd International Earthquake Symposium, March.
- Ansary, M., Siddiquee, M. A., Siddique, A., and Safiullah, A. M. (2001). Status of static pile load tests in Bangladesh. In *Soil mechanics and geotechnical engineering. Eleventh Asian Regional Conference* (pp. 241-244).
- Asaadi, A., and Sharifipour, M. (2015). Numerical simulation of liquefaction susceptibility of soil interacting by single pile. *International Journal of Mining and Geo-Engineering*, 49(1), 47-56.
- Ashford, S. A., Juirnarongrit, T., Sugano, T., and Hamada, M. (2006). Soil–pile response to blast-induced lateral spreading. I: field test. *Journal of geotechnical and geoenvironmental engineering*, 132(2), 152-162.
- ASTM. (1994). *Standard test method for piles under static axial compressive load* ASTM (Ed.). West Conshohocken: ASTM D-1143.
- Au, F. T., Leung, C. C., and Kwan, A. K. (2011). Flexural ductility and deformability of reinforced and prestressed concrete sections. *Computers and Concrete*, 8(4), 473-489.

- Bai, X., Zeng, G., and Guo, Z. (2020). Analysis of the influence of pile embedded cap depth on horizontal bearing capacity of PHC pipe pile group with cap. Paper presented at the E3S Web of Conferences.
- Baladi, G. Y., and Rohani, B. (1979). Elastic-plastic model for saturated sand. *Journal of the Geotechnical Engineering Division*, 105(4), 465-480.
- Banerjee, S., and Shirole, O. N. (2014). Numerical analysis of piles under cyclic lateral load. *Indian Geotechnical Journal*, 44(4), 436-448.
- Banerjee, S., Stanton, J., and Hawkins, N. (1987). Seismic performance of precast prestressed concrete piles. *Journal of Structural Engineering*, 113(2), 381-396.
- Bang, J.-W., Hyun, J.-H., Lee, B.-Y., Lee, S.-S., and Kim, Y.-Y. (2013). Flexural strength of PHC pile reinforced with infilled concrete, transverse and longitudinal reinforcements. *Journal of the Korea Concrete Institute*, 25(1), 91-98.
- Belinchón, P., Sørensen, K. K., and Christensen, R. (2016). Finite Element Investigation of the Interaction between a Pile and a Soft Soil focussing on Negative Skin Friction. *Proceedings of the 17th Nordic Geotechnical Meeting Challenges in Nordic Geotechnic 25<sup>th</sup> – 28<sup>th</sup> of May*.
- Bhattacharya, S., Blakeborough, A., and Dash, S. (2008). Learning from collapse of piles in liquefiable soils. Paper presented at the Proceedings of the Institution of Civil Engineers-Civil Engineering.
- Bhattacharya, S., Madabhushi, S., and Bolton, M. (2003). Pile instability during earthquake liquefaction. University of Cambridge Cambridge, UK.
- Bhattacharya, S., Madabhushi, S., and Bolton, M. (2004). An alternative mechanism of pile failure in liquefiable deposits during earthquakes. *Geotechnique*, 54(3), 203-213.
- Bingkang, L., and Hai, L. J. Z. X. S. (2007). Test of moment bearing capacity and ductility performance of filled prestressed concrete pipe pile. *Industrial Construction*, 03.
- Bolton Seed, H., Tokimatsu, K., Harder, L., and Chung, R. M. (1985). Influence of SPT procedures in soil liquefaction resistance evaluations. *Journal of geotechnical engineering*, 111(12), 1425-1445.
- Boominathan, A., and Ayothiraman, R. (2006). Dynamic response of laterally loaded piles in clay. *Proceedings of the Institution of Civil Engineers-Geotechnical Engineering*, 159(3), 233-241.
- Brandenberg, S. J., Boulanger, R. W., Kutter, B. L., and Chang, D. (2005). Behavior of pile foundations in laterally spreading ground during centrifuge tests. *Journal of geotechnical and geoenvironmental engineering*, 131(11), 1378-1391.
- Brinch-Hansen, J. (1963), Hyperbolic Stress Strain Response: Cohesive Soils, Discussion, JSMFED, ASCE, Vol. 89, No. SM4, pp. 241-242

- Budek, A., and Priestley, M. (2005). Experimental analysis of flexural hinging in hollow marine prestressed pile shafts. *Coastal Engineering Journal*, 47(1), 1-20.
- Butler, H.D. and Hoy, H.E. (1977), User's Manual for the Texas Quick Load Method for Foundation Load Testing, FHWA-IP-77-8, Federal Highway Administration, Office of Development, Washington, pp.59 .
- Byrne, P. M. (1991). A cyclic shear-volume coupling and pore pressure model for sand. *In Second international conference on recent advances in geotechnical engineering and soil dynamics* (pp. 47–55).
- Cao, X., Dai, G., Gong, W., Zhu, M., and Tang, J. (2020). Experimental study on the seismic behavior of new PHC piles. *Arabian Journal of Geosciences*, 13(16), 1-8.
- Chandrasekaran, S., Boominathan, A., and Dodagoudar, G. (2013). Dynamic response of laterally loaded pile groups in clay. *Journal of Earthquake Engineering*, 17(1), 33-53.
- Chatterjee, K. (2019). Influence of site-specific soil amplification on seismic response of piles in liquefiable soils. *Innovative Infrastructure Solutions*, 4(1), 11.
- Chatterjee, K., and Choudhury, D. (2018). Influence of seismic motions on behavior of piles in liquefied soils. *International Journal for Numerical and Analytical Methods in Geomechanics*, 42(3), 516-541.
- Chen, W.-F., and Baladi, G. Y. (1985). *Soil plasticity: theory and implementation*: Elsevier.
- Chen, Y.-J., and Marcos, M. C. M. (2018). Applicability of various load test interpretation criteria in measuring driven precast concrete pile uplift capacity. *International Journal of Engineering and Technology Innovation*, 8(2), 118.
- Cheng, Z., and Jeremić, B. (2009). Numerical modeling and simulation of pile in liquefiable soil. *Soil Dynamics and Earthquake Engineering*, 29(11-12), 1405-1416.
- Choudhury, D., Chatterjee, K., Kumar, A., and Phule, R. (2014). *Pile Foundations during Earthquakes in Liquefiable Soils—Theory to Practice*. 15SEE.
- Chung, S.-G., Kim, S.-R., Dung, N.-T., and Enebish, N. (2007). Appraisal of true resistance of PHC piles driven in thick soft deposit. Paper presented at the 2007 International Forum on Strategic Technology.
- Comodromos, E. M., Papadopoulou, M. C., and Rentzeperis, I. K. (2009). Pile foundation analysis and design using experimental data and 3-D numerical analysis. *Computers and Geotechnics*, 36(5), 819-836.
- Cubrinovski, M., Kokusho, T., and Ishihara, K. (2006). Interpretation from large-scale shake table tests on piles undergoing lateral spreading in liquefied soils. *Soil Dynamics and Earthquake Engineering*, 26(2-4), 275-286.

- Davisson, M.T. (1973), High Capacity Piles: Proc. Of Lecture Series on Innovation in Foundation Construction, Soil Mechanics Division, Illinois Section, ASCE, Department of Civil Engineering, Illinois Institute of Technology, Chicago, IL, 1973.
- Deendayal, R. Finite element analysis of a single pile under cyclic loading. *International Journal of Civil Engineering and Technology*, 10, 918-924.
- Dewi, S., and Liong, G. T. (2011). Analysis on laterally loaded group piles by plaxis 3D foundation. *Jurnal ComTech*, 2(02), 1023-1030.
- Dung, N., Chung, S., Kim, S., and Beak, S. (2011). Applicability of the SPT-based methods for estimating toe bearing capacity of driven PHC piles in the thick deltaic deposits. *KSCE Journal of Civil Engineering*, 15(6), 1023-1031.
- Dungca, J. R., Kuwano, J., Takahashi, A., Saruwatari, T., Izawa, J., Suzuki, H., and Tokimatsu, K. (2006). Shaking table tests on the lateral response of a pile buried in liquefied sand. *Soil Dynamics and Earthquake Engineering*, 26(2-4), 287-295.
- El-Mossallamy, Y. M., Hefny, A. M., Demerdash, M. A., and Morsy, M. S. (2013). Numerical analysis of negative skin friction on piles in soft clay. *HBRC Journal*, 9(1), 68-76.
- Elgamal, A., He, L., Lu, J., Abe, A., Abdoun, T., Dobry, R., Shantz, T. (2006). Liquefaction-induced lateral load on piles. Paper presented at the Fourth international conference on earthquake engineering.
- Fatahi, B., Basack, S., Ryan, P., Zhou, W.-H., and Khabbaz, H. (2014). Performance of laterally loaded piles considering soil and interface parameters. *Geomechanics and Engineering*.
- Finn, W., and Fujita, N. (2002). Piles in liquefiable soils: seismic analysis and design issues. *Soil Dynamics and Earthquake Engineering*, 22(9-12), 731-742.
- Fuziol, J. (2009). Numerical modeling of the seismic performance of prestressed pile to cast in place pile cap connections with plain embedment. *Unpublished MS. Thesis. University of South Carolina, Columbia, SC*.
- Gao, A. (2012). Experimented research on seismic performance of PHC pipe pile and analysis of bearing capacity. *Tianjin University, Dissertation*.
- Gautam, D., de Magistris, F. S., and Fabbrocino, G. (2017). Soil liquefaction in Kathmandu valley due to 25 April 2015 Gorkha, Nepal earthquake. *Soil Dynamics and Earthquake Engineering*, 97, 37-47.
- Gowthaman, S., Nasvi, M., and Krishnya, S. (2017). Numerical Study and Comparison of the Settlement Behaviours of Axially Loaded Piles using Different Material Models.
- Guo, Z., He, W., Bai, X., and Chen, Y. F. (2017). Seismic performance of pile-cap connections of prestressed high-strength concrete pile with different details. *Structural Engineering International*, 27(4), 546-557.

- Haldar, S., and Babu, G. S. (2010). Failure mechanisms of pile foundations in liquefiable soil: Parametric study. *International Journal of Geomechanics*, 10(2), 74-84.
- Hamouma, D., Messameh, A., and Tallah, N. Finite element analysis of soil-pile interface under cyclic loading. *International Journal of Civil Engineering and Technology (IJCET)*, 11, 49-57.
- Han, J., Kim, S., Hwang, J., and Kim, M. (2007). Evaluation of the dynamic characteristics of soil-pile system in liquefiable ground by shaking table tests. Paper presented at the 4th International Conference on Earthquake Geotechnical Engineering.
- Harries, K. A., and Petrou, M. F. (2001). Behavior of precast, prestressed concrete pile to cast-in-place pile cap connections. *PCI journal*, 46(4), 82-93.
- Hasancebi, N., and Ulusay, R. (2007). Empirical correlations between shear wave velocity and penetration resistance for ground shaking assessments. *Bulletin of Engineering Geology and the Environment*, 66(2), 203-213.
- He, L., Elgamal, A., Abdoun, T., Abe, A., Dobry, R., Meneses, J., Tokimatsu, K. (2006). Lateral load on piles due to liquefaction-induced lateral spreading during one-g shake table experiments. Paper presented at the 8th US National Conference on Earthquake Engineering 2006.
- Heidari, M., El Naggar, H., Jahanandish, M., and Ghahramani, A. (2014). Generalized cyclic p-y curve modeling for analysis of laterally loaded piles. *Soil Dynamics and Earthquake Engineering*, 63, 138-149.
- Heidari, M., Jahanandish, M., El Naggar, H., and Ghahramani, A. (2014). Nonlinear cyclic behavior of laterally loaded pile in cohesive soil. *Canadian Geotechnical Journal*, 51(2), 129-143.
- Hokmabadi, A. S., Fatahi, B., and Samali, B. (2015). Physical modeling of seismic soil-pile-structure interaction for buildings on soft soils. *International Journal of Geomechanics*, 15(2), 04014046.
- Huang, F.-y., Wu, S.-w., Luo, X.-y., Chen, B.-c., and Lin, Y. (2018). Pseudo-static low cycle test on the mechanical behavior of PHC pipe piles with consideration of soil-pile interaction. *Engineering Structures*, 171, 992-1006.
- Huang, F., Qian, H., Zhuang, Y., and Fu, C. (2017). Experimental study on the dynamic response of PHC pipe-piles in liquefiable soil. *Journal of Testing and Evaluation*, 45(1), 230-241.
- Huang, F., Shan, Y., Javanmardi, A., Luo, X., and Chen, B. (2020). Seismic Performance of Various Piles Considering Soil-Pile Interaction under Lateral Cycle Loads for Integral Abutment Jointless Bridges (IAJBs). *Applied Sciences*, 10(10), 3406.
- Huang, Y., and Yu, M. (2017). *Hazard analysis of seismic soil liquefaction*: Springer.

- Idriss, I., and Boulanger, R. (2006). Semi-empirical procedures for evaluating liquefaction potential during earthquakes. *Soil Dynamics and Earthquake Engineering*, 26(2-4), 115-130.
- Imai, T. (1977). *P and S wave velocities of the ground in Japan*. Paper presented at the Proc. 9th ICSMFE.
- Irawan, C., and Djamaluddin, R. (2018). Confinement Behavior of Spun Pile using Low Amount of Spiral Reinforcement—an Experimental Study. *International Journal on Advanced Science, Engineering and Information Technology*, 8, 501-507.
- IS: 2911 – Part 1 (1979), Design and Construction of Pile Foundations- Driven Cast In Situ Concrete Piles, Burea of Indian Standards, 1979.
- Janalizadeh, A., and Zahmatkesh, A. (2015). Lateral response of pile foundations in liquefiable soils. *Journal of rock mechanics and geotechnical engineering*, 7(5), 532-539.
- Jawad, F. W., and Al-Ameri, A. F. I. (2018). Numerical analysis of piles foundation to reduce the zone of liquefaction of sandy soil under dynamic loads. *nternational Journal of Civil Engineering and Technology*, 9(10), 1059–1071.
- Joen, P. H., and Park, R. (1990). Simulated seismic load tests on prestressed concrete piles and pile-pile cap connection. *PCI journal*, 35(6), 42-61.
- Johnson, R. T., Varghese, R. M., and Joseph, J. (2019). Parametric Study on the Behavior of Combined Pile Raft Foundation Founded on Multi-layered Soil Using PLAXIS 3D *Soil Dynamics and Earthquake Geotechnical Engineering* (pp. 217-225): Springer.
- JRA. (1980). Specification and interpretation of bridge design for highway—Part V: resilient design. JAPANESE ROAD ASSOCIATION.
- Kardoğan, P. S. Ö., and Bhattacharya, S. (2017). Review of Liquefaction Around Marine and Pile-Supported Wharf Structures. Paper presented at the International Sustainable Buildings Symposium. *International Sustainable Buildings Symposium*. Springer, 893-903.
- Kim, S., Whang, S.-W., and Kim, S. (2017). Pile Foundation Design Through the Increased Bearing Capacity of Extended End Pile. *Journal of Asian Architecture and Building Engineering*, 16(2), 395-402.
- Kishida, S., Horii, M., Kuwabara, F., and Hayashi, S. (1998). Experimental study on shear strength of the PHC pile with large diameter. *J Struct. Const. Eng*, 8(519), 123-130.
- Klar, A., Baker, R., and Frydman, S. (2004). Seismic soil–pile interaction in liquefiable soil. *Soil Dynamics and Earthquake Engineering*, 24(8), 551-564.
- Knappett, J., and Madabhushi, S. (2009). Influence of axial load on lateral pile response in liquefiable soils. Part I: physical modelling. *Geotechnique*, 59(7), 571-581.

- Knappett, J. A., and Madabhushi, S. G. (2006). Modelling of liquefaction-induced instability in pile groups. *In Seismic Performance and Simulation of Pile Foundations in Liquefied and Laterally Spreading Ground* (pp. 255-267).
- Kokusho, S., Wada, A., Kobayashi, K., Mitsugi, S., and Ueda, K. (1987). Experiments on the seismic behavior of PHC piles: study of the improvement in the bearing capacity and deformability of the prestressed high strength concrete (PHC) pile, Part 1. *Journal of Structural and Construction Engineering (Transactions of AIJ)*, 376, 71-80.
- Kyi, C. M., and Yangon, M. Analysis and design of spun pile Foundation of Sixteenth Storyed Building in cohesion less soil. *International Journal of Science and Engineering Applications*, 8(11), 476-484.
- Lee, S. H.-H. (1992). Analysis of the multicollinearity of regression equations of shear wave velocities. *Soils and Foundations*, 32(1), 205-214.
- Li, Y., Xing, K., Liu, H., and Chen, M. (2013). Experimental study of seismic performance of PHC pipe pile considering soil-pile-structure interaction. *Chinese Journal of Rock Mechanics and Engineering*, 32(2), 401-410.
- Li, Y. F., Liu, P., and Zhang, J. X. (2015). Experimental Research on Seismic Performance of PHC Pipe Piles. *Paper presented at the Applied Mechanics and Materials*.
- Lignola, G. P., Prota, A., Manfredi, G., and Cosenza, E. (2009). Analysis Of Reinforced Concrete Hollow Piers Behavior: Benefits Of FRP Confinement.
- Lin, M., ZHANG, J., TANG, Z.-x., and Qian, C. (2016). Simulation of Vertical Bearing Capacity for PHC-Steel Composite Pile. *DEStech Transactions on Materials Science and Engineering(msce)*.
- Liyanapathirana, D. S., and Poulos, H. (2005). Seismic lateral response of piles in liquefying soil. *Journal of geotechnical and geoenvironmental engineering*, 131(12), 1466-1479.
- Lozovyi, S., and Zahoruiko, E. (2014). Plaxis simulation of static pile tests and determination of reaction piles influence. *preprint arXiv:1411.0929*.
- Maheshwari, B., Nath, U., and Ramasamy, G. (2008). Influence of liquefaction on pile-soil interaction in vertical vibration. *ISET Journal of Earthquake Technology*, 45(1), 1-13.
- Maheshwari, B., and Sarkar, R. (2011). Seismic behavior of soil-pile-structure interaction in liquefiable soils: Parametric study. *International Journal of Geomechanics*, 11(4), 335-347.
- Maheshwari, B., and Sarkar, R. (2012). Effects of soil nonlinearity and liquefaction on seismic response of pile groups. *International Journal of Geotechnical Engineering*, 6(4), 497-506.
- Maheshwari, B., Truman, K., El Naggar, M., and Gould, P. (2004). Three-dimensional nonlinear analysis for seismic soil-pile-structure interaction. *Soil Dynamics and Earthquake Engineering*, 24(4), 343-356.

- Maheshwari, B., Truman, K., Gould, P., and El Naggar, M. (2005). Three-dimensional nonlinear seismic analysis of single piles using finite element model: Effects of plasticity of soil. *International Journal of Geomechanics*, 5(1), 35-44.
- Marcos, M. C. M., Chen, Y.-J., and Kulhawy, F. H. (2013). Evaluation of compression load test interpretation criteria for driven precast concrete pile capacity. *KSCE Journal of Civil Engineering*, 17(5), 1008-1022.
- Marjanović, M., Vukićević, M., König, D., Schanz, T., and Schäfer, R. (2016). Modeling of laterally loaded piles using embedded beam elements. *Zbornik radova 4. Međunarodne konferencije Savremena dostignuća u građevinarstvu 2016*, 32, 349-358.
- Martin, G. R., Seed, H. B., and Finn, W. L. (1975). Fundamentals of liquefaction under cyclic loading. *Journal of the Geotechnical Engineering Division*, 101(5), 423-438.
- Meyerhof, G. G. (1976). Bearing capacity and settlement of pile foundations. *Journal of the Geotechnical Engineering Division*, 102(3), 197-228.
- Mohey Mohamed, A., Abd El Fattah, M., Mohamed Hassan, A., and Moussa Abu Bakr, A. (2020). Numerical analysis of liquefaction phenomenon by using UBC3D-PLM constitutive model. *Journal of Advanced Engineering Trends*, 38(2), 81-96.
- Mokhtar, A.-S. A., Abdel-Motaal, M. A., and Wahidy, M. M. (2014). Lateral displacement and pile instability due to soil liquefaction using numerical model. *Ain Shams Engineering Journal*, 5(4), 1019-1032.
- Motamed, R., Sesov, V., Towhata, I., and Anh, N. T. (2010). Experimental modeling of large pile groups in sloping ground subjected to liquefaction-induced lateral flow: 1-G shaking table tests. *Soils and Foundations*, 50(2), 261-279.
- Nagae, T., and Hayashi, S. (2003). Earthquake-resistant property of prefabricated high-strength concrete pile *High Performance Materials in Bridges* (pp. 173-182).
- Nakazawa, A., M. C., Namba, S., Nakazawa, Y. (1996). Damage investigation report of building pile foundation due to Hyogo-ken Nanbu Earthquake: Case of Ashiya City. *AIJ J. Technol*, 2(3), 77-82.
- Nakazawa, A, S. N., Sotetsu, A., Tokimatsu, K., Oh-oka, H., Yasuhiro, and Nakazawa, S. a. Y. (1999). Estimation on pile foundations of high-rise building inclined largely in the Hyogoken-Nanbu earthquake. *J. Struct. Constr. Eng., AIJ, J(520)*, 69-76.
- Ohba, S., and Toriuma, I. (1970). Research on vibrational characteristics of soil deposits in Osaka, part 2, on velocities of wave propagation and predominant periods of soil deposits. Paper presented at the technical meeting of Architectural Institute of Japan.
- Ohta, Y., and Goto, N. (1978). Empirical shear wave velocity equations in terms of characteristic soil indexes. *Earthquake Engineering and Structural Dynamics*, 6(2), 167-187.



- Oka, F., Lu, C.-w., Uzuoka, R., and Zhang, F. (2004). Numerical study of structure-soil-group pile foundations using an effective stress based liquefaction analysis method. Paper presented at the Proceedings of the 13th World Conference on Earthquake Engineering, Vancouver, Canada.
- Phanikanth, V., Choudhury, D., and Reddy, G. (2013). Behavior of single pile in liquefied deposits during earthquakes. *International Journal of Geomechanics*, 13(4), 454-462.
- Piling, P. P. C. J. P. J. (2019). Recommended Practice for Design, Manufacture, and Installation of Prestressed Concrete Piling.
- Poulos, H. G., and Davis, E. H. (1980). *Pile foundation analysis and design*.
- Puebla, H., Byrne, P. M., and Phillips, R. (1997). Analysis of CANLEX liquefaction embankments: prototype and centrifuge models. *Canadian Geotechnical Journal*, 34(5), 641-657.
- Rahmani, A., and Pak, A. (2012). Dynamic behavior of pile foundations under cyclic loading in liquefiable soils. *Computers and Geotechnics*, 40, 114-126.
- Rao, V., Chatterjee, K., and Choudhury, D. (2013). Analysis of single pile in liquefied soil during earthquake using FLAC3D. Paper presented at the Proceedings of the International Conference on “State of the Art of Pile Foundation and Pile Case Histories” PILE–2013, June.
- Rostami, R., Hytiris, N., Bhattacharya, S., and Giblin, M. (2017). Seismic analysis of pile in liquefiable soil and plastic hinge. *Geotechnical Research*, 4(4), 203-213.
- Saha, P., Paul, I., and Takahashi, A. Liquefaction susceptibility of artificially filled soil in dhaka city and potential countermeasures against liquefaction induced damages. *Taiwan-Japan Joint Symposium on the Advancement of Urban Earthquake Hazard Mitigation Technology*.
- Saha, P., Uddin, A. F., and Hasnat, A. (2012). Liquefaction characteristics of in-filled soil at banasree in dhaka city. *Proceedings of the 1st International Conference on Civil Engineering for Sustainable Development (ICCESD-2012)*.
- Sarkar, R., and Maheshwari, B. (2012). Effect of soil nonlinearity and liquefaction on dynamic stiffness of pile groups. *International Journal of Geotechnical Engineering*, 6(3), 319-330.
- Seed, H. B., and Idriss, I. (1981). Evaluation of liquefaction potential sand deposits based on observation of performance in previous earthquakes. Paper presented at the ASCE national convention (MO).
- Seed, H. B., Idriss, I., and Arango, I. (1983). Evaluation of liquefaction potential using field performance data. *Journal of geotechnical engineering*, 109(3), 458-482.
- Seed, H. B., and Idriss, I. M. (1971). Simplified procedure for evaluating soil liquefaction potential. *Journal of the Soil Mechanics and Foundations division*, 97(9), 1249-1273.

- Setiawan, A. F., Darmawan, M. F., Ismanti, S., Mukhlis, S., and Muria, A. G. (2020). Numerical model for investigating seismic performance of Prestressed Hollow Concrete (PHC) piles with Fiber section element. Paper presented at the E3S Web of Conferences.
- Shafieezadeh, A., DesRoches, R., Rix, G. J., and Werner, S. D. (2012). Seismic performance of pile-supported wharf structures considering soil-structure interaction in liquefied soil. *Earthquake Spectra*, 28(2), 729-757.
- Shafiq, Q. S. M., and Sa'ur, R. H. M. (2017). Numerical Analysis of a Pile-Soil System under Earthquake Loading. *Al-Nahrain Journal for Engineering Sciences*, 20(2), 446-451.
- Shi, F. (2004). Experimental research on load transfer mechanism of pretensioned high strength spun concrete piles. *Chinese journal of geotechnical engineering-chinese edition*-, 26(1), 95-99.
- Shin, M., Choi, Y. Y., Sun, C.-H., and Kim, I.-H. (2013). Shear strength model for reinforced concrete rectangular hollow columns. *Engineering Structures*, 56, 958-969.
- Singh, H., Garg, P., and Jha, J. (2021). Modeling the Response of a Piled-Raft Footing: Ultimate Bearing Capacity. *Iranian Journal of Science and Technology, Transactions of Civil Engineering*, 45(1), 359-371.
- Sugimura, Y., Karkee, M. B., and Mitsuji, K. (2004). An investigation on aspects of damage to precast concrete piles due to the 1995 Hyogoken-Nambu earthquake. Paper presented at the Proceedings Third UJNR Workshop on Soil-structure Interaction, Menlo Park, California, USA.
- Suzuki, H., Tokimatsu, K., Sato, M., and Abe, A. (2006). Factor affecting horizontal subgrade reaction of piles during soil liquefaction and lateral spreading. *Seismic performance and simulation of pile foundations in liquefied and laterally spreading ground* (pp. 1-10).
- Sweigart, S. P. (2010). Seismic performance of prestressed concrete piles in CIP reinforced concrete pile caps. University of South Carolina.
- Tamura, S., and Tokimatsu, K. (2006). Seismic earth pressure acting on embedded footing based on large-scale shaking table tests *Seismic performance and simulation of pile foundations in liquefied and laterally spreading ground* (pp. 83-96).
- Tao, G., Zhou, Q., and Qiao, Z. (2017). Seismic Performance of PHC Pipe Piles Considering Soil-pile Interaction. Paper presented at the 2017 6th International Conference on Energy, Environment and Sustainable Development (ICEESD 2017).
- Teguh, M., Duffield, C., Mendis, P., and Hutchinson, G. (2006). Seismic performance of pile-to-pile cap connections: An investigation of design issues. *Electronic Journal of Structural Engineering (EJSE)*, 6(1), 8-18.

- Terzaghi, K. (1942), Discussion of the Progress Report of the Committee on the Bearing Value of Pile Foundations, Proc. ASCE, Vol. 68, pp. 311-323.
- Teguh, M., Mendis, P., Duffield, C., and Hutchinson, G. Finite Element Modeling of Pile-to-pile Cap Connections under Lateral Loads. Paper presented at the The 18th Australasian Conference on the Mechanics of Structures and Materials (ACMSM).
- Ter-Martirosyan, A. (2020). Calculation of the settlement of pile foundations taking into account the influence of soil liquefaction. Paper presented at the IOP Conference Series: Materials Science and Engineering.
- Tokimatsu, K., and Yoshimi, Y. (1983). Empirical correlation of soil liquefaction based on SPT N-value and fines content. *Soils and Foundations*, 23(4), 56-74.
- Towhata, I., Sesov, V., Motamed, R., and Gonzalez, M. (2006). *Model tests on lateral earth pressure on large group pile exerted by horizontal displacement of liquefied sandy ground*. Paper presented at the Proceedings of the 8th US National Conference on Earthquake Engineering.
- Tradigo, F., Castellanza, R., Partovi, M., and Schreppers, G. (2015). Calibration procedure for embedded pile modeling based on in situ pile load tests.
- Ukritchon, B., Faustino, J., and Keawsawasvong, S. (2016). A numerical study of load distribution of pile group foundation by 2D model. *Walailak Journal of Science and Technology (WJST)*, 13(8), 669-688.
- Uzuoka, R., Sento, N., Kazama, M., Zhang, F., Yashima, A., and Oka, F. (2007). Three-dimensional numerical simulation of earthquake damage to group-piles in a liquefied ground. *Soil Dynamics and Earthquake Engineering*, 27(5), 395-413.
- Wang, T., Du, Z., Zhao, H., Liu, X., and Wang, M. (2015). Experimental research on seismic behavior of pipe piles with hybrid reinforcement. *Journal of Civil Engineering and Management*, 32(3), 27-32.
- Wang, T., Yang, Z., Zhao, H., and Wang, W. (2014). Seismic performance of prestressed high strength concrete piles. *Materials Research Innovations*, 18(sup2), S2-515-S512-521.
- Wang, Y., Liu, X., Zhang, M., Yang, S., and Sang, S. (2020). Field Test of Excess Pore Water Pressure at Pile–Soil Interface Caused by PHC Pipe Pile Penetration Based on Silicon Piezoresistive Sensor. *Sensors*, 20(10), 2829.
- Wei, Y., Wang, D., Li, J., Jie, Y., Ke, Z., Li, J., and Wong, T. (2020). Evaluation of ultimate bearing capacity of pre-stressed high-strength concrete pipe pile embedded in saturated sandy soil based on in-situ test. *Applied Sciences*, 10(18), 6269.
- Wen, X. W. H., F.Y. Zheng, JS. (2016). Experiment on seismic failure mode of PHC pipe-piles in liquefiable soil under Shaking Table. *GEO-China*.

- Wu, P., Guo, Y., Zhu, D., Jin, W., and Lee, C.-f. (2020). Flexural performances of pre-stressed concrete piles reinforced with hybrid BFRP and steel bars. *European Journal of Environmental and Civil Engineering*, 1-20.
- Xia, X., Xu, H., Xu, H. D., and Gu, R. J. (2013). Study on bending behaviors of  $\Phi 500$  PHC pile. *Paper presented at the Advanced Materials Research*.
- Xiao, Y. (2003). Experimental studies on precast prestressed concrete pile to CIP concrete pile-cap connection. *PCI journal*, 48(6).
- Xizhi, Z., Shaohua, Z., Shengbo, X., and Sixin, N. (2020). Study of seismic behavior of PHC piles with partial normal-strength deformed bars. *Earthquake Engineering and Engineering Vibration*, 19(2), 307-320.
- Xu, C., Dou, P., Du, X., El Naggar, M. H., Miyajima, M., and Chen, S. (2020). Seismic performance of pile group-structure system in liquefiable and non-liquefiable soil from large-scale shake table tests. *Soil Dynamics and Earthquake Engineering*, 138, 106299.
- Xu, J., and Ma, L. (2017). Study on bearing capacity of prestressed pipe pile foundation under horizontal load. *The Open Construction and Building Technology Journal*, 11(1).
- Yamazoe, M., Sakuta, J., Mitsuji, K., and Maeda, M. (2012). Field investigation and dynamic analysis of damaged structure on pile foundation during the 2011 off the Pacific Coast of Tohoku Earthquake. *Paper presented at the Proceedings of the 15th World Conference on Earthquake Engineering*.
- Yang, Z., Guo, W., Zha, F., Jardine, R., Xu, C., and Cai, Y. (2015). Field behavior of driven prestressed high-strength concrete piles in sandy soils. *Journal of geotechnical and geoenvironmental engineering*, 141(6), 04015020.
- Yang, Z., Li, G., and Wang, W. (2018). Experimental investigation and nonlinear finite element analysis on seismic performance of PHC piles. *Structural Engineering International*, 28(4), 475-488.
- Yang, Z., and Wang, W. (2016). Experimental and numerical investigation on the behaviour of prestressed high strength concrete pile-to-pile cap connections. *KSCE Journal of Civil Engineering*, 20(5), 1903-1912.
- Yanyan, R. X. X. L. (2013). Experimental research on aseismic behavior of prestressed high strength concrete pipe piles [J]. *Industrial Construction*, 7.
- Yazici, V. (2012). Strengthening hollow reinforced concrete columns with fibre reinforced polymers.
- Yongchao, L., Gang, Z., Guyi, K., and Qinglong, W. (2011). Test on shear bearing capacity in oblique section for pre-stressed concrete pipe piles. *Building Structure*, 41(5), 93-97.
- Youd, T. L., and Idriss, I. M. (2001). Liquefaction resistance of soils: summary report from the 1996 NCEER and 1998 NCEER/NSF workshops on evaluation of liquefaction

- resistance of soils. *Journal of geotechnical and geoenvironmental engineering*, 127(4), 297-313.
- Yu, F., and Yang, J. (2012). Base capacity of open-ended steel pipe piles in sand. *Journal of geotechnical and geoenvironmental engineering*, 138(9), 1116-1128.
- Zein, Z. Z., Hussein, Z., Jaber, J. L., and Temsah, T. Y. (2021). Dynamic Soil-Structure Interaction Analysis: Detecting the Reliability of Modelling the Piles as a Plate Element for a Multistory Building Resting on Deep Foundation. *BAU Journal-Science and Technology*, 2(2), 8.
- Zhanfang, H., Xiaohong, B., Chao, Y., and Yanping, W. (2020). Vertical bearing capacity of a pile-liquefiable sandy soil foundation under horizontal seismic force. *PloS one*, 15(3), 0229532.
- Zhang, J., and Hutchinson, T. C. (2012). Inelastic pile behavior with and without liquefaction effects. *Soil Dynamics and Earthquake Engineering*, 36, 12-19.
- Zhang, L. (2009). Nonlinear analysis of laterally loaded rigid piles in cohesionless soil. *Computers and Geotechnics*, 36(5), 718-724.
- Zhang, X., Niu, S., Yan, J.-B., and Zhang, S. (2019). Seismic behaviour of prestressed high-strength concrete piles under combined axial compression and cyclic horizontal loads. *Advances in Structural Engineering*, 22(5), 1089-1105.
- Zhang, Z., Li, J., Xie, Z., and Zhang, R. (2011). Experimental study on flexural and shearing properties of modified concrete pipe piles. *Chinese Journal of Geotechnical Engineering*, 33(2), 271-277.
- Zhou, J.-j., Yu, J.-l., Gong, X.-n., Zhang, R.-h., and Yan, T.-l. (2019). Influence of soil reinforcement on the uplift bearing capacity of a pre-stressed high-strength concrete pile embedded in clayey soil. *Soils and Foundations*, 59(6), 2367-2375.
- Zhou, J., Wang, R., Dong, F., and Oh, E. 2019. Behavior of precast concrete pipe piles under compressive loading.
- Zhou, J., Zhang, X., Jiang, H., Lyu, C., and Oh, E. (2017). Static and dynamic load tests of shaft and base grouted concrete piles. *Advances in Civil Engineering*, 2017.
- Zhou, X., and Fang, G. (2015). A Study of PHC Pipe Pile Vertical Ultimate Bearing Capacity Calculation Method and its Numerical Simulation Analysis. Paper presented at the MATEC Web of Conferences.
- Ziehl, P. H., Caicedo, J. M., Rizos, D., Mays, T., Larosche, A., ElBatanouny, M. K., and Mustain, B. (2012). Behavior of pile to bent cap connections subjected to seismic forces: University of South Carolina. Dept. of Civil and Environmental Engineering.